TERMINAL BALLISTICS

Marvin E. Backman

Naval Weapons Center
China Lake, California

February 1976

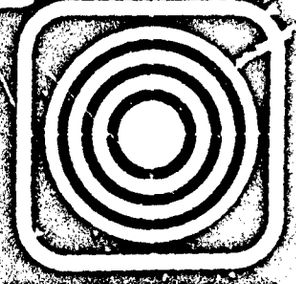

TERMINAL BALLISTICS

NWC TP 5780

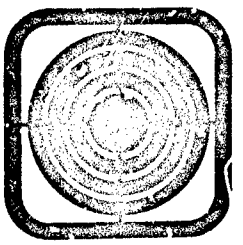

TERMINAL BALLISTICS

Marvin E. Backman
Research Department
Naval Weapons Center

February 1976

Naval
Weapons
Center
China Lake
California 93555

NWC Technical Publication 5780

Published by ..... Technical Information Department
Collation ..... Cover, 118 leaves
First printing ..... 500 unnumbered copies

Additional copies, at $12.50 each, available from
National Technical Information Service
Springfield, Virginia 22161

if

UNCLASSIFIED

SECURITY CLASSIFICATION OF THIS PAGE (When Data Entered)

REPORT DOCUMENTATION PAGE		READ INSTRUCTIONS BEFORE COMPLETING FORM
1 REPORT NUMBER NWC TP 5780	2 GOVT ACCESSION NO.	3 RECIPIENT'S CATALOG NUMBER
4 TITLE (and Subtitle) TERMINAL BALLISTICS		5 TYPE OF REPORT & PERIOD COVERED 6 PERFORMING ORG. REPORT NUMBER
7 AUTHOR(s) Melvin E. Backman		8 CONTRACT OR GRANT NUMBER(s)
9 PERFORMING ORGANIZATION NAME AND ADDRESS Naval Weapons Center China Lake, California 93555		10 PROGRAM ELEMENT, PROJECT, TASK AREA & WORK UNIT NUMBERS
11 CONTROLLING OFFICE NAME AND ADDRESS Naval Weapons Center China Lake, California 93555		12 REPORT DATE 13 NUMBER OF PAGES 232
14 MONITORING AGENCY NAME & ADDRESS (if different from Controlling Office)		15 SECURITY CLASS. (of this report) UNCLASSIFIED 15a DECLASSIFICATION/DOWNGRADING SCHEDULE

16 DISTRIBUTION STATEMENT (of this Report)

Approved for public release, distribution unlimited.

17 DISTRIBUTION STATEMENT (of the abstract entered in Block 20, if different from Report)

18 SUPPLEMENTARY NOTES

19 KEY WORDS (Continue on reverse side if necessary and identify by block number)

Terminal Ballistics	Fragmentation	Impact Mechanics
Projectiles	Soil and Rock Penetration	
Warheads	Armor Penetration	
Explosives	Blast	
Detonation	Shaped Charges	

20 ABSTRACT (Continue on reverse side if necessary and identify by block number)

See back of form.

DD FORM 1 JAN 73 1473 EDITION OF 1 NOV 65 IS OBSOLETE
S/N 0102-014-6601

UNCLASSIFIED
SECURITY CLASSIFICATION OF THIS PAGE (When Data Entered)

ia

(U) *Terminal Ballistics*, by Morton J. Rochester. China Lake, Calif., Naval Weapons Center, February 1976. 230 pp. (NWC TP 5788, publication UNCLASSIFIED.)

(U) This report is an introductory summary of the main phenomena of the detonation and fragmentation of explosive warheads and of the phenomena of high-velocity impact. It covers the techniques for measuring and predicting the extremely rapid and intense exchanges of energy and momentum that occur in the interaction of a warhead with a target.

(U) Beginning with the ballistics of gun-launched projectiles, the report develops a parallel discussion of warhead phenomena. In this process parts of several specialized fields of physical science are used: impact mechanics, the deflagration and detonation of explosives, and the behavior of materials under extremely high loads and high rates of loading.

Naval Weapons Center
AN ACTIVITY OF THE NAVAL MATERIAL COMMAND
R. G. Freeman, III, RAdm., USN ..... Commander
G. L. Hollingsworth ..... Technical Director

Foreword

This book is based on lecture notes for a course offered at the Naval Weapons Center as part of its training program of day classes in science and engineering. Its publication was jointly sponsored by the Research Department and the Personnel and Organization Development Division, Personnel Department of NWC. The course was designed to summarize the fundamental concepts of terminal ballistics for employees who would use the information directly in assignments in research, development, or analysis of weapons, or who would use the information as background in the planning and management of weapons programs. For this audience terminal ballistics is the science of the interaction of a ballistic weapon with a target and must include sophisticated warheads as well as the classical concepts of the defeat of armor.

Typically the student was a recent engineering or physical science graduate; however, many technicians who were directly involved in weapon design and testing also took the course. For these and many others associated with ordnance science, there is a continuing need for an introductory summary of the main phenomena of the detonation and fragmentation of explosive warheads and of the phenomena of high-velocity impact and the techniques for measuring and predicting the extremely rapid and intense exchanges of energy and momentum that occur in the interaction of a warhead with a target. Warhead design and analysis will often require the development of these concepts beyond this introductory level. The object here is to provide the starting point from which the direction for further development will be more clear.

The book begins with the ballistics of gun-launched projectiles, the subject matter of classical ballistics, and develops from this base a parallel description of warhead phenomena. In this process parts of several specialized fields of physical science are used: impact mechanics, the deflagration and detonation of explosives, and the behavior of materials under extremely high loads and high rates of loading. Thus, in this

progression from classical ballistics to current technology the reader is exposed to a synthesis of specializations in physical science that are not readily available and are not usually interrelated, but which are the basis for warhead analysis and design.

released by
JOHN PEARSON, *Head*
Detonation Physics Division
1 December 1975

Under authority of
H. W. HUNTER, *Head*
Research Department

ACKNOWLEDGMENT

The author wishes to acknowledge the assistance given by the members of the Detonation Physics Division of the Research Department at the Naval Weapons Center through discussions, criticism, and encouragement. The contributions of John Pearson and Carl Austin as guest lecturers are particularly appreciated. The sections on warhead fragmentation and soil and rock penetration are based on their lectures. Thanks is due also to Toni Goff for preparation of the manuscript. The vision and concern of the Command at the Naval Weapons Center which has been embodied in the Science and Engineering Day Class Program made the original presentations possible.

Contents

Part II. Warhead Ballistics

Introduction

Scientific methods have been applied to the problem of improving the accuracy and range of guns for at least two centuries. An important part of this effort has been the prediction of the trajectories of projectiles from the weight and composition of the charge, the weight and shape of the projectile, and the dimensions and elevation of the gun barrel. The data and theories needed to make these predictions are part of the science of ballistics. The events occurring in the barrel of the gun are vastly different from the events occurring during free flight of the projectile. Both sets of events are obviously important in determining accuracy and range, but the methods of analyzing them are sufficiently different to make separate treatment useful and natural. Information about the events in the barrel is called *interior ballistics*; information about events in free flight is called *exterior ballistics*.

Contact between the projectile and the target ends all considerations of accuracy and range. The projectile impacts against the object at the aimpoint, and that object loses its meaning as a target and becomes important as a barrier. The interactions of a projectile with a barrier that are of most interest are the penetration into the barrier, or passage of the projectile through the barrier. Quantitative measures of these interactions are correlations of penetration depth to impact velocity, correlations of residual velocity of the projectile to the impact velocity, and the ballistic limit, which is the lowest velocity for perforation. These are data on trajectories, and the study of the projectile/barrier interaction completes the investigation of projectile motion begun under interior and exterior ballistics. The study of projectile/barrier interactions is called *terminal ballistics*.

Developments in military technology have changed the methods of delivering weapons. Aerial bombs and rocket-propelled weapons are now just

as important as gun-fired weapons. Interior and exterior ballistics still provide the basis for systematic improvement of the accuracy and range of these devices. Yet another development is the use of explosives in projectiles. The terminal phase of an explosive projectile differs drastically from that of an inert projectile. The explosive event and its consequences are the new center of interest. Projectile motion loses much of its importance in the projectile barrier interaction. The ballistic limit, penetration, and theories of residual velocity, which are the essence of projectile terminal ballistics, have few counterparts in explosive phenomena, so that classical terminal ballistics does little to explain the workings of explosive projectiles.

The terminal phase of an exploding ballistic weapon is composed of events that occur so fast and under such intense force that it is difficult to observe the phenomena much less analyze them. For this reason, any body of knowledge that will help interpret these events by comparison or analogy is definitely needed. The terminal ballistics of inert projectiles is too limited to meet this need. There are, however, strong similarities between *all of the ballistics of inert projectiles* and the *terminal phase of an explosive warhead.* The acceleration of fragments from the case of the warhead is like interior ballistics, the flight of fragments to the target is like exterior ballistics, and the interaction of the fragments with the target as a barrier is like terminal ballistics. Added to these phenomena of fragments is the generation, transmission, and interaction of blast with the target. Blast has no significant counterpart in projectile ballistics, but it is an addition that can be considered separately without detracting from the advantages gained by the analogy between projectile and warhead fragment.

To summarize, the study of the terminal phase of the operation of an explosive warhead is certainly necessary and will profit from systematic use of analogy, but it is not feasible to base the study of the warhead terminal phase on the terminal phase of projectile ballistics; rather, the whole of projectile ballistics is required. The warhead is a new ballistic system complete with interior, exterior, and terminal ballistic phases, and the study of this new system has useful parallels to the projectile ballistic system.

The warhead and projectile ballistic systems have a common purpose to convert energy stored as chemical energy into mechanical form and transfer the energy to a remote target. The two systems differ most in the limitations that are imposed on the energy transfer process. The projectile system involves an energy transfer apparatus—the gun that must not be damaged by the process. The warhead system is completely free of this limitation, but it has

the imitation that every component of the energy transfer apparatus must function with maximum efficiency and minimum weight.

The present treatment begins with a discussion of projectile ballistics. Only those parts of interior and exterior ballistics of gun-fired projectiles that are particularly relevant to warhead ballistics are discussed. (For example, the complexities of spin stabilization imparted by the rifled barrel are given minimal attention, not because these are unimportant in projectile ballistics, but because there is little carryover into warhead ballistics.) Projectile terminal ballistics is considered in greater detail. Warhead ballistics is developed by showing the elaboration and modification of projectile interior ballistics that is needed for explosive devices, the changes needed in exterior ballistics, and the changes needed in terminal ballistics to account for the special characteristics of warhead fragments and the effect of blast.

Nomenclature

A	Area, usually cross-sectional area
A_b	Base area, the effective area of the base of a projectile
A_s	Wetted area, area a fluid can contact on a projectile
B_1, B_2	Combination of ballistic parameters in the expression for projectile deflection
C	The mass of a propellant or explosive charge
C_v	Specific heat at constant volume
C_p	Specific heat at constant pressure
C_L	Aerodynamic coefficient of lift
C_D	Aerodynamic coefficient of drag
C_M	Aerodynamic coefficient of yaw
C_l	Yaw-dependent coefficient of lift
C_m	Yaw-dependent coefficient of yaw moment
C_{1lim}, C_0	Drag coefficients for soils
C_{llim}, C_{l0}	Lift coefficients for soils
C_H	Thermodynamic constant
D	Detonation velocity
d_g	Grain dimension
E	Internal energy
E_0	Energy converted to nonkinetic form
F	Force in general discussion
F_c	Internal ballistic force constant
F_D	Drag force
F_g	Force due to gravity
F_I	Force due to inertia
F_L	Lift force
F_p	Force due to pressure

F_r	Force resisting penetration
G	$\dfrac{A^2 n_g^2 k_2}{a^2 m k_1 C F_c}$
H	Material hardness
J	Mechanical equivalent of heat
K	Velocity decay constant
L_g	Grain dimension
M	Mach number
M_s	Yaw moment
P	Penetration
Q	Heat (amount of heat released at constant volume)
R	Gas constant
R_f	Radius of gyration
R_1	The mass ratio $m_1/(m_1 + m_2)$
R_2	The mass ratio $m_2/(m_1 + m_2)$
S	Petry constant
SN	Empirical constant in the Sandia equations
T	Temperature
T_a	Ambient temperature
T_0	Stagnation temperature
T_r	Recovery temperature
U	Shock velocity
V_0, V_1, V_2	Velocities in shaped charge liner collapse
V_j	Jet velocity
V_s	Slug velocity
W	Work
W_p	Weight of projectile
Z	A length variable
a, b, a_1, a_2, a_3	Empirical constants. (In Chap. 5, Eq. 5-16 and following, a and b are inner and outer diameters of a cylinder)
c	Speed of sound
c_0	Speed of sound for small disturbances
c_1, c_2, c_3	Poncelet constants
c_a	Speed of sound in air
c_s	Speed of sound in soil
d	Diameter of projectile, rod, or other object

e	Energy density
f	Fraction of a grain dimension that has been consumed
g	Gravitational constant
h	Thickness of principal dimension
h_f	Heat of fusion
k	Shape factor
k_1, k_2	Lagrange constants
l	A length measurement
l_0	Added bore length to account for free space in barrel
l_1, l_2, l_3	Lengths of an element of a body
l_p	Projectile length
m	Mass
m_c	Mass of warhead case
m_g	Instantaneous mass of a propellant grain
m_{g0}	Initial mass of a propellant grain
m_1	Mass of the projectile (Chapter 5, mass ahead of the shock)
m_2	Mass of the barrier (Chapter 5, mass behind the shock)
m_3	Mass of the plug
m_j	Mass of the jet
m_s	Mass of the slug
n	Number of moles of a given material
p_0, p_1, p	Breech pressure, base pressure, and mean pressure in the interior ballistics of a gun Also, p_1, p_2, the pressure ahead of a shock and behind it
p^*	Overpressure
q_j	Energy flux
q_m	Mass flow
r	Radial coordinate
r_f	Recovery factor
s	Distance parameter
$s_{ij}, \bar{s}$	Stress deviators and mean normal stress
t	Time parameter
u	Particle velocity
u_i	Particle velocity of an incident wave
u_r	Particle velocity of a reflected wave
u_t	Particle velocity of a transmitted wave
v	Projectile velocity
v_0	Initial velocity of a projectile

v_1	Final velocity of a projectile
v_2	Final velocity of a barrier
v_c	Velocity of expansion of a warhead case
v_x	x-component of velocity
v_y	y-component of velocity
v_{BL}	Ballistic limit velocity
w_1	Projectile velocity component off the line of flight
w_2	Barrier velocity component off the line of flight
x, y	Cartesian coordinates
z	Fraction of propellant mass that has been consumed
α, β	Angles in shaped charge liner collapse process
γ	Ratio of the specific heats
δ	Yaw angle
ϵ	Constant of integration
ϵ_{ij}	General strain components
ϵ_1, ϵ_2	Strain components
$\epsilon_x, \epsilon_z, \epsilon_\theta$	Strain components in cylindrical coordinates
θ	Form function (in internal ballistics)
	Also, angle parameter
λ	Lamé's constant. λ is also a geometric ratio
μ	Lamé's constant
ν	Poisson's ratio
ξ	Displacement of the flame front
ξ_i	Displacement of the flame front in direction i
ρ	Density
ρ_a	Density of air
ρ_g	Density of a gas
ρ_p	Propellant density
ρ_s	Density of soil
ρ_1, ρ_2	Densities ahead of and behind a shock
σ	Aerodynamic stability parameter
σ_{ij}	General stress components
$\sigma_\theta, \sigma_r, \sigma_z$	Components of stress in cylindrical coordinates
σ_y	Yield strength
τ	Volume
ψ	Deflection angle for barrier
Ω	Deflection angle for projectile

PART I

PROJECTILE BALLISTICS

1

The Interior Ballistics of Guns

A smooth-bore, muzzle-loading cannon is shown in Fig. 1. It consists of a barrel that is a strong metal tube open on one end and thickest at the closed end. There is a small opening in the closed end, the touch hole, that provides access to ignite the main charge of black powder. The burning of the charge results in the release of gases and heat. Pressure develops behind the projectile and pushes it out of the barrel.

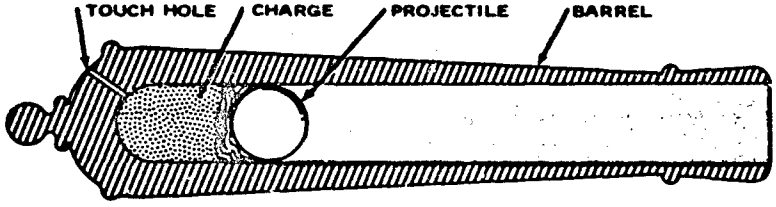

FIG. 1. Smooth-Bore Muzzle-Loading Cannon.

Modern guns are much more complicated devices, largely because of mechanisms that serve subsidiary functions such as the automation of loading, the control of the aimpoint, or the increasing of mobility. The barrel of a modern gun is usually rifled to provide spin stabilization of the projectile in free flight. The propellant charge has a carefully specified composition and a controlled granular configuration. The projectile may be a combination of many materials that help to seal it into the barrel and give it good exterior

and terminal ballistic performance, but its essential property in internal ballistics is its mass.

The processes that occur between the operation of the igniter and the expulsion of the projectile from the barrel can be described as follows:

1. The igniting system applies the heat that is required to ignite the propellant charge.

2. A steady chemical reaction on the surface of the propellant grains is quickly set up that results in the liberation of heat and gases. The evolution of heat and gases causes the pressure and temperature in the chamber to build up.

3. The projectile is accelerated by the pressure. The displacement of the projectile changes the volume in which the chemical reaction takes place. The rate of chemical reaction is affected by the change of pressure and temperature brought about by the change of volume, but is also dependent on the propellant grain shape and size. The rate of combustion of the charge, the changes of pressure and temperature behind the projectile, and the motion of the projectile continue an interdependent development until the charge is consumed.

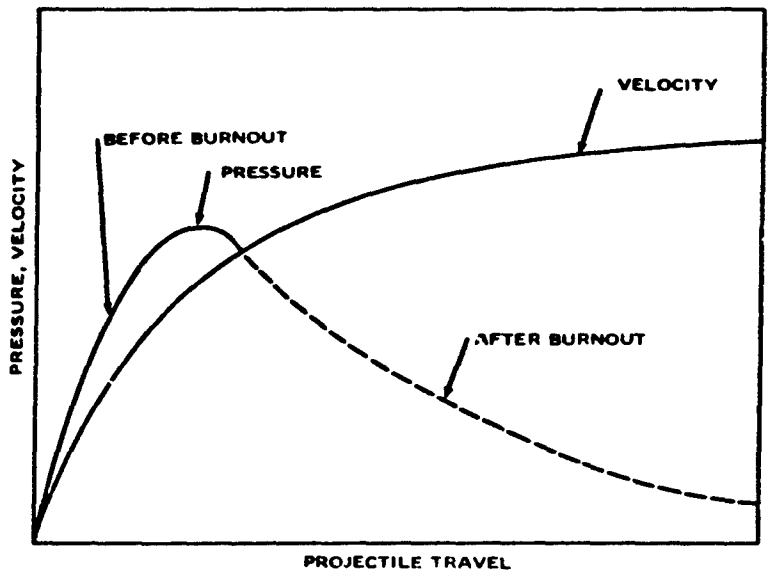

FIG. 2. Velocity and Pressure on the Base of a Projectile as a Function of Distance Along the Bore.

4. After the charge is consumed, the hot product gases continue to push the projectile until it is expelled from the muzzle.

The final result of these processes is a pressure on the base of the projectile and a velocity of the projectile that vary with distance down the bore roughly as shown in Fig. 2.

The forces on the projectile may be very large, but the projectile must not deform and the pressures in the gun barrel must be below the failure limit. *The central problem of interior ballistics, therefore, is to determine those parameters of the charge, the projectile, and the barrel that are important in assuring that the pressures in the chamber and bore are held to safe values but still produce a maximum muzzle velocity.*

IGNITION

The function of the igniting system is to produce the high temperature that is required to ignite the propellant charge. Ideally, all of the propellant grains should be exposed to the ignition temperature of about 170 to 500°C in a very short time. The igniting system is usually actuated by a firing pin (plunger) that strikes a device called the percussion cap (Fig. 3). This cap

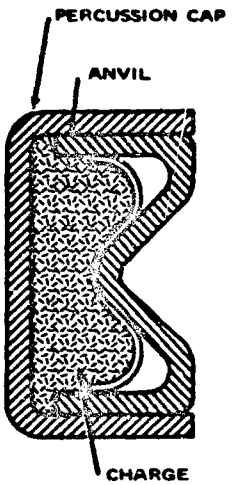

FIG. 3. Percussion Cap.

contains an explosive mixture that reacts rapidly as a result of the impact of the firing pin against the anvil. The explosive may be pure lead styphnate or a mixture of lead styphnate, DDNP (diasonitrophenol), and tetracene, which are primary explosives that will be discussed in greater detail later. The reaction of the explosive produces hot particles and gases that are projected into the case. The flame acts directly on the grains of the main charge in small arms ammunition. In larger caliber rounds the flame ignites a charge of black powder, which then augments the flame from the percussion cap and improves the distribution of the flame throughout the main propellant charge. An example is shown in Fig. 4. The black powder is enclosed in an ignition tube that serves to distribute the flame from the black powder through the propellant charge.

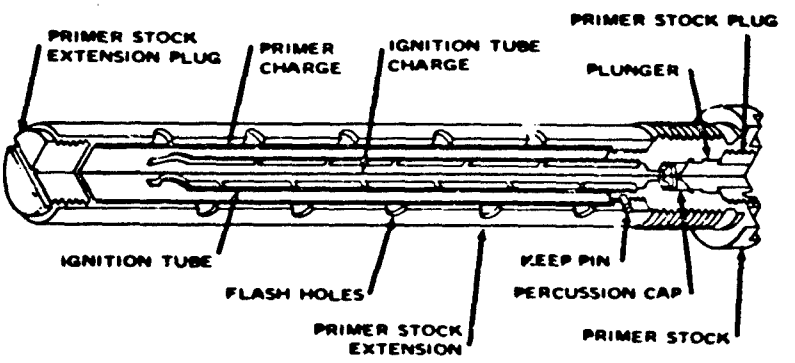

FIG. 4. Ignition Primer.

CHEMISTRY AND THERMODYNAMICS OF BURNING

Black powder, which is now used only in ignition primers, is one of the oldest propellants to be used in guns. It is a mixture of 75% potassium nitrate, 15% charcoal, and 10% sulphur. The stoichiometric equation for its combustion is

$$2KNO_3 + 3C + S = N_2 + 3CO_2 + K_2S$$

This is an exothermic reaction; that is, it releases energy in the form of heat when the products on the right side of the equation are formed. A gram of

dry powder releases about 800 gram-calories of heat in the formation of 200 to 300 cubic centimeters of gases.

The details of the reaction are believed to be much more complex than is indicated by the above equation (Ref. 1). One theory is that there are two main parts to the reaction, which are as follows:

1. A rapid oxidation process

$$10KNO_3 + 8C + 3S = 2K_2CO_3 + 3K_2SO_4 + 6CO_2 + 5N_2$$

This is believed to be the most rapid process and to contribute the most energy.

2. Much slower reduction reactions

a. $4K_2CO_3 + 7S = K_2SO_4 + 3K_2S_2 + 4CO_2$

b. $4K_2SO_4 + 7C = 2K_2CO_3 + 2K_2S_2 + 5CO_2$

These increase the total amount of gas formed but reduce the amount of energy released.

In heat transfer by radiation the emissivity of the materials is important. The emissivity of solids is many times that for gases. Thus the solid particles of K_2CO_3 and K_2SO_4 that occur in the above reactions are an asset when black powder is used as an igniter.

Black powder was formerly used as the main charge. Its greatest disadvantage is the formation of solid products of combustion that foul the barrel and produce smoke and excessive muzzle flash that give away the gun location. Black powder has been replaced by nitrocellulose and combinations of nitrocellulose and nitroglycerin.

Nitrocellulose was discovered in 1845, but it was 40 years before it became a practical propellant. The reason is that the simple nitration of cellulose gives a product that has the porosity of the cellulose. A propellant with this porosity has a very high reaction rate and produces excessive pressures that can damage the barrel and also can lead to a runaway process called detonation. (Detonation will be discussed in greater detail later. For the purposes of the immediate discussion, detonation is an extremely violent energy release process that cannot be used effectively in the barrel of a gun.) Nitrocellulose became usable with the development of processing methods that led to a better macrostructure and controlled burning rate.

A stoichiometric equation of the explosion of nitrocellulose is

$$2C_{24}H_{29}O_9(NO_3)_{11} \rightarrow 41CO + 7CO_2 + 29H_2O + 11N_2$$

The final products of this ideal reaction are all gases. Actual products do include some solids and liquids, but far fewer than the products of black powder. Nitrocellulose releases 750 to 950 g-cal/g, and combinations with nitroglycerin have calorimetric values up to 1,250 g-cal/g.

Propellants that contain nitrocellulose as the chief ingredient are called *single-base propellants*. Propellants that use both nitrocellulose and nitroglycerin as major constituents are called *double-base propellants*. Examples of propellant compositions are given in Tables 1 through 5 (Ref. 2).

TABLE 1. Compositions of Single-Base Propellants for Small Arms.

Ingredient	% of ingredient for indicated propellant				
	I	II	III	IV	V
Nitrocellulose	97.4[a]	99.3[b]	98.3[b]	99.0[c] 99.6	96.95[d]
Tin	2.0	...	...	...	..
Potassium sulfate	...	...	1	...	..
Diphenylamine	0.6	0.7	0.7	0.4-1.0	1.05

[a] 13.15% nitrogen.
[b] 13.15 or 13.25% nitrogen.
[c] 13.10% minimum nitrogen.
[d] 12.95% nitrogen.

TABLE 2. Compositions of Double-Base Propellants for Small Arms.

Ingredient[a]	% of ingredient for indicated propellant		
	Ballistite	Bullseye	Infallible
Nitrocellulose[b]	60	59.6	60.25
Nitroglycerin	39	40.0	39.00
Diphenylamine	1	0.4	0.75

[a] Graphite is used as a coating for all propellants.
[b] 13.25% nitrogen.

TABLE 3. Compositions of Propellants for .30- and .50-Caliber Ammunition.

Ingredient	Ingredient for indicated propellant		
	%	%	%
Nitrocellulose[a]	74.70	76.55	84
Nitroglycerin	19.90	20.40	15
Starch	2.25	2.30	...
Barium nitrate	1.50	...	...
Potassium nitrate	0.90	...	...
Diphenylamine	0.75	0.75	0.75
Graphite	...	...	0.25

[a] 13.15 or 13.25% nitrogen.

TABLE 4. Compositions of Double-Base Cannon Propellants.

Ingredient	% of ingredient for indicated propellant	
	M2	M5
Nitrocellulose[a]	77.45	81.95
Nitroglycerin	19.50	15.00
Barium nitrate	1.40	1.40
Potassium nitrate	0.75	0.75
Ethyl centralite	0.60	0.60
Graphite	0.30	0.30

[a] 13.25% nitrogen.

TABLE 5. Compositions of Mortar Propellants.

Ingredient	% of ingredient for indicated propellant	
	M8 increment	M9 ignition
Nitrocellulose[a]	52.15	57.75
Nitroglycerin	43.00	40.00
Diethylphthalate	3.00	...
Potassium nitrate	1.25	1.50
Diphenylamine	...	0.75
Ethyl centralite	0.60	...

[a] 13.25% nitrogen.

The evolution of heat and gases causes the temperature and pressure to build up. Thermodynamic principles can be applied to find the relation between the temperature and pressure, the physical properties of the products of combustion, and the amount of heat released (Ref. 3 and 4). According to the first law of thermodynamics, the heat added to a system is the sum of the change in its internal energy and the work done by the system

$$Q = \Delta E + W \tag{1-1}$$

Let the system consist of unit mass of propellant burned to its final products in the free space of the gun chamber. The internal energy E can be given as

$$E = \int_0^{T_0} C_v \, dT \tag{1-2}$$

and if Q is the amount of heat released at constant volume (so that $W = 0$),

$$Q = \int_0^{T_0} C_v \, dT - \int_0^{T} C_v \, dT = \int_{T_0'}^{T_0} C_v \, dT \tag{1-3}$$

where T_0' is the temperature of the products corresponding to their initial state, T_0 is the temperature of the products (the adiabatic flame temperature), and C_v is the specific heat at constant volume. The pressure can be obtained from the equation of state of the product gases. Using a form of the van der Waals equation of state

$$p(\tau - b) = RT$$

$$p = \frac{RT}{\tau - b} \tag{1-4}$$

where $\tau = \tau_c - \tau_p$ if τ_c is chamber volume, τ_p is propellant volume, and $\tau_p = C/\rho_p$ is the charge mass divided by the propellant density.

The projectile is accelerated by the pressure acting on the base of the projectile

$$Ap_1 = m\frac{dv}{dt} \tag{1-5}$$

where p_1 is the pressure at the base of the projectile, A is the projectile cross-sectional area, m is the projectile mass, and v is the projectile velocity. If the pressure were known as a function of the displacement of the projectile as shown in Fig. 2, the muzzle velocity could be calculated directly and the central problem of interior ballistics would be solved. Unfortunately, interior ballistics investigations have not found any explicit dependence of pressure on projectile displacement, but rather show that the pressure depends on the amount of propellant burned behind the projectile and on the volume of the space behind the projectile. The relation between pressure, the amount of charge burned, and the change in volume brought about by projectile displacement is derived from conservation of energy. This relation is called Resal's equation.

Resal's Equation

Let z be the fraction of the charge mass C that is burned at a given instant; then (where J is the mechanical equivalent of heat)

$$E = JCz \int_0^{T_0} C_v dT \tag{1-6}$$

is the internal energy of the combustion products if there is no work done by the system. Projectile displacement means that (1) the gases have expanded and changed the internal energy and (2) the gases have done work. The expansion of the gases lowers the temperature from T_0 to T, and the internal energy is

$$E = JCz \int_0^{T} C_v dT \tag{1-7}$$

The change in the internal energy is

$$\Delta E = JCz \int_0^{T} C_v dT - \int_0^{T_0} C_v dT = -JCz \int_T^{T_0} C_v dT \tag{1-8}$$

from Eq. 1-5 and 1-6, and the work of expansion is

$$W = A \int_0^x p_1 dx \tag{1-9}$$

(It is implicit in the thermodynamic assumptions that p is uniform over the chamber. The fact that this is only approximately true will be considered later.) Using the first law of thermodynamics and Eq. 1-7 and 1-8,

$$-\Delta E = W$$

$$JC_v \int_T^{T_0} C_v dT = A \int_0^x p_1 dx \tag{1-10}$$

It is usually assumed that the variation in C_v over the range from T to T_0 is small so that C_v can be replaced under the integral sign by its mean value $\bar{C}_v$; hence, Eq. 1-10 becomes

$$JC_z\bar{C}_v T_0 = JC_z\bar{C}_v T + A \int_0^x p_1 dx \tag{1-11}$$

and T is replaced by using an equation of state

$$p(\tau - b) = nRT \tag{1-12}$$

so that

$$JC_z\bar{C}_v T_0 = \frac{J\bar{C}_v Cp(\tau - b)}{nR} + A \int_0^x p_1 dx \tag{1-13}$$

Use the thermodynamic relation $C_p - C_v = nR/J$ and the definition of the force constant, $F = nRT_0$, which is common in internal ballistics, to obtain

$$\frac{FC_z}{\gamma - 1} = \frac{PC_z(\tau - b)}{\gamma - 1} + A \int_0^x p_1 dx$$

where τ is the volume occupied by the unit mass of gas and $Cz\tau$ is the volume of gas at the time considered and consists of these parts: chamber volume (τ_c) plus volume of bore behind the projectile (Ax) minus the volume of propellant burned at the given time ($C(1 - z)/\rho_p$). The initial volume of the free space is expressed for analytical convenience as added length of bore l_0,

$$Al = \tau_c - \frac{C}{\rho_p}$$

and the final result is Resal's equation

$$\frac{FCz}{\gamma - 1} = \frac{p}{\gamma - 1} A(x + l_0) - Cz\frac{(b - 1)}{\rho_p} + A\int_0^x p_1 dx \qquad (1\text{-}14)$$

The quantity $(b - 1)/\rho_p$ is small and is frequently neglected to give a simpler form

$$\frac{FCz}{\gamma - 1} = \frac{p}{\gamma - 1} A(x + l_0) + A\int_0^x p_1 dx \qquad (1\text{-}15)$$

The term $A\int_0^x p_1 dx$ in Resal's equation includes all forms of energy changes that are brought about by the pressure p. The kinetic energy of the projectile is of most immediate interest and importance. A second major contribution is the kinetic energy that the expanding gases in the chamber acquire as the projectile is driven down the bore. An estimate of the magnitude of this term can be made by using the Lagrange approximation. This estimate is based on the assumption that the density of the gases and unburned propellant is constant and that the velocity is linearly distributed between the breech and the base of the projectile.

$$E_{kg} = A\int_0^{x_1} \rho\frac{v^2}{2} dx \qquad \text{for } v = v_1 y, \quad y = x/x_1$$

$$= \frac{Ax_1\rho v_1^2}{2}\int_0^1 y^2 dy$$

$$= \frac{Cv_1^2}{6}$$

The two major terms together are

$$\frac{mv^2}{2} + \frac{Cv^2}{6} = \left(m + \frac{C}{3}\right)\frac{v^2}{2}$$

and can be lumped together by defining

$$k_2 = \left(1 + \frac{C}{3m}\right) \tag{1-16}$$

so that

$$\left(m + \frac{C}{3}\right)\frac{v^2}{2} = k_2\frac{mv^2}{2}$$

Other energy changes that are either neglected or included as apparent changes in projectile mass are the energy of the recoil of the gun, the elastic and heat energy absorbed by the gun, and the rotational energy imparted to the projectile by rifling.

Resal's equation becomes

$$\frac{F_c Cz}{\gamma - 1} = \frac{p}{\gamma - 1}A(x + l_0) + \frac{k_2 mv^2}{2} \tag{1-17}$$

The equation of motion of the projectile has to be supplemented by information on the dependence of the pressure at the base of the projectile on the displacement of the projectile down the bore. Resal's equation partially fulfills this need. It is a relation between projectile velocity, the pressure, the amount of charge that has been burned, and the change in volume brought about by projectile displacement. To complete the required information, the dependence of burning on the pressure and temperature within the barrel must be determined.

RATE OF BURNING

Studies of propellant burning under constant pressure show that the chemical reaction advances into the propellant material at a steady rate. The

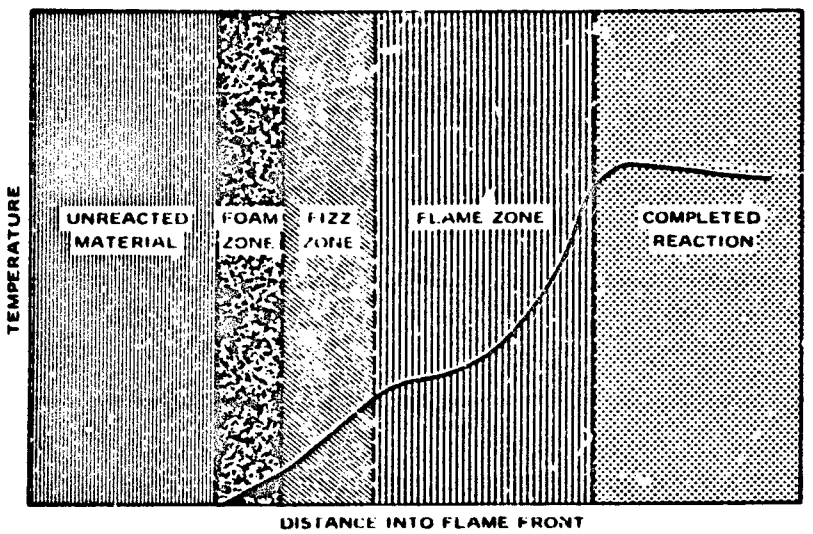

FIG. 5. Flame Front.

structure of the cross section of a material that is undergoing reaction is shown in Fig. 5. The reaction consists of several parallel zones. The reaction is advancing from right to left with unreacted material on the far left. Each zone of the reaction is given a descriptive label that indicates qualitatively the main features of the zone. The solid line indicates qualitatively the temperature variation in the zones. In the first zone, called the *foam zone*, heat from radiation and convection melts the propellant and liberates gases that move to the right (opposite to the direction of the advance of the flame front) into the next zone, the *fizz zone*, where the speed of reaction increases. The products of the second zone flow into the *flame zone* and, after an induction period, enter into the final reaction, which yields the highest temperature and is luminous.

In the discussion of warheads the properties of the flame front of a propellant will be compared to the properties of the detonation front of a high explosive. In anticipation of that comparison it should be noted that the flow of material in the burning of propellants is in the opposite direction to the advance of the flame front. In detonation the motion of reacted material is in the *same direction* as the advance of the detonation front.

Many tests on the burning of propellants indicate that the rate of

advance of the propellant depends on the pressure. The form of the mathematical relation that holds for many materials is

$$\frac{d\xi}{dt} = ap_0^b \tag{1-18}$$

where ξ is the displacement of the flame front, p_0 is the pressure at the breech where the propellant is burned, and a and b are empirical constants. This equation is referred to as Vieille's law.

It is usually assumed that the reaction of the propellant is initiated on the entire surface of all the propellant grains and advances into the grain parallel to the grain surface. The law that propellants burn parallel to the initial grain surface is called Piobert's law. Although it may not be accurate in minute detail, it is believed to be a reasonable description of the net effect of burning. Piobert's law is the basis for analytical expressions of the relation between the rate of chemical reaction and the grain shape and size.

It is convenient to express the burning rate in terms of the fraction f of a typical grain dimension ($\xi = fd_g$), since this is a parameter that must ultimately be considered.

Thus

$$\frac{d\xi}{dt} = d_g \frac{df}{dt} = ap_0^b \tag{1-19}$$

A particular expression that is used frequently is

$$z = (1 - f)(1 + \theta f) \tag{1-20}$$

which is called the form function. $\theta = \theta(f)$, and the particular analytical expression of θ represents the effect of shape.

The following sections discuss three propellant (powder) grain configurations: cylindrical, tubular, and multitubular (Fig. 6).

Cylindrical Grain

A very simple grain configuration is a cylindrical grain (Fig. 6a). The

volume of the cylinder is

$$\tau_0 = \pi d_g^2 l/4$$

$$\tau_0 = \pi d_g^3 \lambda/4$$

where d_g is the diameter of the cylinder and l is the length of the cylinder (let $l = \lambda d_g$).

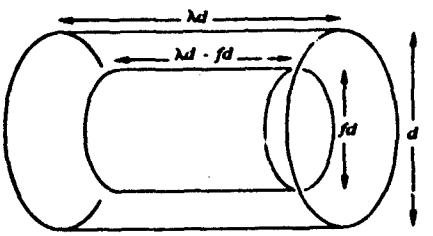

(a) Cylindrical grain.

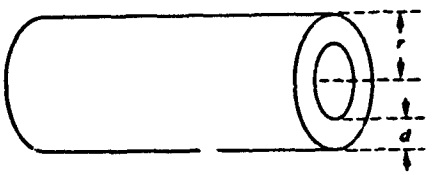

NOTE THAT d IS THE THICKNESS OF THE WALL.

(b) Tubular grain.

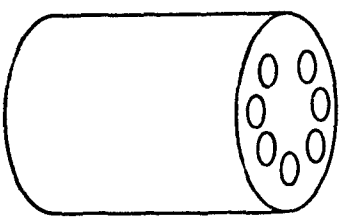

(c) Multitubular grain.

FIG. 6. Propellant Grains.

The dimensions of the cylinder are reduced by fd_g at a given time. Since

$$z = \frac{m_{g0} - m_0}{m_{g0}} = \frac{\tau_0 - \tau}{\tau_0}$$

and

$$\tau = \pi\lambda f^2 d_g^2 [d_g - (1 - f)d_g]$$

then

$$z = (1 - f)[1 + (1 + f/\lambda)f]$$

and

$$\theta = 1 + f/\lambda$$

and for $\lambda >> 1$

$$\theta = 1$$

The burning surface of powder with this shape decreases as burning proceeds, and the powder is called a *degressive powder*.

Tubular Grain

For a tubular grain (Fig. 6b) the same types of considerations yield the following equations for the initial and current volumes

$$\tau_0 = 2\pi d_g r l$$

$$\tau_0 = 2\pi d_g r \lambda d$$

and z becomes equal to

$$1 - f(\lambda - 1 + f)/\lambda$$

which is the same as

$$(1 - f)(1 + f/\lambda)$$

and

$$1 - f \text{ (if } \lambda >> 1 \text{ and } \theta = 0)$$

The burning surface of powder with this shape remains essentially constant as burning proceeds, and the powder is called a *neutral powder.*

Multitubular Grain

Another common grain configuration is a cylinder with multiple perforations (Fig. 6c). θ for a seven-perforation grain is estimated at -0.172. The burning surface continually increases as burning proceeds, and the powder is called a *progressive powder.*

Lagrange Correction

The pressure behind the projectile cannot be uniform since there is a positive velocity gradient from the breech to the base of the projectile; so the pressure gradient must be negative. The pressure at the base of the projectile is estimated by using a factor called a *Lagrange correction* for converting breech pressure to base pressure (Fig. 7). This correction is derived by assuming that pressure will drop in proportion to the momentum acquired by the propellant gases. Specifically it is assumed that

$$\frac{p_1}{p_0} = \frac{mv}{\left(m + \frac{C}{2}\right)v} \tag{1-21}$$

where $Cv/2$ is the momentum of the propellant gases estimated by using the same assumptions employed in estimating the energy of the gases in the discussion of the corrections to Resal's equation. Thus,

$$p_1 = \frac{p_0}{1 + \frac{C}{2m}} = \frac{p_0}{k_1} \tag{1-22}$$

where $k_1 = 1 + \frac{C}{2m}$

A mean value of pressure p is used in the internal energy term of Resal's equation. This is estimated by assuming that the ratio of the pressure at the base of the projectile to the mean pressure is equal to the ratio of the

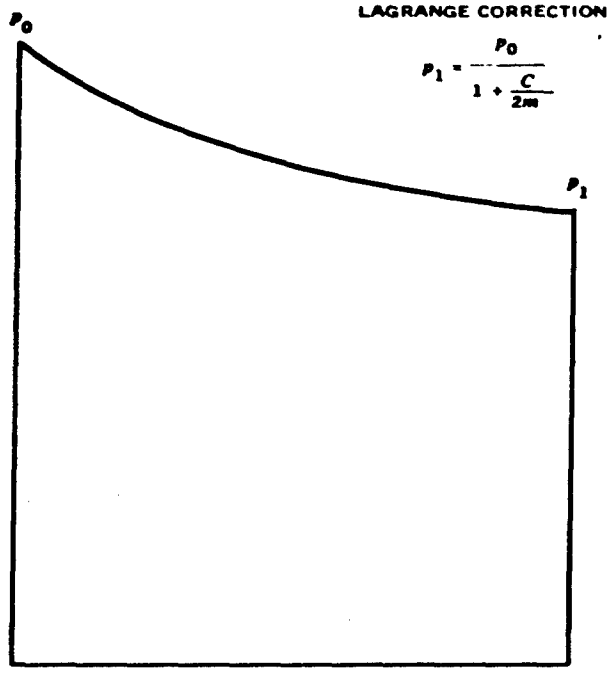

FIG. 7. Pressure Distribution Between Breech and Base of a Projectile.

projectile kinetic energy to the sum of the projectile and gas kinetic energies

$$\frac{p_1}{\bar{p}} = \frac{mv^2/2}{[m + (C/3)](v^2/2)} \tag{1-23}$$

so that $p = p_1 k_2$ where k_2 is defined by Eq. 1-16. Equation 1-5 is expressed in terms of the mean pressure as

$$Ap = k_2 m \frac{dv}{dt} \tag{1-24}$$

The pressure at the breech is found by using Eq. 1-22 and 1-23 to give

$p_0 = p(k_1/k_2)$, and the burning rate, Eq. 1-19, becomes

$$\sigma_g \frac{df}{dt} = -a\left(p\frac{k_1}{k_2}\right)^b \tag{1-25}$$

The equation of motion, the burning rate equations, Resal's equation, and the form function are mathematically sufficient information to determine the motion of the projectile and the pressures in the barrel for a given propellant and barrel dimensions. These equations are expressed in terms of the mean pressure p as follows:

$$Ap = k_2 m\frac{dv}{dt} \tag{1-24}$$

$$\frac{F_c Cz}{\gamma - 1} = \frac{p}{\gamma - 1} A(x + l_0) - Cz\left(b - \frac{1}{\rho_p}\right) + A\int_0^x p_1 dx \tag{1-14}$$

$$\sigma_g \frac{df}{dt} = -ap\left(\frac{k_1}{k_2}\right)^b \tag{1-25}$$

$$z = (1 - f)(1 + \theta f) \tag{1-20}$$

in which the constant k_1 equals $1 + C/2m$ (the correction for obtaining base pressure from breech pressure), the constant k_2 equals $1 + C/3m$ (the Lagrange correction for Resal's equation), and p is the mean pressure in the chamber.

These four equations are four separate and independent restrictions on changes in pressure, velocity, and fraction of the charge that is burned as the projectile moves down the barrel. The difficulties at this point are largely mathematical—the problem of extracting the required information in convenient form.

Two of these equations can be simplified to give (from Eq. 1-17 and 1-19)

$$F_c Cz = pA(x + l_0) \tag{1-17a}$$

in which kinetic energy is deleted, and

$$d_g \frac{df}{dt} = -ap \frac{k_1}{k_2} \tag{1-19a}$$

which is the linear form, $b = 1$. Equations 1-17a and 1-19a are reasonably accurate in the early stages of projectile acceleration and are easier to solve. Equations 1-24 and 1-19a are satisfied by

$$v = \frac{Ad_g(1 - f)}{ak_1 m} \tag{1-26}$$

Equations 1-26, 1-17, and 1-17a imply

$$\frac{dx}{df} = \frac{A^2 d_g^2 (x + l_0)}{a^2 m(1 + \theta f)} \tag{1-27}$$

which has the solution

$$x + l_0 = l_0 \left(\frac{1 + \theta}{1 + \theta f}\right)^{G/\theta} \qquad \theta \neq 0 \tag{1-28a}$$

and

$$x + l_0 = l_0 \exp\left[G(1 - f)\right] \qquad \theta = 0 \tag{1-28b}$$

where

$$G = \frac{A^2 d_g^2 k_2}{a^2 m k_1 \bar{C} F_c} \tag{1-29}$$

The pressure is also found as a function of f from the above equations for $x + l$ and from Eq. 1-17a

$$p = \frac{F_c C k_1 (1 - f)(1 + \theta f)}{A l_0 k_2} \left(\frac{1 + f}{1 + \theta}\right)^{G/\theta} \qquad \theta \neq 0 \tag{1-30a}$$

$$p = \frac{F_c C k_1 (1 - f) \exp\left|-G(1 - f)\right|}{A l_0 k_2} \qquad \theta = 0 \qquad (1\text{-}30b)$$

These equations are sufficient to calculate the pressure as a function of projectile displacement. In general the pressure peaks before the propellant is used up and the pressure curve has a rounded top, but this depends on the constants of the system, and the propellant may be used up on the ascending part of the curve (Fig. 8).

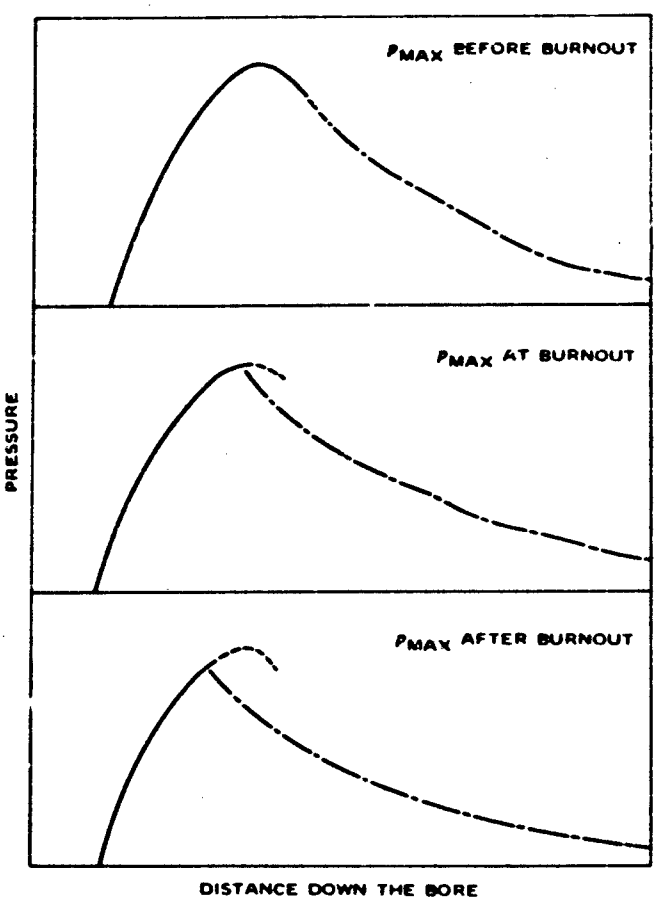

FIG. 8. Maximum Pressure Compared to Location of Burnout.

At $f = 0$ all of the propellant is burned, and the values of v, p, and x are

$$v_b = \frac{Ad_g}{ak_1 m} \tag{1-31}$$

$$p_b = \frac{F_c C k_1}{A k_2 (1 + \theta)^{G/n}} \qquad \theta \neq 0 \tag{1-32a}$$

$$p_b = \frac{F_c C k_1 \exp(G)}{A k_2} \qquad \theta = 0 \tag{1-32b}$$

$$x_b + l_0 = l_0 (1 + \theta)^{G/n} \qquad \theta \neq 0 \tag{1-33a}$$

$$x_b + l_0 = l_0 \exp(G) \qquad \theta = 0 \tag{1-33b}$$

PROJECTILE ACCELERATION AFTER BURNING

After burning is completed, z is equal to 1, and only two of the original four equations apply to the phenomena; thus for $z = 1$, Eq. 1-17 is

$$\frac{F_c C}{\gamma - 1} = \frac{pA(x + l_0)}{\gamma + 1} + \frac{k_2 m v^2}{2} \tag{1-34}$$

and using $dv/dt = v(dv/dx)$, Eq. 1-24 is

$$k_2 m v \frac{dv}{dx} = Ap \tag{1-35}$$

These equations can be solved by differentiating Eq. 1-34 and eliminating v from the result, using Eq. 1-35, so that

$$dp\, A(x + l_0) + pA\, dx + (\gamma - 1) k_2 m v\, dv = 0$$

$$dp\, A(x + l_0) + pA\, dx + (\gamma - 1) Ap\, dx = 0 \tag{1-36}$$

which has the solution

$$p = p_b\left(\frac{x + l_0}{x_b + l_0}\right)^{\gamma} \tag{1-37}$$

Resal's equation after burning is

$$\frac{F_c C}{\gamma - 1} = p_b A(x_b + l_0) + \frac{k_2 m v_b^2}{2} = pA(x + l_0)\frac{k_2 m v^2}{2} \tag{1-38}$$

This equation can be combined with the previous result for p_b and $x_b + l$ to determine v as a function of x and system parameters,

$$v^2 = v_b^2 + \frac{2F_c C}{mk_2(\gamma - 1)}\left[1 - \left(\frac{x + l_0}{x_b + l_0}\right)^{1-\gamma}\right] \tag{1-39}$$

From the definition of G and v_b

$$v_b^2 = \frac{GCF_c}{mk_2} \tag{1-40}$$

and

$$v^2 = \frac{F_c C}{mk_2}\left\{G + \frac{2}{\gamma - 1}\left[1 - \left(\frac{x + l_0}{x_b + l_0}\right)^{1-\gamma}\right]\right\} \tag{1-41}$$

The general shapes of pressure/distance curves for different types of powders are compared in Fig. 9. The advantages of a progressive powder are shown in this figure. For the limitation placed on the pressure/distance curve by the strength of the barrel, the progressive powder may give the greatest muzzle velocity. Small arms and cannon up to 20 mm usually use single-perforation grains, and all larger guns use multiperforated grains.

An example of a specific pressure/distance curve is shown in Fig. 10. Figure 11 compares a calculation of the pressure and velocity curves obtained for instantaneous burning with that for the same powder burned gradually.

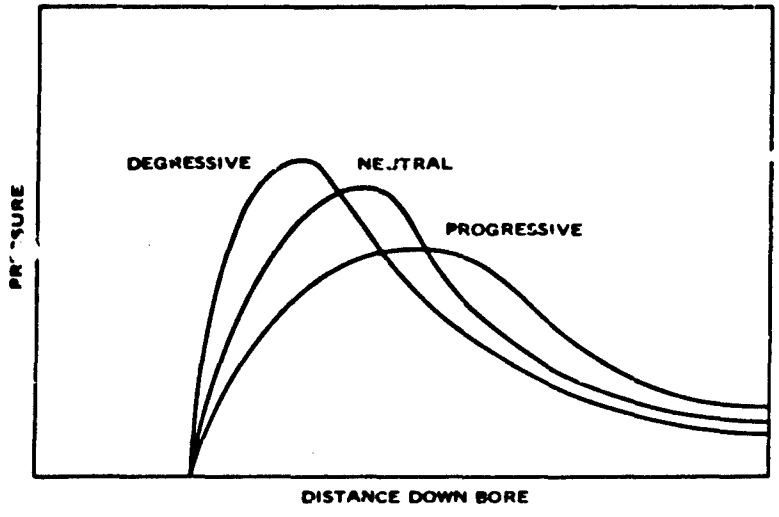

FIG. 9. Pressure/Distance Curves for Different Forms of Propellant.

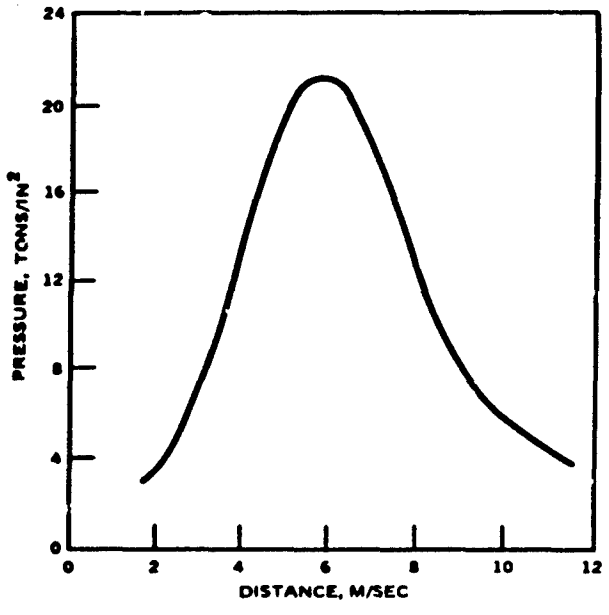

FIG. 10. Pressure/Distance Curve for a 3.7-Inch Antiaircraft Gun.

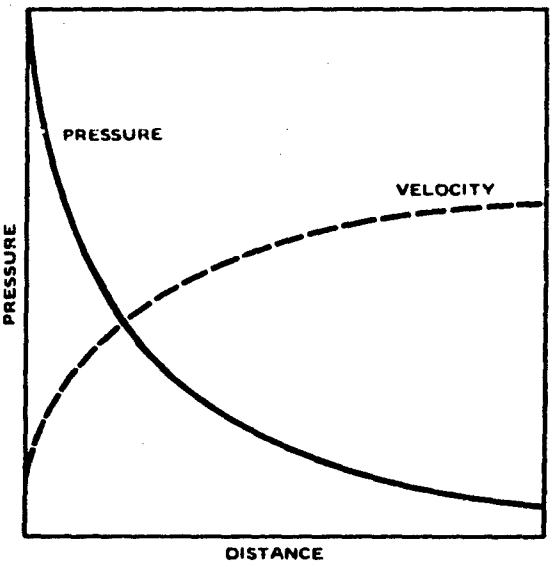

FIG. 11. Pressure/Distance Curve for Instantaneous Burning.

This comparison is interesting since the instantaneous burning is like the process of energy release in a warhead. It will be noted that the instantaneous burning gives the greater velocity (but at the price of very high pressures at the start of the process).

The velocity/distance curve for instantaneous burning (Ref. 5) is given by

$$v = v_{lim}\sqrt{1 - \left(\frac{x + l_0}{l_0}\right)^{1-\gamma}} \tag{1-42}$$

which is Eq. 39 with $v_b = 0$, $x_b = 0$ and

$$v_{lim} = \sqrt{\frac{2F_c C/(\gamma - 1)}{mk_2}} \tag{1-43}$$

Examples of muzzle velocities for several weapons are given below

Weapon	Muzzle velocity, ft/sec
240-mm howitzer M1	1,500 to 2,300
155-mm gun M1	2,745
105-mm howitzer M2	650
105-mm howitzer M2A1	1,235 to 1,550
75-mm gun M3	2,030

SUMMARY

A gun gives a projectile kinetic energy by the controlled burning of the propellant charge in the barrel of the gun. The pressure must always be less than a critical pressure for barrel failure. An objective of internal-ballistic design is to obtain maximum kinetic energy under the restriction on pressure. This objective can be achieved by an appropriate control of the pressure applied to the projectile as it travels along the barrel. Such control is feasible because propellant materials burn rapidly but at variable rates that depend on the pressure and temperature within the barrel. In order to exploit this control the equations of motion of the projectile, the equations of burning of the propellant, and the equations of the thermodynamics of the burning process are formulated and solved so as to relate parameters for the design of the gun, projectile, and propellant charge to the pressure behind the projectile and its velocity. These relationships then allow a choice of gun, projectile, and propellant design that gives maximum kinetic energy to the projectile but under safe barrel conditions.

2

The Exterior Ballistics of Projectiles

Exterior ballistics is concerned with the motion of the unconstrained projectile under the influence of gravitational, inertial, and aerodynamic forces that are experienced in free flight. The initial conditions for exterior ballistics are determined by the internal ballistic phase. Ideally this motion consists of the muzzle velocity of the projectile with all rigid body rotations zero except for the specified rotation rate of a spin-stabilized projectile. These ideal initial conditions are usually achieved to a high degree of precision, but slight-to-moderate departures have to be considered as causes of dispersion.

DYNAMICS OF A PROJECTILE IN FREE FLIGHT

At a given instant the projectile motion is described by the translational velocity v of the center of mass and rotations about the center of mass. For most of the following discussion it is assumed that the projectile does not spin. For simplicity, rotations are limited to yaw. In Fig. 12 an angular displacement, δ, called the yaw, and its rate, $\dot{\delta}$, are indicated in a reference frame that has x-direction parallel to the surface of the earth and y-direction normal to the earth and in the direction of the gravitational force. Two other rotations are possible, (1) spin and (2) pitch about a third axis.

The forces acting on the projectile are the inertial forces mdv/dt, gravitational forces mg, and the aerodynamic forces, the lift F_L and drag F_D. The inertial and gravitational forces are body forces that have their resultant

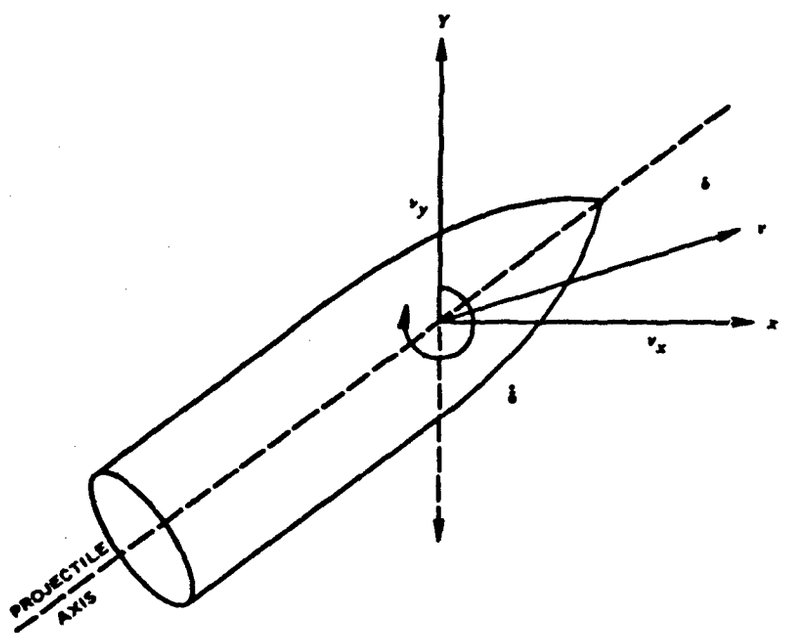

FIG. 12. Reference Frame for the Motion of a Projectile.

force at the center of mass of the projectile, the inertial force in the direction of motion and the gravitational force normal to the earth's surface. The aerodynamic forces are contact forces that have their resultant force at the center of lift. This force is resolved into a force at the center of mass and a torque that produces rotation about the center of mass. Figure 13 illustrates the relation between these various forces.

PROJECTILE TRAJECTORIES

Large-caliber guns have ranges that are large enough to make the inclusion of the curvature of the earth a part of the basic assumption. For intercontinental missiles the assumptions about the variation of gravity with distance that are used by the astronomers in orbit calculations should be

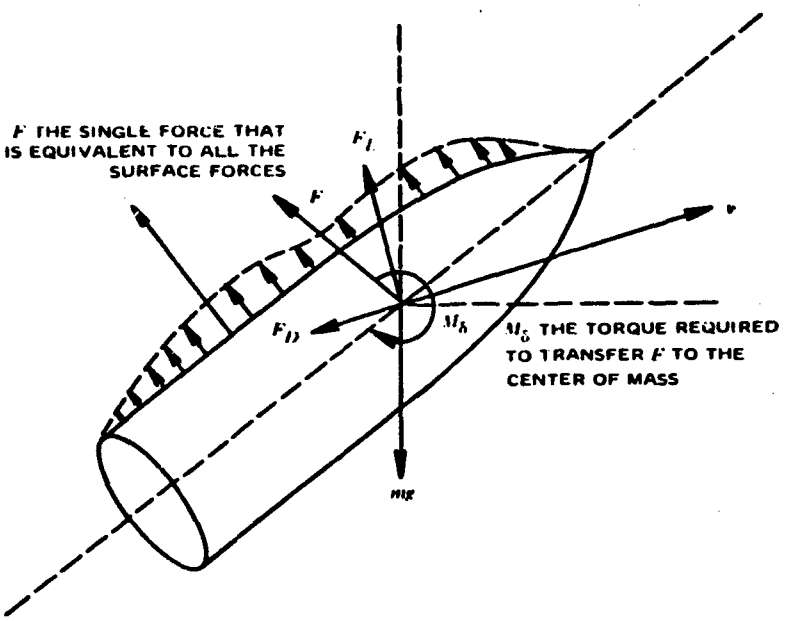

FIG. 13. Forces on a Projectile.

included. The exterior ballistics of most weapons, however, can be based on the assumption that gravity is constant and that the earth is flat.

Vacuum Trajectories

The basic equations for a ballistic trajectory in a vacuum and a gravitational field that is constant in magnitude and direction throughout the trajectory are the following:

$$m\frac{dx^2}{dt^2} = 0$$

$$m\frac{dy^2}{dt^2} = -mg$$

The initial conditions are

$$x = 0$$

$$y = y_0$$

$$v_x = \frac{dx}{dt} = v_0 \cos\theta$$

$$v_y = \frac{dy}{dt} = v_0 \sin\theta$$

The vertical and horizontal motions are given by the equations

$$x = v_0 \cos\theta t$$

and

$$y = v_0 \sin\theta t - \frac{gt^2}{2} + y_0$$

and the time required for the projectile to reach the height y_f is

$$t = \frac{v_0 \sin\theta \pm \sqrt{v_0^2 \sin^2\theta + 2g(y_f - y_0)}}{g} \tag{2-1}$$

The range of the projectile is

$$x_f = \frac{v_0 \cos\theta \left(v_0 \sin\theta + \sqrt{v_0^2 \sin^2\theta + 2g(y_f - y_0)}\right)}{g}$$

$$= \frac{v_0^2 \sin 2\theta}{g}\left(1 \pm \sqrt{1 + \frac{2g(y_f - y_0)}{v_0^2 \sin^2\theta}}\right) \tag{2-2}$$

Trajectories With Air Resistance

The foregoing calculation of trajectories neglects the effect of the atmosphere on the projectile. More accurate calculations include a resistance to the motion of the projectile that is along the instantaneous direction of motion. This resisting force is computed as

$$F_D = \frac{C_D \rho A v^2}{2} \tag{2-3}$$

where C_D is the drag coefficient, ρ is the density of the atmosphere, and A is the cross-sectional area of the projectile. The equations of motion are

$$m\frac{d^2x}{dt^2} = -F_d \cos\theta \tag{2-4}$$

and

$$m\frac{d^2y}{dt^2} = -F_d \sin\theta - mg \tag{2-5}$$

in which θ is the angle subtended between the tangent to the trajectory and the horizontal. These equations cannot be solved in terms of simple algebraic equations, but require either approximate solutions or solution by numerical methods.

AERODYNAMICS OF A PROJECTILE

The aerodynamic forces on a projectile are due to the action of the surrounding atmosphere as it is set in motion. The fluid exerts forces on the projectile through frictional and fluid dynamic effects. It is convenient to describe the motion of the atmosphere and projectile such that the projectile is at rest and the fluid flows over it. A small element of the atmosphere might flow over the projectile as is shown in Fig. 14. The rate of flow depends on the velocity of the projectile, but since the projectile does not slow down

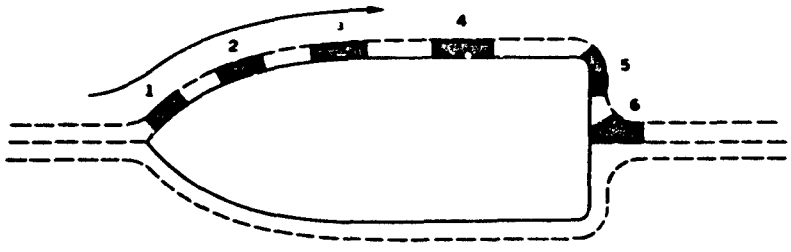

FIG. 14. Flow of Fluid Over a Projectile.

rapidly, the flow is approximately steady. This means that although an element of the volume of the atmosphere will change velocity as it goes from position 1 to position 6, all elements follow the same path and go through the same changes of velocity. Thus, the velocity of the element of atmosphere at a given position on the projectile is always the same, and distribution of velocity is constant. The total force exerted on the projectile by all such elements makes up the net aerodynamic force.

Steady Flow

Steady flow means that the paths of fluid elements through any point do not change with time. Such paths are called streamlines. The shape of a streamline is fixed, but the velocity of an element as it traverses the streamline will vary. The points at which the velocity is zero, called *stagnation points*, are of particular interest. In general, the velocity can be expressed as a function of the time and the distance along the streamline, $v = v(s, t)$.

The dynamics of a fluid element can be analyzed by considering the dynamic equilibrium of the forces on it. The equilibrium is between the contact forces due to the hydrostatic pressure and viscosity of the atmosphere and the body forces due to inertia and gravitation. A fluid has a hydrostatic pressure at any point, i.e., it exerts a force per unit area normal to any given surface so that the total normal force on a plane surface is

$$F_p = \int_{(A)} p \, dA$$

The hydrostatic pressure pushes in on all surfaces of the element of volume,

and if the pressure is uniform, there is no net force on the element. The pressure may vary from point to point and then a net force can develop due to the difference in the pressures on opposite sides of the element. The element accelerates along the streamline so that the force due to hydrostatic pressure will come from the difference in pressure on the forward and rear surfaces of the element:

$$F_p = \left(p + \frac{dp}{ds}\,ds \quad p\right)dA = \frac{dp}{ds}\,dA\,ds \tag{2-6}$$

The inertial force is

$$F_i = m\frac{dv}{dt}$$

and since $v = v(s, t)$

$$\frac{dv}{dt} = \frac{\partial v}{\partial t} + \frac{\partial v}{\partial s}\frac{\partial s}{\partial t} = \frac{\partial v}{\partial t} + \frac{\partial v}{\partial s}v$$

Since the motion is steady, $\partial v/\partial t = 0$ so that

$$F_i = mv\frac{\partial v}{\partial s} \tag{2-7}$$

The force due to gravity in this direction is

$$F_g = \rho d\tau g \cos\theta$$

$$= \rho d\tau g\frac{dy}{ds} \tag{2-8}$$

The equilibrium of forces is

$$F_i = F_p + F_g$$

which, from Eq. 2-6, 2-7, and 2-8, is

$$\rho v\frac{\partial v}{\partial s} = -\frac{dp}{ds} - \rho g\frac{dy}{ds}$$

which can be integrated to give

$$\rho v^2/2 + p + \rho g y = \text{constant} \tag{2-9}$$

thus the hydrostatic pressure is related to the flow rate and the height. The equation is called Bernoulli's equation and has wide applicability to steady-state fluid dynamic problems. The aerodynamic forces on a projectile are important in regions of flow in which the gravitational effect is insignificant so that

$$v^2/2 + p/\rho = \text{constant} \tag{2-10}$$

is sufficient to relate flow rate and pressure.

In Fig. 15 there is a stagnation point at zero, and since v is zero, the pressure has a maximum value that is equal to the constant for that streamline. At a large distance the velocity has its maximum value equal to the projectile velocity and the pressure is a minimum, the atmospheric pressure for undisturbed conditions. The theory of incompressible flow has been developed to determine the properties of steamlines from the contour of

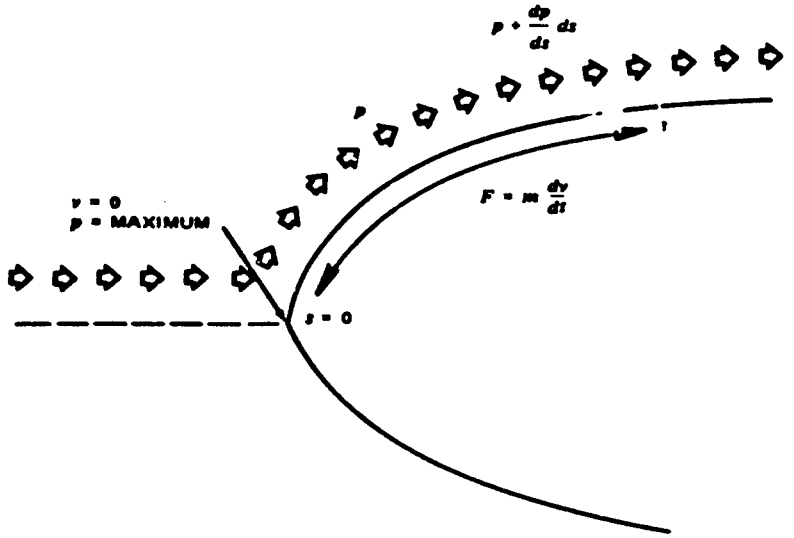

FIG. 15. Forces on a Fluid Element.

the objects over which flow occurs and from these properties to determine the pressures and velocities at all points.

The net fluid dynamic force turns out to be *zero* for flow that follows the contour of the projectile without regard to friction along the projectile surface or within the fluid as viscosity. The friction between the projectile and the fluid causes the fluid to slow down at the projectile surface, shears develop in a thin layer, and there is a shearing traction exerted on the projectile. The net force on the projectile is still not enough to account for the fluid dynamic forces that are known to exist.

Effect of Viscosity

Fluid dynamic theory that includes viscosity of the fluid allows the possibility that there will develop layers of intense shearing that are capable of changing the character of the flow. For a projectile the shearing begins on the ogival surface but separates from the projectile behind it and has the net effect of setting up a low-pressure region behind the projectile. This is illustrated in Fig. 16. For a more complete treatment of fluid dynamics, see Ref. 6.

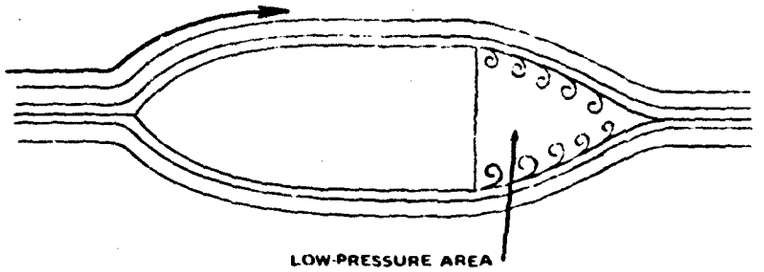

FIG. 16. Flow With a Detached Boundary Layer.

Lift, Drag, and Yawing Moments

A quasi-empirical method of representing the forces recognizes the dynamic pressure $\rho v^2/2$ as the dominant factor in the relation of the forces to projectile motion. The aerodynamic forces are most conveniently expressed as lift and drag forces acting at the center of mass in the direction normal to the

projectile motion and parallel to it and a torque that acts about the center of mass (Ref. 7 and 8). These are lift

$$F_L = \frac{C_L \rho A v^2}{2} \tag{2-11}$$

drag

$$F_D = \frac{C_D \rho A v^2}{2} \tag{2-12}$$

and yawing moment

$$M_\delta = \frac{C_M \rho A l v^2}{2} \tag{2-13}$$

where l is the distance from the center of pressure to the center of mass.

The dimensionless coefficients C_D, C_L, and C_M correct the dynamic pressure $\rho v^2/2$ for the effects of the shape and orientation of the projectile and the Mach number of the flow. The coefficients C_l and C_m can be defined to express the approximately linear dependence on yaw at small yaw angles

$$C_M = C_m \delta \tag{2-14}$$

and

$$C_L = C_l \delta \tag{2-15}$$

The restoring torque tends to induce angular accelerations about the yaw axis according to the relation

$$m R_I^2 \frac{d^2\delta}{dt^2} = \frac{A C_m \rho v^2 \delta l}{2} \tag{2-16}$$

where R_I is the radius of gyration of the projectile about the yaw axis. If the center of mass of the projectile is ahead of the center of pressure, then the

moment tends to oppose the existing yaw δ, the right side of the equation is negative, and the equation has the solution

$$\delta = \delta_1 \cos\left(\frac{2\nu}{\sigma} t + \epsilon\right) \tag{2-17}$$

in which δ_1 and ϵ are constants of integration that depend upon the initial yaw and yaw rates and

$$\sigma = 2\pi\sqrt{\frac{2mR_I^2}{\rho AlC_m}} \tag{2-18}$$

The quantity σ turns out to be the distance of projectile travel for one cycle of oscillation. Figure 17 represents a trajectory with a yaw oscillation. The net lift for such an oscillating projectile is zero, and the aerodynamic effects on the trajectory depend only on the drag.

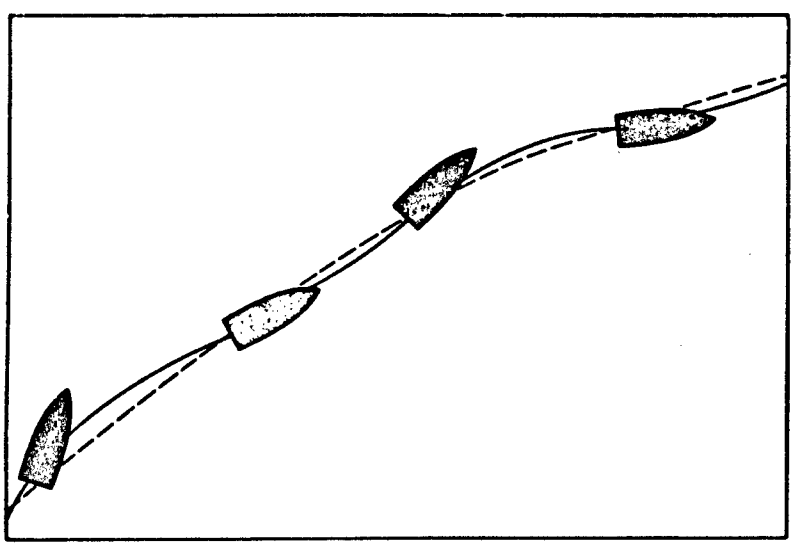

FIG. 17. Section of a Trajectory With Yaw Oscillations.

Causes of Drag

The foregoing shows that for stable behavior of projectiles the most important part of the aerodynamic forces is the drag.

There are three contributions to the total drag: skin friction, base drag, and wave drag (Ref. 9 and 10). Each of these contributes to the drag force through different processes and depends on different aspects of projectile configuration. The skin friction is the effect of the interaction between the flowing gases and the surface of the projectile. This contribution to the total drag depends on the shape of the projectile and in particular on the area of the base of the projectile, which should be small for the least drag. Wave drag is the effect of the compression and expansion of the air as it flows over the body. This contribution to the total drag depends on projectile shape and is least for slender bodies, i.e., it decreases for an increase in the ratio of length to diameter. This contribution to drag is only important as the Mach number increases, and at subsonic speeds it is negligible. Wave drag is defined with reference to the cross-sectional area.

The total drag coefficient is defined with reference to the cross-sectional area; hence, it is related to skin friction and base and wave components as

$$C_D = \underset{\text{(wave drag)}}{C_{Dw}} + \underset{\text{(skin friction)}}{\frac{C_{Df} A_s}{A}} + \underset{\text{(base drag)}}{C_{Db} \frac{A_b}{A}}$$

when A_s equals the wetted area of the body, A_b equals the effective area of the base, and A equals the cross-sectional area of the body.

To determine the values of the drag coefficient experimentally, accurate measurements are made over short distances that are known accurately and over which the effect of gravity is negligible and atmospheric effects are constant. A factor K can be defined

$$K = \frac{AC_D}{2m} \tag{2-19}$$

then the equation of motion, neglecting gravitational effects, is

$$\frac{dv}{dt} = -Kv^2$$

the first integral with respect to time is

$$v = \frac{v_0}{1 + v_0 K t} \tag{2-20}$$

and the second integral is

$$s = \frac{1}{K} \ln(v_0 K t + 1) \tag{2-21}$$

where s is the distance over which the measurement has been made. The distance s and the transit time t determine an average velocity $\bar{v}$. The average velocity can be used in the above equation to eliminate the dependence on t and yield an equation in $\bar{v}$ and s:

$$\bar{v} = \frac{Ks}{\exp(Ks) - 1} v_0 \tag{2-22a}$$

This equation can be used to determine the value of K if v_0 is known (from measurements directly at the muzzle, for example), or the value of v_0 can be obtained if a value of K is known.

The equation of motion can be transformed by using the relation

$$\frac{dv}{dt} = \frac{dv}{ds}\frac{ds}{dt} = v\frac{dv}{ds}$$

so that

$$v\frac{dv}{ds} = -Kv^2$$

and this has the solution

$$v = v_0 \exp(-Ks) \tag{2-22b}$$

If the velocity can be obtained at two points along the path, the value of K is given by

$$K = \frac{\ln(v_1/v_2)}{s} \tag{2-23}$$

The drag coefficient is a function of Mach number M, i.e., the projectile velocity divided by the speed of sound for ambient conditions

$$M = v/c$$

Figures 18 and 19 present the variation of drag coefficient for several projectile shapes.

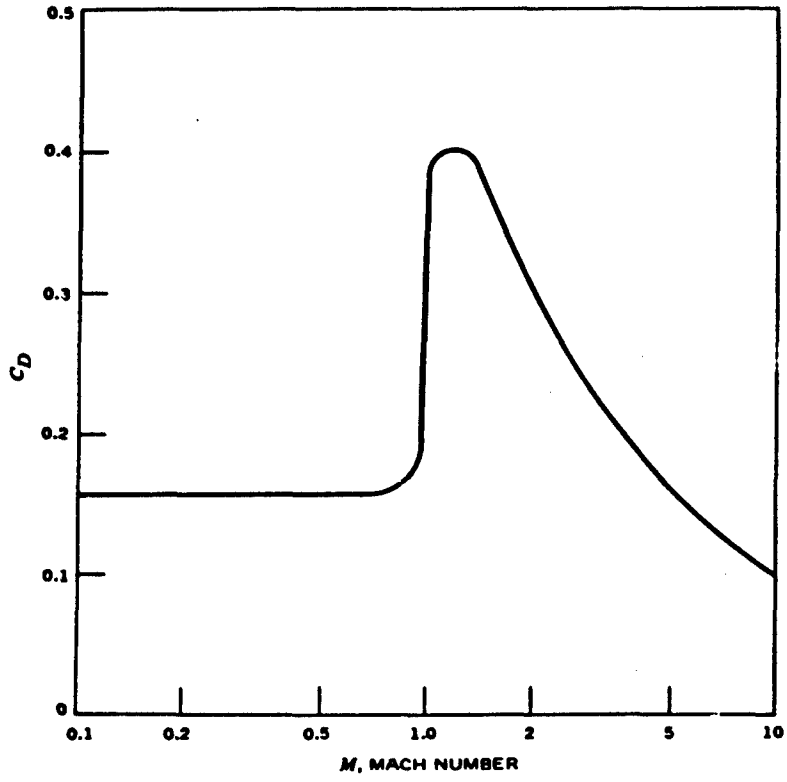

FIG. 18. Drag Coefficient as a Function of Mach Number Typical of Common Projectile Shapes.

3

The Terminal Ballistics of Projectiles

Terminal ballistics is that part of the science of ballistics that relates to the interaction between a projectile and target. The target could be a tank, truck, command post, aircraft, missile, ship, etc., so that the possible interactions could depend on a myriad of structural details. Fortunately, terminal ballistics is simplified by the common observation that a projectile traveling at ordnance velocities produces the hole through which the projectile passes and extremely localized material failure immediately adjacent to the hole. The only relevant properties of the target are those along the path of the projectile and a few projectile diameters to the side. Thus, the overall interaction of a projectile with a complex target is simplified to the impact of the projectile with an array of barriers. The way these barriers are interconnected and supported is not very important.

EXAMPLES OF TARGETS

A simple example of a target is a building that stores munitions (Ref. 11). The building is usually a reinforced concrete structure with soil pushed up against its walls. The concrete and soil barriers protect the vulnerable munitions that are stored inside. The thicknesses and obliquities that are presented to a projectile depend on the trajectory of the projectile. If the projectile still has velocity after perforating the barriers, it may either cause mechanical damage or detonate the munitions.

A tank is a much more sophisticated target. Its military value lies in its

mobile firepower. Anything that decreases its mobility or impairs its firepower destroys its military value. The components of greatest value are the ammunition, engine parts, personnel, fuel, and the guns and fire-control system. These are protected by the armor plate of the turret, sides, and bottom of the vehicle (Fig. 20). The terminal interaction of a projectile with this target is a series of perforations through these barriers that impacts against vulnerable components. The weight that a tank designer can allot to armor is limited by the power of the engine, and therefore the armor material has to be very tough.

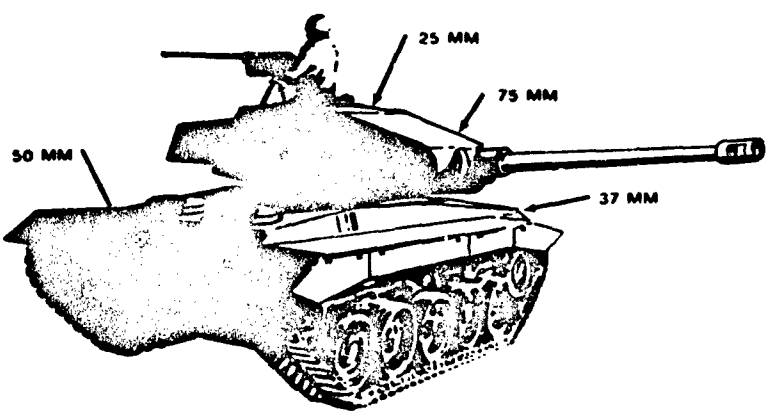

FIG. 20. Distribution of Armor Thicknesses, Typical World War II Tank.

An aircraft is still another target that derives its military value from its mobility and firepower. The vulnerable components of an aircraft are comparable to those of the tank. Weight limitations on aircraft prevent the use of thick protective barriers. In fact, there are few protective barriers as such, but the structural elements that comprise the airframe must also serve as protective barriers.

These and many other examples show that the terminal ballistics of a projectile can almost always be viewed as one or more interactions with barriers that serve to deny the projectile access to vulnerable components at velocities that could destroy the vulnerable components. A barrier succeeds by (1) simply decelerating the projectile, (2) breaking the projectile into fragments and decelerating the fragments, or (3) deforming the projectile and decelerating the projectile in its less efficient shape. This discussion of inert projectiles will be primarily concerned with the first of these. It is assumed

that the projectile is properly designed so that the barrier decelerates the projectile but never succeeds in resisting the projectile with sufficient force to cause it to shatter or deform. This is actually the assumption of a majority of the theories of armor penetration. It is at least approximately correct for many real situations and vastly simplifies analysis.

EXAMPLES OF PROJECTILES

Figure 21 shows different types of projectiles and the features of

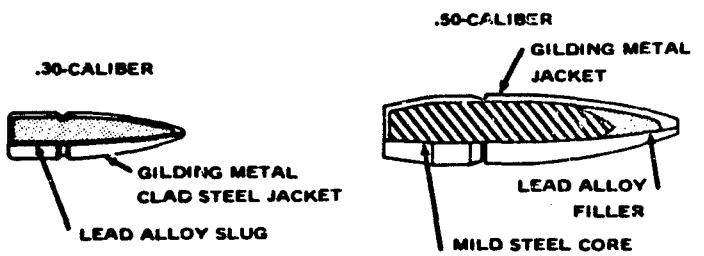

(a) Bullets (ball).

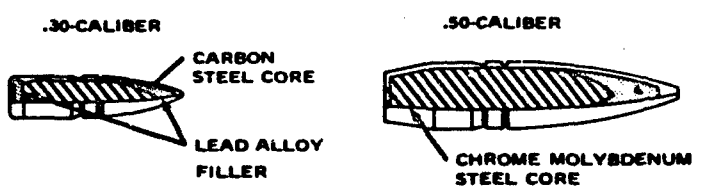

(b) Bullets (armor-piercing).

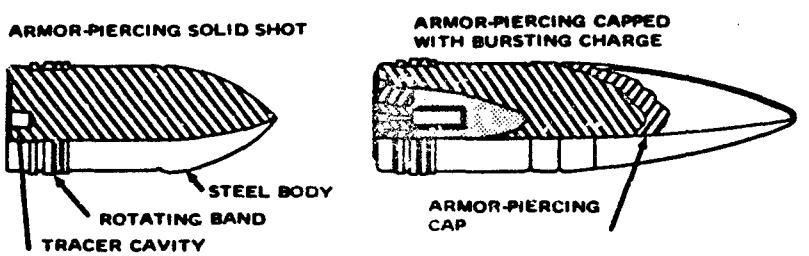

(c) Projectiles.

FIG. 21. Examples of Nondeforming Projectiles.

internal design that are used to make the projectile nondeforming during impact. Figure 21a shows the cross sections of .30- and .50-caliber bullets that are intended to attack lightly protected personnel and equipment. These consist of a lead alloy or mild steel core and a jacket. These will be nondeforming only in the attack of light armor and extended barriers that are not very resistant to penetration. Figure 21b shows bullets of the same calibers that are intended to attack armor. The cores of these armor-piercing bullets are hard, tough steels or a material like tungsten carbide. The nose shape of the core is chosen to attain reasonable performance at obliquities. The jacket includes a windshield that gives the bullet optimum aerodynamic properties. As long as the core material has an advantage in hardness over the barrier material, the projectile will be essentially nondeforming. Figure 21c shows larger-caliber projectiles, one that is solid steel, and one that has a cap on the nose of the core to assist in armor penetration.

PENETRATION RESISTANCE OF VARIOUS MATERIALS

The deceleration of a nondeforming projectile is given by the ratio of the total force on the projectile to the mass of the projectile. A convenient form for the specification of the total force on the projectile is a correlation of total force to the distance traveled into the barrier. The area under the curve that represents this correlation is the amount of kinetic energy that the projectile has lost in traveling the given distance. The details of the force/distance curve depend on the mechanism of failure and flow in the specific material. Different materials can be compared by their force/distance curves for identical kinetic energy dissipation. Two important measurements of such curves are the *peak force* and the *total distance* covered. Figure 22 is an example of the comparison of three different materials penetrated by a single type of projectile. These are more or less typical of the curves for soils, masonry, and metals.

The peak forces for penetration into many soils are comparatively low. Loosely packed sands and wet clays typically offer low resistance to projectile penetration. The resistance to penetration correlates most conspicuously with porosity, moisture content, and macrostructure. These physical parameters vary considerably, depending on the makeup of the soil and its history. A highly compacted soil may offer resistance comparable to that for some types of rock, but under favorable conditions soils will offer the least resistance of

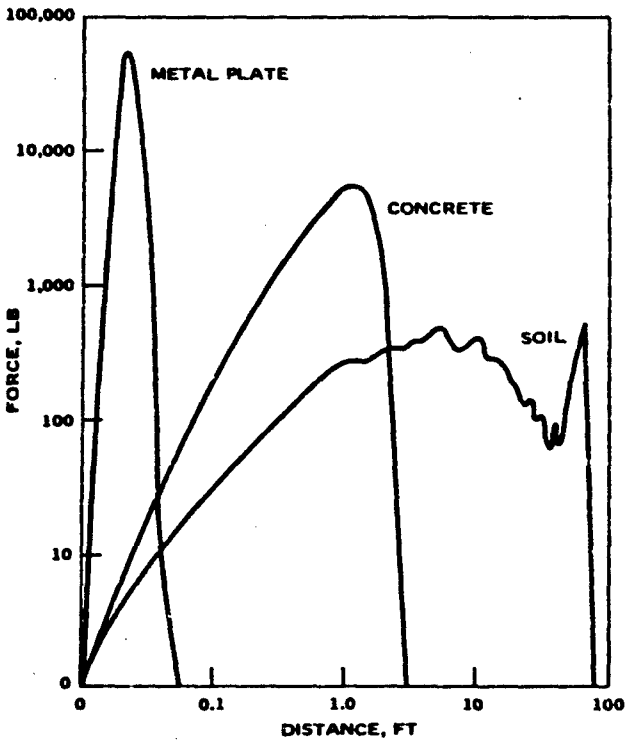

FIG. 22. Force/Distance Curves for Metal Plate, Concrete, and Soil.

any of the commonly encountered barriers. For the soil to have a specified energy dissipation, the total distance over which the force acts must be large.

Masonry and concrete barriers have a penetration resistance that is intermediate between soil breastworks and armors or very hard rock. In general these barriers may be thought of as an array of high-strength elements held together by a lower-strength binder to make up a composite material. The passage of the projectile through the material depends on the operation of brittle failure of the rock and binder and the flow of the pulverized debris.

Metals have still higher penetration resistance but are almost always used in comparatively small thicknesses. The failure and flow mechanisms for metals have been investigated extensively and are significantly different from the processes in soils and concrete. The one property that is in the sharpest contrast to rock, masonry, and concrete is ductility, the tendency of a metal

to undergo large, permanent deformation before breaking. This is a common property of structural metals, and the continuous permanent deformation accounts for a major part of the energy of deformation.

PENETRATION INTO SOILS

Soils offer comparatively low resistance per unit distance of penetration and are usually encountered in large thicknesses. Figure 23 is an example of fortifications in which structures of concrete and steel are given extra protection by a covering of soil. Projectiles must penetrate the covering to attack the structure. The required terminal ballistic information is the penetration of a given thickness of a reasonably homogeneous soil. Explosive projectiles can damage the structure by a remote detonation, but the efficiency of transmission of explosive blast effects depends on the depth of penetration. The desired information in this case is the trajectory of the projectile into natural soil either to the point of complete deceleration or at a time established by preset fuzing. Thus, the central problem of the terminal ballistics of projectiles in soil barriers is to determine penetration as a function of projectile and barrier parameters.

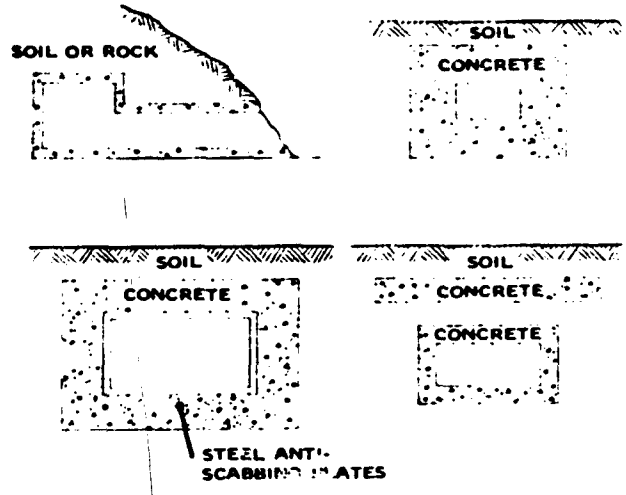

FIG. 23. Elevation Views of Bomb-Resistant Structures.

Stable Trajectories

Soils such as wet sands and clays are low-resistance materials that require several projectile lengths of travel to have significant effect. Major sections of the trajectories are uninfluenced by boundaries, so that the terminal interaction is primarily a steady interaction between the projectile and the low-resistance material. This interaction has many similarities to air resistance in exterior ballistics except that the forces are much larger. The method of exterior ballistics can be applied in which the surface forces are resolved into the drag force, lift force, and restoring moments, and these forces and moments are defined in terms of their coefficients if the correlation of surface forces to projectile motion is known at least by empirical observation.

Trajectories of missiles, shells, and bombs in soils are not usually stable. Projectiles tumble on entry, or the trajectories have large curvatures. Unstable trajectories are too complex to allow the correlation, and therefore it is most convenient to start with the available information on stable motions of projectiles.

Stability can be achieved consistently if the center of mass of the projectile is moved as far forward on the projectile as possible and the projectile has a length that is from 10 to 20 times its diameter. This conclusion has been carefully established for the penetration of small projectiles into dry sand (Ref. 12 and 13) and less conclusively for large projectiles penetrating a wide range of soils.

If we assume that the motion is stable and also *without yaw*, then the deceleration is expressed in exterior ballistics as

$$m\frac{dv}{dt} = \frac{C_D \rho v^2 A}{2} \tag{3-1}$$

This should be a useful form in terminal ballistics if the dynamic pressure $\rho v^2/2$ is the principal factor in the resistance of the medium, and it would be most useful if the correlation of drag to dynamic pressure is *approximately constant* as it is for much exterior ballistics. Much data supports the idea that the dynamic pressure is a major factor in soil penetration, but the proportionality is definitely not linear in the range of velocities of interest.

Constant C_D is unrealistic because it requires an exponential decrease in the velocity of the projectile (as was indicated in the discussion of exterior

ballistics, Eq. 2-22b) and this means that the projectile never comes to rest. Other mathematical expressions for the dependence of drag force on velocity have been tried that successfully predict deceleration in a finite time and also match experimental penetration measurements with reasonable accuracy. Two of these are (1) $F_D = (c_1 + c_2 v + c_3 v^2)A$ and (2) $F_D = (c_1 + c_3 v^2)A$ where A is the cross-sectional area of the projectile. The first is a general representation of the drag as a quadratic function of the velocity. The second is a particular case but is singled out because of its historical prominence and prevalent use. This second form of the resistance force when equated to the deceleration of the projectile gives Poncelet's equation

$$m \frac{dv}{dt} = (c_1 + c_3 v^2)A \tag{3-2}$$

Poncelet's equation has been successfully applied to soils, masonry, and armor in the sense that empirical constants c_1 and c_3 can be determined for a given combination of projectile and barrier so that then Poncelet's equation determines projectile velocities and trajectories with reasonable accuracy. This success appears to be due to the common feature among these barriers that at higher velocities the resistance depends most strongly on the dynamic pressure, whereas at lower velocities effects that are less velocity-dependent—such as the residual strength of the barrier—are dominant.

The Poncelet form for the resisting force can be given as an equivalent drag coefficient that has an explicit velocity dependence,

$$C_D = C_{\text{lim}} + \frac{C_0}{v^2} \tag{3-3}$$

This procedure has been suggested in Ref. 12 and 13 in the discussion of penetration into sand. They report a change in the dependence of the drag on velocity at a critical velocity, and this effect justifies the drag coefficient form of the resisting force, especially since the drag coefficient is constant above the critical velocity. It is largely a matter of convenience whether a specific analytical form or the equivalent drag coefficient is used. In the following discussion both are used since much of the work on penetration into soils has been in terms of resisting forces of the Poncelet type, but it sometimes is desirable to interpret these data and theories in terms of the lift, drag, and restoring moment resolution of surface forces.

The equation for the penetration of a stable projectile as a function of velocity under the Poncelet assumptions is obtained by integrating

$$m \frac{dv}{ds} v = A(c_1 + c_3 v^2)$$

and is

$$s = \frac{m}{2c_3 A} \ln\left(\frac{c_1 + c_3 v_0^2}{c_1 + c_3 v^2}\right) \tag{3-4}$$

where s is the distance along a linear trajectory. The columns at the right of Table 6 give values of Poncelet's constants for the tabulated soils and "bomb-shaped" projectiles. The velocity after passing through a barrier of thickness h is

$$v^2 = v_0^2 \exp(-2c_3 Ah/m) + \frac{c_1}{c_3} \exp(-2c_3 Ah/m) - 1 \tag{3-5}$$

If the maximum penetration is required, then $v = 0$ and

$$P = \frac{m}{2c_3 A} \ln\left(\frac{c_1 + c_3 v_0^2}{c_1}\right) = \frac{m}{2c_3 A} \ln\left(1 + \frac{c_3 v_0^2}{c_1}\right) \tag{3-6}$$

In large-scale testing of projectiles it is sometimes only feasible to measure the total penetration, but the main interest in analytical predictions is in the maximum penetration (Ref. 14 and 15). Empirical equations have been derived that relate the maximum penetration to the impact velocity. These equations have the general form of the Poncelet penetration equation, but the constants do not have the Poncelet interpretation. Two equations that are widely used are the Petry equation:

$$P = \frac{W}{A} K \log_{10}\left(1 + \frac{v^2}{215{,}000}\right) \tag{3-7}$$

TABLE 6. Penetration Resistance Constants for Three Soils.

Soils	S/N for long slender weapons	K for Petry equation	Density, g/cm^3	Historical values		General trafficability estimate
				lb/in^2	lb/ft^3	
1. Soft:						Too soft for ordinary wheeled vehicles
Partially saturated clays	...	12-20	1.6-2.0			
Wet tide flat muds	40	55	1.1-1.5			
Soft wet clays	50	...	1.5-2.0			
Typical soft soil (sand, 30%; silt, 30%; clay, 40%)				160	79	
2. Medium:						Passable for wheeled vehicle with varying degrees of difficulty
Loose, moist sand	6.5	5.1-7.1	1.6			
Loess (loam)	...	...				
Loose, dry, sandy alluvium	...	...				
Moist, sandy, silty clay	...	...				
Typical loam (sand, 50%; silt, 35%; clay, 15%)				350	92	
3. Hard:						Passable for all wheeled vehicles
Dry, silty sand	2.5	2.5-2.8	2.7			
Frozen clayey silt	3.8	3.0-3.3	...			
Glacier ice	4.2	4	1.0			
Hard, dense, clayey silt	5.2	...	2.6			
Typical sand (sand, 95%; silt, 5%)				750	110	

and the Sandia equations:

$$P = 0.53\,SN\left(\frac{W}{A}\right)^{1/2} \ln(1 + 2v^2\,10^{-5}) \qquad v < 200 \text{ ft/sec} \qquad (3\text{-}8)$$

$$P = 0.0031\,SN\left(\frac{W}{A}\right)^{1/2} (v - 100) \qquad v \geq 200 \text{ ft/sec}$$

where SN is an empirical constant.

It is also desirable to have the dependence of penetration on time, and this can be obtained by integrating the equation of motion in the form

$$m\frac{dv}{dt} = A(c_1 + c_3v^2)$$

The derivation is straightforward, and the final result is

$$s = \frac{m}{2c_3A}\ln\frac{\cos\left(\tan^{-1}\sqrt{\frac{c_3}{c_1}}v_0\right) - \sqrt{c_3c_1/m}\,At}{\cos\left(\tan^{-1}\sqrt{\frac{c_3}{c_1}}v_0\right)} \tag{3-9}$$

This equation gives the instantaneous penetration for a projectile at a specified time; for example, the preset time for a fuze.

An example of a practical application is the estimation of the energy degradation brought about by a given thickness of barrier of a specified material. Velocities as a function of distance are plotted in Fig. 24 for two sample soils of Table 6. The constants used in the equations might come from

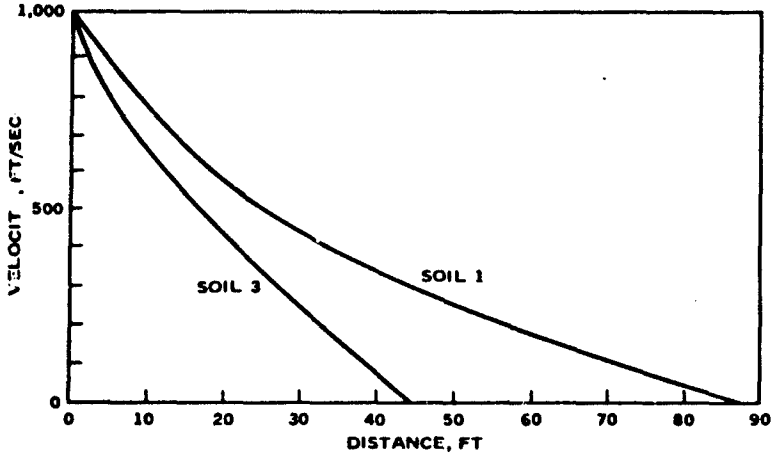

FIG. 24. Calculations of Velocity as a Function of Distance for the Poncelet Form of Resistance to Projectile Motion.

values determined from previous firing programs (the constants of Table 6, for example), or from a firing program set up to obtain the required data. The constants would certainly be dependable if the projectiles were identical to those of primary interest. It may happen that the projectiles used in previous work or in future work are of a different size but the same shape. The question then arises, "Do the same constants apply if the shape is the same but the dimensions are different?"

This is a question that is important in the interpretation of the meaning of the constants in expressions for the resisting force. A definitive answer to the question is not available because of the difficulties in doing large-scale testing and the complexities caused by the instability of terminal trajectories. Work has been done (Ref. 15) that has led to some useful conclusions about scaling. If the projectiles have a length-to-diameter ratio that is between 10 and 20, thus assuring stability, and if the diameter is between 3 and 18 inches, then a single set of constants used in the Sandia equations will give reasonably accurate estimates of the penetration performance of the projectile in the specified barrier. Below the 3-inch diameter the scaling of the constants depends on the soil. Above the 18-inch diameter there have not been sufficient data collected to justify a firm conclusion. A possible explanation for the dependence of scaling on the type of soil is the granular texture of soils, so that there is a characteristic particle size for the soil. This parameter is most significant for the dynamics of the interaction of small projectiles with the granular component of the medium.

Assuming that the Sandia empirical equations are basically representations of the Poncelet equations but in more convenient analytical form, then the scaling relationship of the Sandia equations implies that c_1 and c_3 scale by the same factor so that there is no resultant scaling for the combined constant c_3/c_1 in the argument of the natural logarithm function. The scaling of penetration is due to the scaling of the factor c_3 alone since this parameter appears in the multiplier $m/2Ac_3$. True dimensionless constants c_1' and c_3' can be written

$$c_3 = \sqrt{\frac{m}{A}}\, c_3', \quad c_1 = \sqrt{\frac{m}{A}}\, c_1' \tag{3-10}$$

There are some aspects of the interaction of a soil to projectile penetration that appear to be significantly different from the interaction of a projectile with the atmosphere. The diameters of penetration craters are

readily observed, at least at the surface, and some general conclusions can be reached on the basis of such observations. The diameters in dry hard soils are close to the diameter of the projectile, but the diameters in soft wet sands and clays may be considerably larger than the projectile diameter. Apparently the inertia and cohesiveness of these soils cause radial flow that continues after the passage of the projectile. Thus it is incorrect to think of the projectile as completely in contact with the soil.

Tests have been conducted in which projectiles were instrumented with accelerometers and transmitters for telemetering the data to a remote recorder. The accelerometer records indicate that early decelerations are low, but that at the end of the penetration there are sudden increases. The low values in the early part of the records have been interpreted to be the result of the radial flows which produce a limited contact with the projectile in the early phase of interaction, but when the projectile is slowed down, contact with the projectile is greatly increased. A sample record shown in Fig. 25 is that of the deceleration of a 1,160-pound projectile 9 inches in diameter penetrating a sandy soil. The abrupt increase in the decelerations at low velocities is evident in this record. The record is complicated by the structure of the soil. It is not a homogeneous medium, but consists of layers put down by geologic processes that led to variations in the layers with depth.

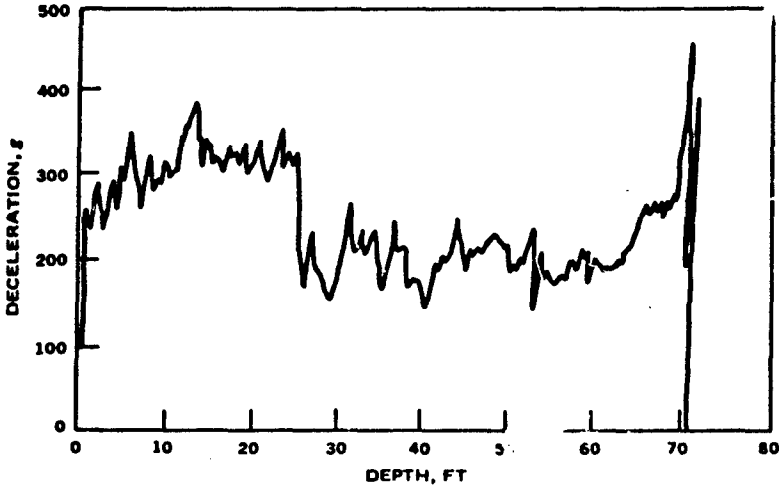

FIG. 25. Deceleration Record for Penetration of a Pointed Projectile Into Sandy Soil.

The idea that the flow of a soil may result in limited contact surface between the projectile and the soil is not a new discovery, and these accelerometer records merely give new evidence for an old concept. It is well to bear in mind that values of Poncelet constants determined by firing programs implicitly include this effect.

Projectile Instability

Projectiles are designed so that they are stable in free flight. The axis of the projectile tends to line up with the direction of motion, and if there is a misalignment the aerodynamic forces tend to remove it. The path of the projectile is a smooth curve determined by the gravitational field and aerodynamic forces. Terminal trajectories on the other hand are more likely to be unstable. The disturbance of the soil along the trajectory shows that projectiles frequently tumble immediately after entry or at least undergo violent yawing. Trajectories are often hooked, with sharp curves at the last part of the trajectory. Several factors can contribute to instability of trajectories in soils: (1) the upsetting forces at entry are large, (2) the inhomogeneities of the medium generate upsetting forces along the trajectories, or (3) the distribution of terminal ballistic forces is sometimes intrinsically unstable because of the response of the soil to the high-speed projectile.

Forces at Entry. Direct measurements show that the forces on a projectile during entry into a soil are very large. The forces on the projectile during entry include the transient response of the soil to the motion of the rigid projectile in which steady flow conditions are set up. The resistance at this time is due more to direct compression of the material than to the inertia of the material. This force can be estimated by means of the impact pressure $p_I = \rho c u$, where c is the wave speed in the soil for compressive forces, and u is the particle velocity of the soil induced by the motion of the projectile. By way of contrast, the inertial force is given by the dynamic pressure $p = \rho u^2/2$. The pressure p_I will be discussed later. Its significance for this discussion is that it represents the pressure associated with a wave that propagates a state of compression through the material. The rate of propagation, c, depends primarily on the properties of the material and is very rapid, usually of the order of thousands of feet per second. By this process of rapid propagation the soil is able to accommodate to the motion of the entering projectile

through the rapid transmission of small displacement over a large region. The distribution of stresses in the soil then leads to flow toward the free surface, and the internal stresses are reduced and are soon dominated by the inertia of the flow.

Figure 26 shows accelerometer records from the penetration of flat-ended, instrumented projectiles into sandy soil. The high intensity of the entry phase is evident. The entry forces are well forward on the projectile and therefore tend to worsen yaw and induce high yaw rates.

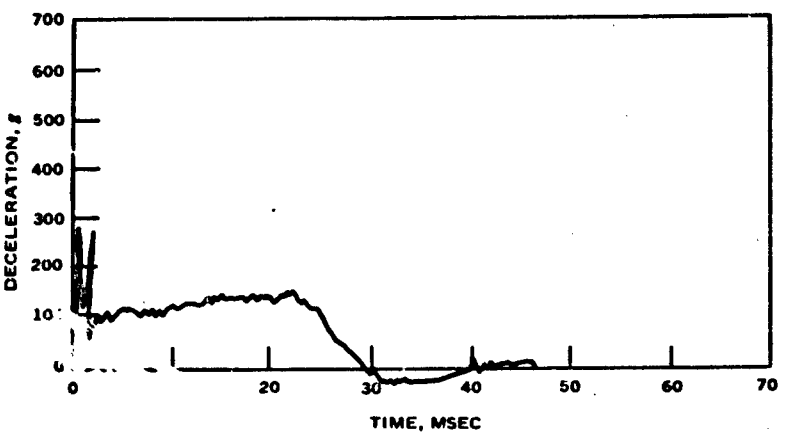

FIG. 26. Deceleration record for Penetration of a Blunt Projectile Into Sandy Soil.

Effect of Inhomogeneities. The terminal trajectory is apt to be strewn with rocks that have to be either broken up or moved aside. These obstructions induce forces that can be estimated by the strength of the rock times its cross-sectional area. Since rocks often have very high strength, highly localized forces are produced in general off the projectile axis.

Natural soils tend to be increasingly compacted with depth so that the projectile experiences changes of resistance as it penetrates. Figure 27 illustrates the variations of density with depth that are likely for a homogeneous soil. This property of a soil corresponds to the standard atmosphere that is used in exterior ballistics to estimate variations of density with altitude. The depth scale depends on the factors indicated in the illustration (the length of time the soil has been in place, for example).

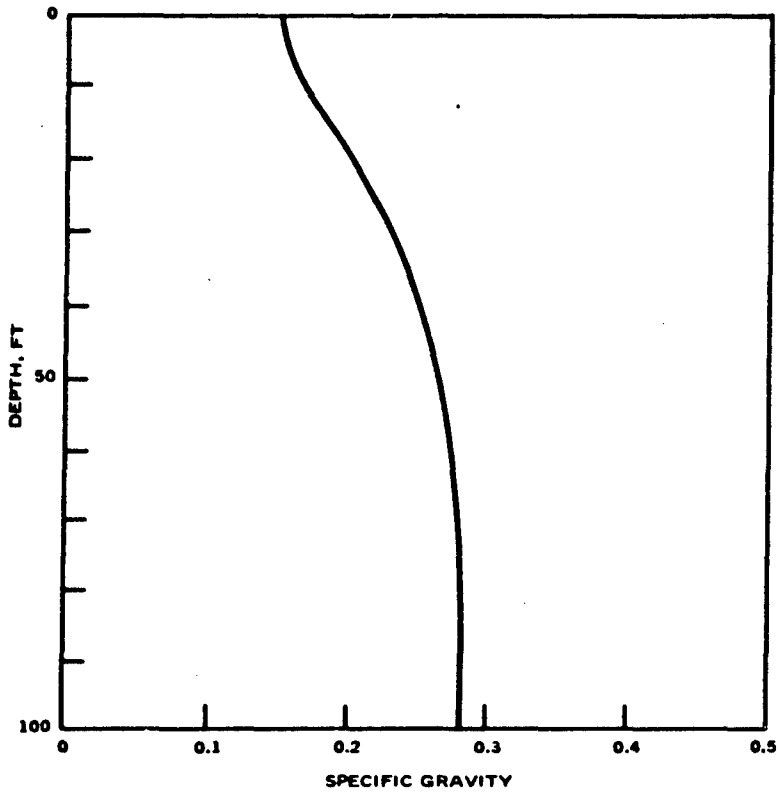

FIG. 27. Changes of Soil Density With Depth. The distance required for these density variations depends on the total time the strata have been in place and on the grain structure.

Soils are seldom homogeneous but rather are stratified. Figure 28 illustrates a typical change of density and soil composition. This particular stratification is representative of a soil in the vicinity of the Naval Weapons Center and is intended to show the possible variability of a soil; it is in no way a model of a soil. The point is that soils are *not homogeneous.* The details of the inhomogeneities are also not easily determined. This means that if the penetration into an unknown soil is attempted, say on the basis of the general geology of the area, the results are highly uncertain.

Unstable Distributions of Surface Forces. It has already been noted that the flow of a soil around a pointed projectile (conical ended or ogival) is such

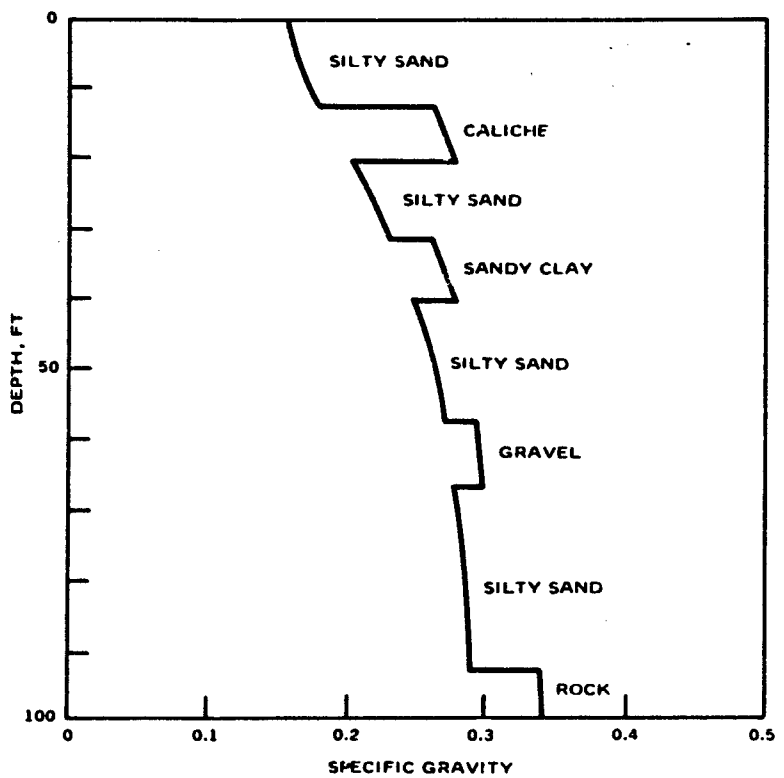

FIG. 28. Changes of Soil Density With Depth and Differing Strata.

that the projectile makes contact with the soil only on its nose. The center of pressure is therefore well forward on the projectile, and if the center of pressure is ahead of the center of mass, the resisting force will tend to increase the yaw angle. The dynamics of the projectile response to the resisting forces consist of the rotational and translational accelerations. These are the changes of yaw rate, the deceleration component in the instantaneous direction of motion that is due to the drag force, and the change of motion due to lift force. These may be written as follows (the equation for the yaw is Eq. 2-16):

$$mR_I^2 \frac{d^2\delta}{dt^2} = \frac{AC_{m_\delta}\rho v^2 \delta l}{2}$$

and the equation for the drag deceleration is equivalent to Eq. 3-1.

$$m\frac{d^2s}{dt^2} = \frac{AC_D\rho v^2}{2}$$

The lift force can be equated to the centrifugal force

$$F_L = \frac{mv^2}{r} = \frac{AC_l\rho v^2\delta}{2} \tag{3-11}$$

so that the radius of the curvature of the trajectory is

$$r = \frac{2m}{A\rho C_l\delta} \tag{3-12}$$

The solution of the yaw equation is either

$$\delta = \delta_0 \sin\left(\frac{2\nu}{\sigma}t + \epsilon\right)$$

if the yaw is stable or

$$\delta = \delta_0 \exp\left(\frac{\nu}{\sigma}t\right) \tag{3-13}$$

if the yaw is unstable. In the latter case the yaw may increase to the point of tumbling if the parameter σ is sufficiently small compared to ν, but as σ increases the rate of yaw decreases so that the projectile can decelerate before tumbling occurs. The trajectory of the projectile will of course have a radius of curvature that depends on the lift coefficient and instantaneous yaw. If it is assumed that the lift coefficient depends on velocity in an analogous way to the drag coefficient, then the Poncelet form of the resisting force will give

$$C_l = C_{l\lim} + \frac{C_{l0}}{v^2} \tag{3-14}$$

Thus for unstable yaws both the lift coefficient and the yaw tend to increase toward the end of the trajectory, reducing the radius of curvature and causing the hooked shape that is so commonly observed.

HIGH-STRENGTH BARRIERS

The major structural components of targets like tanks, aircraft, and command posts are metals, concrete, or masonry. These materials are high-strength solids that are efficient penetration resistors so that small-to-moderate thicknesses of these materials are effective barriers. The terminal interaction between these materials and projectiles is not usually described by penetration relations but rather by standardized definitions of the defeat of the projectile that emphasize the conditions for perforation.

Defeat of the Projectile

The ballistic limit measures defeat of the projectile as the velocity of the projectile at which perforation just occurs. More than one definition is possible, depending on how perforation is defined. Several definitions of ballistic limit have been agreed upon to standardize the nomenclature. If the projectile gets through the armor so that its tip is showing or daylight can be seen through the crater it has made in the armor, then the velocity of the projectile meets the Army criterion for perforation. The velocity of a projectile at which it passes through the armor but has no energy meets the Navy criterion for perforation. Fragmentation by spalling is possible (the ejection of fragments from around the perforation hole), and the "protection ballistic limit" is defined to be the velocity of the projectile at which a 0.020-inch-thick aluminum alloy plate 6 to 12 inches behind the barrier is perforated by either the projectile or a barrier fragment.

Pieces of armor differ to at least a slight degree even if the material properties are carefully controlled, and it is to be expected that near the ballistic limit perforation tests will give erratic results. For this reason tests to determine the ballistic limit for a given material use a statistical criterion for selecting the numerical value. If 50% of a series of impacts of at least six firings that are within 125 ft/sec of the given value are perforations, then that value is the V_{50} ballistic limit.

Complete denial of access to vulnerable components may involve more than one barrier so that other quantitative information on the contribution of individual barrier elements is required. Such information is given as the correlation of residual mass and velocity to the impact velocity of the projectile for perforations without fragmentation of the projectile or barrier, and the distribution of the fragment velocities and sizes for perforations that result in fragmentation. For perforations with fragmentation it is also desirable to know the barrier and projectile parameters that control the onset of fragmentation. The barrier may not only slow down the projectile but it may also change its direction. This is conspicuously a function of the angle between the barrier and the line of flight. The angle between the line of flight of the projectile and the normal to the surface of the barrier is called the *obliquity angle*. At low-to-moderate obliquities the most common effect is a deflection of the line of flight toward the normal to the plate. Deflection is greatest at velocities near the ballistic limit and steadily decreases with increased velocity. At high obliquities the projectile skips off the barrier and is said to *ricochet*.

Mechanical Behavior

Metals, concrete, and masonry have significant differences in the physical properties that govern the forces that resist penetration and the failure processes that cause perforation. It is necessary to describe the mechanical behavior of solids in order to have a proper basis for the selection of the barrier parameters that are important in specifying terminal interactions. Three kinds of response by a material to applied loads suffice to describe the gross mechanical behavior of many solids. These are elastic, brittle, and ductile responses. A material is *elastic* if it follows the rule that when subjected to an external force deformation is proportional to the force, and the deformation is removed by removal of the force. The materials used in building construction, armored vehicles, and aircraft are elastic according to this rule as long as the forces are not too great. The elastic deformations produced under normal loads are small and are usually undetectable. A building, for example, has forces applied to it by the weight of its walls and ceiling, but bending, contraction, or elongation of structural members is not usually obvious.

If structures are loaded beyond some critical amount, there is a change

in the way the material of the structure responds to the forces on it. A concrete member, for example, will develop cracks and come apart. A steel member subjected to equivalent forces will bend or buckle but stay together. If a material, like concrete, typically goes from elastic behavior to failure fracture or rupture, it is called *brittle.* If a material, like steel, typically goes from elastic behavior to large permanent stretching and bending deformations, it is called *ductile.* A ductile material ultimately fails like a brittle material, but only after some degree of plastic deformation. These two kinds of material failure are useful in separating barriers into two groups. Concrete, masonry, and rock are examples of brittle materials. Metals and alloys are examples of ductile materials.

Mechanism of Penetration

It is assumed that the projectile keeps its shape during ballistic impact. The barrier material must be pushed aside or forward through a combination of elastic, plastic, and brittle failures in order to accommodate the barrier to the moving contour imposed by the projectile. In so doing the barrier material exerts its resisting force on the projectile and changes its motion. One aspect of the mechanism of penetration is the specific combinations of deformations that occur within a given material. A few general observations can be made on the role of brittle and ductile processes in penetration that are based on the examination of penetration holes.

The hole that is made in a ductile barrier is very nearly the exact diameter of the projectile. If the barrier is cut along the axis of symmetry of the hole, the cross section reveals a zone of approximately one to three diameters that has been plastically deformed. The plastic deformations are responsible for a lip on the entry side and deformations to the side and in front of the projectile. Consider the penetration of long projectiles into thick targets: as velocity is increased and penetration increases, the lip deformations increase up to a point. These lip deformations can account for some of the material that is displaced, but ultimately are unable to account for all of the increased volume of the penetration hole. Since plastic deformations are very nearly incompressible, the change of volume has to be due to elastic and plastic deformations to the side and in front of the projectile.

The hole that is made in a brittle barrier by ballistic impact may vary from a hole the size of the impacting projectile to one that is several

projectile diameters in width. In any case there is usually some indication that a zone of material immediately in contact with the projectile has undergone changes due to brittle failure. In some cases the zone manages to retain its integrity and the hole is roughly the shape of the projectile; in other cases the zone fails during the impact or at some later time and the material of the zone is removed. The differences in the behavior of brittle materials can be correlated with such properties as strength and porosity.

For either a ductile or brittle barrier the impact of the projectile against the barrier produces stresses in the barrier that are responsible for the full penetration resistance at the surface of the projectile. These stresses decrease in magnitude with distance from the projectile. The failure zone is the zone in which these stresses are above the strength of the material. Beyond this zone the deformations are elastic. Within this zone the deformations are either ductile or brittle failures.

The projectile gets through the barrier by making a separation of the barrier material that goes completely through the barrier. Some forms of failure that are recognized in experimental and theoretical studies are shown in Fig. 29 (Ref. 16 and 17).

Brittle Penetration. The process of brittle penetration illustrated in Fig. 29 can in principle at least be continued until the failure zone reaches the exit surface and fractures run to that surface.

Ductile Penetration. In ductile materials (materials that undergo large amounts of deformation before fracture or rupture) the point of a conical or ogival projectile concentrates stresses at the tip and results in intense deformations along the axis of the crater. Extensive plastic deformation culminates in fractures on the axis. The projectile opens a hole in the barrier along the projectile axis, and the hole is enlarged as the projectile passes through. This is also illustrated in Fig. 29. This mode of perforation is characteristic of extremely ductile materials.

Radial Fractures. Projectiles of a wide variety of shapes may cause failure on the exit side of a ductile barrier that occur in a star pattern about the projectile axis (Fig. 29). In thin barriers the star fractures extend through the entire barrier thickness and, if sufficiently ductile, the angular piece between the cracks folds back into petals. This is called *petalling*. In thick targets the fractures extend only partway through the barrier and combine with other modes of failure to form fragments. There is no common designation for this mode of failure.

Plugging. Cylinders, and blunt projectiles in general, knock out a plug

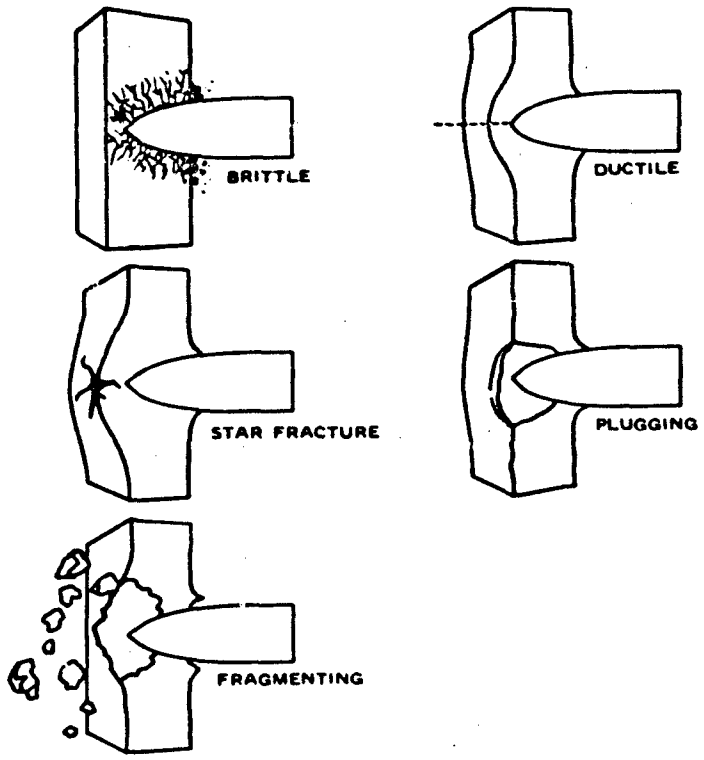

FIG. 29. Primary Modes of Perforation Failure.

that is roughly cylindrical in shape. Even sharp projectiles may do this under the proper conditions. The essential feature is failure on cylindrical or conical surfaces around the projectile axis. This is called *plugging* (Fig. 29).

Spalling and Scabbing. Two other modes of failure that may be associated with high-velocity impact are *spalling* and *scabbing*. Spalling has been intensely studied for explosive loading and is failure caused by the interaction of intense stress waves. The configuration of the fracture surface is determined by the impact configuration and stress wave transmission and reflection. Scabbing may have the same general causes but the fracture surface is determined by patterns of inhomogeneities and anisotropy in the barrier materials. Under certain circumstances these failure processes could contribute

to the formation of a single fragment and resemble plugging.

Fragmenting. The above processes of ductile perforation, radial fractures, and plugging may occur in pure form at lower velocities. At higher velocities these combine with spalling and scabbing or with secondary ductile and brittle failure processes to produce many fragments. It is sometimes convenient to call these *fragmenting mode perforations* (Fig. 29), although there are obviously many finer distinctions possible within this mode.

APPLICATION OF CONSERVATION LAWS

The final results of the interaction of a projectile and a tough barrier are new rigid body motions of the projectile and barrier, changes of shape for these bodies, and changes of energy. Conclusions about the interrelation of initial and final motions and changes of energy can be reached by applying conservation of energy and momentum to the initial and final states with little or no concern for the details of the intervening events.

Conservation of energy and momentum are first applied to the initial and final states of rigid body motion (Fig. 30) of the projectile/barrier system with *clean perforation of the barrier*, i.e., perforations by ductile or petalling modes.

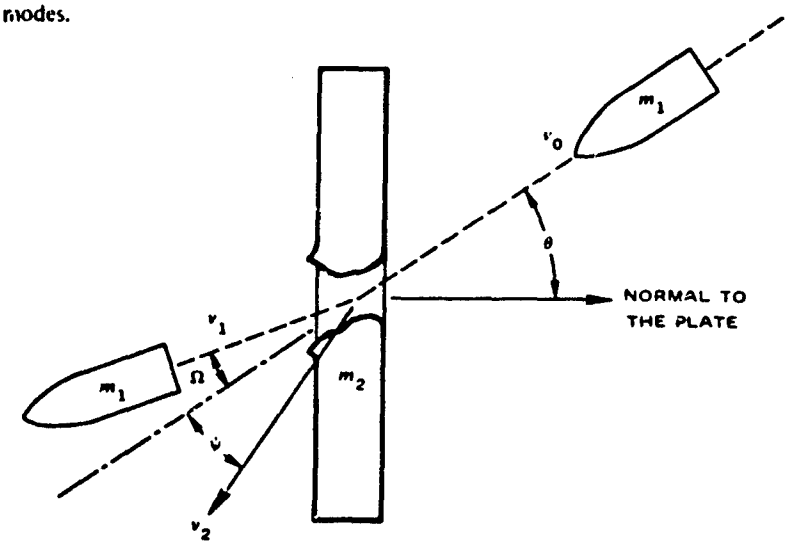

FIG. 30. Perforation at Obliquity With Deflection of the Projectile.

Conservation of momentum requires that

$$m_1 v_0 = m_1 v_1 + m_2 v_2 \quad \text{line-of-flight momentum}$$

$$0 = m_1 w_1 + m_2 w_2 \quad \text{off-line-of-flight momentum} \qquad (3\text{-}15)$$

Conservation of energy requires that

$$\frac{m_1 v_0^2}{2} = \frac{m_1\left(v_1^2 + w_1^2\right)}{2} + \frac{m_2\left(v_2^2 + w_2^2\right)}{2} + E_0$$

where E_0 is the amount of energy that is converted from kinetic to nonkinetic form. This can occur by many processes, in dissipative processes in elastic waves or in the permanent deformations of plasticity and fracture, for example.

The components of off-line-of-flight momentum depend on the deflection angles Ω and ψ

$$w_1 = v_1 \tan \Omega$$

$$w_2 = v_2 \tan \psi$$

and thus ψ and Ω are interrelated

$$\tan \psi = \frac{m_1 v_1}{m_2 v_2} \tan \Omega$$

since

$$m_2 w_2 = m_1 w_1$$

$$= m_1 v_1 \tan \Omega$$

$$w_2 = \frac{m_1 v_1}{m_2} \tan \Omega$$

Conservation of energy is expressed as

$$m_1 v_0^2 = m_1 v_1^2 + m_2 v_2^2 \tan^2 \Omega + \frac{m_1^2}{m_2} v_1^2 \tan^2 \Omega + 2E_0$$

The equation for momentum and energy conservation can be solved for v_1 and v_2

$$v_1 = \left(R_1 v_0 \pm R_2 \sqrt{v_0^2 \left(\frac{2E_0}{R_2 m_1} + \tan^2 \Omega \right) \left| (R_1 - R_2) v_0^2 + \frac{2E_0}{m_1} R_1 \right|} \right) \cos^2 \Omega$$

$$v_2 = \frac{m_1 v_0}{m_2} (1 - R_1 \cos^2 \Omega) \pm R_1 \left(\sqrt{v_0^2 \left(\frac{2E_0}{R_2 m_1} + \tan^2 \Omega \right) \left| (R_1 - R_2) v_0 + \frac{2E_0}{m} R_1 \right|} \right) \cos^2 \Omega \tag{3-16}$$

where

$$R_1 = \frac{m_1}{m_1 + m_2}$$

$$R_2 = \frac{m_2}{m_1 + m_2} \tag{3-17}$$

The quantities E_0 and Ω account for the individual properties of the given impact system, such as the projectile shape, the mechanical properties of the barrier, and the mode of failure of the barrier. Special cases of the above equations make it easier to understand the consequences of the conservation laws and the role of the parameters E_0 and Ω.

Special Cases

(1) Impacts without deflection are important special cases. The final velocities are

$$v_1 = R_1 v_0 + R_2\sqrt{v_0^2 - \frac{2E_0}{R_2 m_1}}$$

$$v_2 = R_1 v_0 + R_1\sqrt{v_0^2 - \frac{2E_0}{R_2 m_1}} \qquad (3\text{-}18)$$

There are two values of v_1 and v_2 for every E_0 except $E_0 = (R_2 m_1 v_0)/2$. If v_1 is plotted as a function of E_0, the curves for five values of R_2 are shown in Fig. 31. For each value of R_2 the upper branch of each curve corresponds to perforations, since for this branch v_1 is greater than v_2 so that the

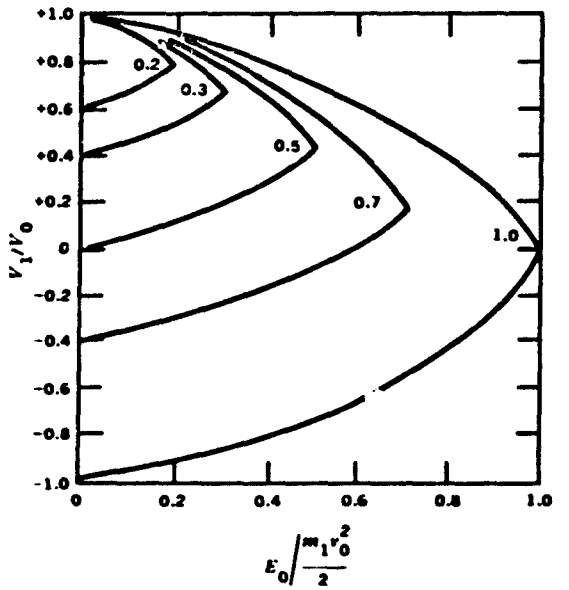

FIG. 31. The ratio of v_1 to v_0 Plotted Against the Ratio of E_0 to $(m_1 v_0^2)/2$ for Five Values of R_2.

projectile has passed through the barrier. The lower branches of these curves correspond to rebounds since on these branches v_1 is less than v_2 and the projectile is rebounding relative to the barrier. Since v_2 is always positive, it is clear that both the projectile and the barrier are moving in the direction of initial projectile motion for R_2 less than 0.5. The identification of equations is as follows:

$$\left.\begin{aligned} v_1^+ &= R_1 v_0 + R_2\sqrt{v_0^2 - 2E_0/R_2 m_1} \\ v_2^- &= R_1 v_0 - R_1\sqrt{v_0^2 - 2E_0/R_2 m_1} \end{aligned}\right\} \text{perforation}$$

$$\left.\begin{aligned} v_1^- &= R_1 v_0 - R_1\sqrt{v_0^2 - 2E_0/R_2 m_1} \\ v_2^+ &= R_1 v_0 + R_1\sqrt{v_0^2 - 2E_0/R_2 m_1} \end{aligned}\right\} \text{rebound} \qquad (3\text{-}19)$$

Note that even the case $E_0 = 0$ has both perforation and rebound. The rebound is $v_1 = 0$, $v_2^+ = v_0$ whereas perforation is $v_1^+ = v_0$, $v_2^- = 0$ (which is a complete miss).

(2) Equal masses $m_1 = m_2$ are interesting because of such common examples as "billiard ball" impacts. In this case $R_1 = R_2 = 1/2$, so that in general

$$v_1 = \frac{v_0}{2} \pm \frac{1}{2}\left(\sqrt{v_0^2 - \frac{4E_0}{m_1} - \frac{4E_0}{m_1}\tan^2\Omega}\right)\cos^2\Omega$$

$$v_2 = v_0\left(1 - \frac{\cos^2\Omega}{2}\right) \pm \frac{1}{2}\left(\sqrt{v^2 - \frac{4E_0}{m_1}\sec^2\Omega}\right)\cos^2\Omega \qquad (3\text{-}20)$$

and if $E_0 = 0$, the elastic impact of billiard balls is one example. For the specific case of contact at 45 degrees the possible velocities are

a. $v_1 = \frac{v_0}{2}, 0 \qquad v_1 = \frac{v_0}{2} \qquad w_1 = 0$

$$\text{b. } v_2 = \frac{v_0}{2}, v_0 \qquad w_2 = -\frac{v_0}{2} \qquad w_2 = 0$$

where set (a) is the only physically meaningful one.

If instead of $E_0 = 0$ the energy is $E_0 = mv_0^2/4$ but $\Omega = 0$, this describes a system in which energy has been dissipated by conversion to heat or other nonkinetic forms of energy in the same amount as is converted to *lateral kinetic energy* in the preceding billiard ball impact. Thus for

$$E_0 = \frac{mv_0^2}{4}, \Omega = 0$$

$$v_1 = \frac{v_0}{2}, \quad w_1 = 0$$

$$v_2 = \frac{v_0}{2}, \quad w_2 = 0$$

The two bodies move together after impact, in this case. The billiard ball impact and penetrating impact are illustrated in Fig. 32.

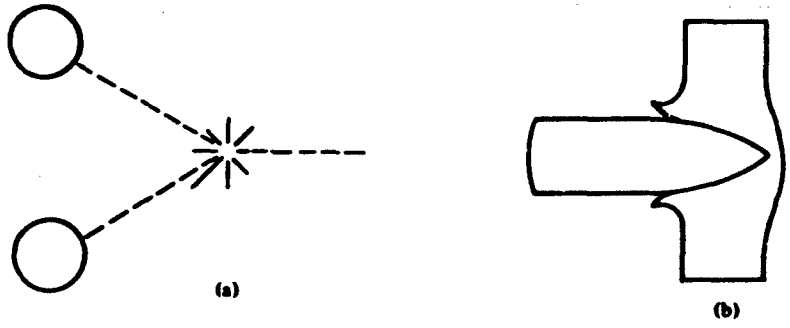

FIG. 32. Impacts Between Bodies of Equal Mass. (a) Billiard ball impact, masses equal and no energy loss. (b) Penetrating impact, energy lost in crater formation.

(3) A very common condition is that the barrier mass is much larger than the projectile mass so that R_1 is very small and R_2 is approximately equal to 1. Then $R_1 = 0$ and $R_2 = 1$ give

$$v_1 = \pm \left(\sqrt{v_0^2 - \frac{2E_0}{m_1}} \right) \cos \Omega \tag{3-21}$$

$$v_2 = 0$$

This condition is implicit in much of the theory of armor penetration, especially theories based on energetic considerations.

SIMPLE TERMINAL BALLISTICS THEORIES

Several theories of the interaction between a projectile and barrier at zero obliquity calculate measures of the defeat of a projectile in tractable form by using simple assumptions about the response of the barrier to impact (Ref. 18). These all result in calculations of the energy E_0 that is changed from kinetic to nonkinetic form. The earlier theories calculate the work done in penetration using specific assumptions on the nature of the contact forces resisting penetration. More recent theories explicitly determine the changes in energy that occur as penetration proceeds. In addition, assumptions are made—often implicitly—on the motion of entry and exit boundaries and on the failure process that terminates resistance or initiates changes in the form of resistance.

Penetration resistance has been estimated by simple expressions that use empirical constants for each barrier of interest. The Euler-Robinson form is

$$F_R = c_1 A$$

where A is the cross-sectional area of the projectile at the current stage of embedment, and c_1 is a constant for the particular projectile and barrier. This is equivalent to assuming that the barrier material has been loaded until it has reached a limit σ_Y beyond which it cannot go. The constant c_1 is then the yield limit σ_Y.

A slightly more complicated form for the penetration resistance is the Poncelet form that was introduced in the discussion of soil penetration

$$F_R = (c_1 + c_3 v^2)A$$

where c_1 and c_3 are empirical constants. This can be interpreted as an extension of the Euler-Robinson form by consideration of inertial effects through an adaptation of the methods of exterior ballistics.

These forms of penetration resistance are gross simplifications of real behavior; attempts to find empirical constants that will apply to a wide range of material and projectile configurations have never been successful. The expressions are useful in showing the general dependence of the measures of defeat on the principal parameters of the barrier. Thus the Euler-Robinson form of penetration resistance can be combined with the assumption that the entry and exit surfaces have negligible motion, and that the mode of perforation is ductile (the barrier material opens at the tip of the projectile and expands about it). The force on the projectile at any penetration is $F_R = kA$, and the energy E_0 that is dissipated in the penetration is $E_0 = \int_0^P kA\,dP = k\tau$, where τ is the volume of the indentation in the barrier.

For nondeforming projectiles the crater volumes are easily estimated from the nose shape and penetration, $\tau = \int_0^P A(P)dP$, where $A(P)$ is the cross-sectional area of the projectile as a function of penetration. Examples of $A(P)$ are

spherical nose $A(P) = \pi(dP - P^2)$ (3-22)

conical nose (cone angle α) $A(P) = \pi\tan^2(d/2)P^2$ (3-23)

flat-ended nose (and penetration beyond complete nose embedding) $A(P) = \frac{\pi d^2}{4}$ (3-24)

An example of the application of these results to penetration data is shown in Fig. 33. The data are penetrations of conically ended steel projectiles into brass targets. The targets were plates 9 inches on a side and

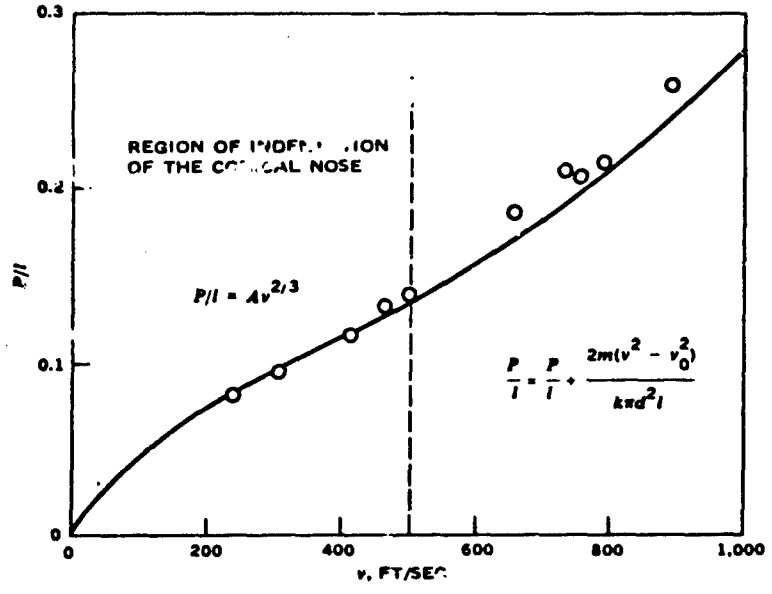

FIG. 33. Penetration Data for a Conical Ended Projectile.

1/4 inch thick. The 0.875-inch-long projectiles were 1/4 inch in diameter with a cone angle of 90 degrees. The values of the mass ratios R_1 and R_2 are 0.002 and 0.009, respectively, so that special case 3 is appropriate. The penetration of the projectile up to the shaft is given by

$$\frac{mv^2}{2} = k\int_0^P \pi \tan^2(\pi/2)P^2 dP$$

$$= k\frac{\pi P^3}{3}$$

or

$$P = \sqrt[3]{\frac{3mv^2}{2k\pi}}$$

and beyond the nose

$$\frac{mv^2}{2} = k\tau_0 + \frac{k\pi d^2}{4}(P - P_0)$$

or

$$P = P_0 + \frac{2m(v^2 - v_0^2)}{k\pi d^2}$$

where τ_0 is the volume of the nose and P_0 is the length of the nose. The constant k was chosen to fit the data.

For complete dissipation of the projectile's energy the ballistic limit is

$$\frac{mv_0^2}{2} = \frac{k\pi d^2 h}{4} \quad \text{(using the Navy criterion for perforation)}$$

This has the form of the Thompson equation (Ref. 21) for the ballistic limit

$$v_{BL} = \sqrt{\frac{k\pi d^2 h}{2m}} \tag{3-25}$$

The residual velocity for an impact above the ballistic limit is

$$\frac{mv^2}{2} - \frac{mv_0^2}{2} = \frac{mv_1}{2}$$

$$v_1 = \sqrt{v^2 - v_0^2} \tag{3-26}$$

If the resistance to penetration is of the form

$$F_R = \frac{\pi d^2}{4}(c_1 + c_3 v^2)$$

then the equation of motion is

$$m\frac{dv}{ds}v = \frac{\pi d^2}{4}(c_1 + c_3 v^2)$$

and this has the solution given in the section on soil penetration. The ballistic limit is given by the equation

$$v_{BL} = \sqrt{\frac{c_1}{c_3}\left[\exp\left(\frac{2c_3\tau}{m}\right) - 1\right]} \tag{3-27}$$

and this implies that the energy E_0 is

$$E_0 = \frac{c_1 m}{c_3}\left[\exp\left(\frac{2c_3\tau}{m}\right) - 1\right] \tag{3-28}$$

If the exponential function is approximated by a series, then the ballistic limit velocity is

$$v_{BL} = \sqrt{\frac{c_1\tau}{m} + \frac{c_1\tau^2 c_3}{2m^2} + \frac{4c_1\tau^3 c_3^2}{3m^3}}$$

$$= \sqrt{\frac{c_1\pi d^2 h}{2m}\left[1 + \frac{\pi d^2 c_3 h}{2m} + \frac{2}{3}\left(\frac{\pi d^2 c_3 h}{m}\right)^2 + \cdots\right]} \tag{3-29}$$

which then corrects the ballistic limit for the Euler-Robinson resistance for the effect of inertia. In comparing the two forms of resistance, $c_1 = k$.

Another procedure for determining ballistic limits and residual velocities consists of the direct calculation of the work that is done by the projectile in forming the indentation that is required for ductile perforation. These calculations apply the theory of plasticity to the known deformations of the barrier in a ductile perforation. The details of a calculation by W. Thomsen are given in the Appendix. H. Bethe calculated the energy required to expand the hole formed at the projectile tip to the radius of

the projectile (Ref. 19). His calculation explicitly includes distinct regions of elastic deformation and plastic or ductile deformation. Both calculations have similar forms

$$W = \frac{\pi h d^2}{4}\left[\rho\left(\frac{vd}{2l_\rho}\right)^2 + \frac{\sigma_y}{2}\right] \qquad \text{(Thomsen)} \qquad (3\text{-}30)$$

$$W = \pi d^2 h\left[\rho\left(\frac{\pi v d}{2l_\rho}\right)^2 (3.8912)\frac{(1+\nu)^2}{(5-4\nu)^2} + \frac{\sigma_y}{2}\log\left(\frac{\mu_g}{(5-4\nu)\sigma_y}+1\right)\right] \qquad \text{(Bethe)} \qquad (3\text{-}31)$$

These calculations are equivalent to assuming a penetration resistance of the Poncelet type (Ref. 18) and neglect frictional effects. The neglect of friction is justified by measurement of the frictional force (Ref. 22).

DEFLECTION AND RICOCHET

Most of the investigations of projectile penetration have been at normal incidence because of the great simplicity of that condition. At oblique incidence the problem is more difficult to formulate and solve because the contact forces and the boundary conditions imposed on the barrier are not symmetrical with respect to the axis of the projectile. There are no generally accepted methods of calculating the deflection angle Ω. It is known that at velocities near the ballistic limit the deflections are greatest and are often close to the original obliquity, and hence the projectile tends to emerge normal to the plate. As impact velocity increases, the deflection decreases.

An estimate of the angle Ω can be made by assuming that the component of the contact forces L that causes deflection is related to normal contact force F_R by $F_L = F_R \cos(\theta - \Omega)$ where θ is the initial angle of obliquity, Ω is the instantaneous deflection, and $(\theta - \Omega)$ is the instantaneous obliquity (deflection is toward the exit side of the barrier). This assumption is plausible in that it accounts for decreased resistance on

the exit side that results from the zero stress on the exit surface and the acceleration of the surface outward, but it oversimplifies since it does not make the effect dependent on barrier thickness and does not account for the reversal of the deflecting force at the very large obliquities at which ricochet occurs. The assumption serves one purpose here: to show that the general phenomena of impact at oblique incidence can be explained by a deflecting force of the proposed type including the role of major impact and material parameters.

It is assumed that the deflecting force is

$$F_L = A(c_1 + c_3 v^2) \sin(\theta - \Omega)$$

for which the inertial reaction is

$$\frac{mv^2}{r} = F_L$$

and the curvature of the trajectory is then

$$d\Omega/ds = \frac{1}{r}$$

so that

$$d\Omega/ds = \frac{A(c_1 + c_3 v^2) \sin(\theta - \Omega)}{mv^2}$$

Assuming that the deceleration along the trajectory is given by the equation derived for normal incidence, the velocity is

$$v^2 = v_0^2 \exp\left(\frac{-2c_3 A}{m}\right) + \frac{c_1}{c_3}\left[\exp\left(\frac{-2c_3 A}{m}\right) - 1\right]$$

Put this expression for the velocity in the equation for the curvature and a differential equation for the angle of deflection is obtained that can be solved to determine the deflection as

$$\Omega = \theta - 2\tan^{-1}\left[\tan\left(\frac{\theta}{2}\right)\exp\left(c_3 B_1 s + B_1 \log_e |B_2|\right)\right] \qquad (3\text{-}32)$$

where

$$B_1 = \frac{A}{m}\left(\frac{c_3 v_0^2 + c_1}{c_3 v_0^2 - c_1}\right)$$

and

$$B_2 = \frac{c_3 v_0^2 + c_1 \left|1 - \exp\left(2c_3 As/m\right)\right|}{c_3 v_0^2} + \frac{v_0^2 - v_{BL}^2}{v_0^2}$$

At high velocities c_1 is not important, and the above expression reduces to the simpler form

$$\Omega = \theta - 2\tan^{-1}\left[\tan\left(\frac{\theta}{2}\right)\exp\left(\frac{c_3 As}{m}\right)\right] \tag{3-33}$$

Small velocities reduce the velocity-dependent effects; hence $c_3 = 0$ and the equation for deflection can be simplified to

$$\Omega = \theta - 2\tan^{-1}\left[\tan\left(\frac{\theta}{2}\right)\left(\frac{v_0^2 - \frac{c_1 As}{m}}{v_0^2}\right)\right] \tag{3-34}$$

To complete the calculation of ballistic limits and residual velocities it is necessary to determine the intersection of the curved trajectory with the rear surface of the barrier. This turns out to be analytically cumbersome, but it is possible to reach useful conclusions without these procedures. At low velocities the deflections increase with thickness and tend toward a maximum deflection that is equal to the angle of incidence; thus at its greatest deflection the projectile emerges normal to the barrier. At a given barrier thickness the deflection decreases with increased impact velocity. These conclusions are in quantitative agreement with the experimental observations on impacts at obliquities. Figure 34 shows typical curves representing the dependence of the deflection angle on the impact velocity.

The equation

$$F_L = F_R \cos\left(\theta - \Omega\right) \tag{3-35}$$

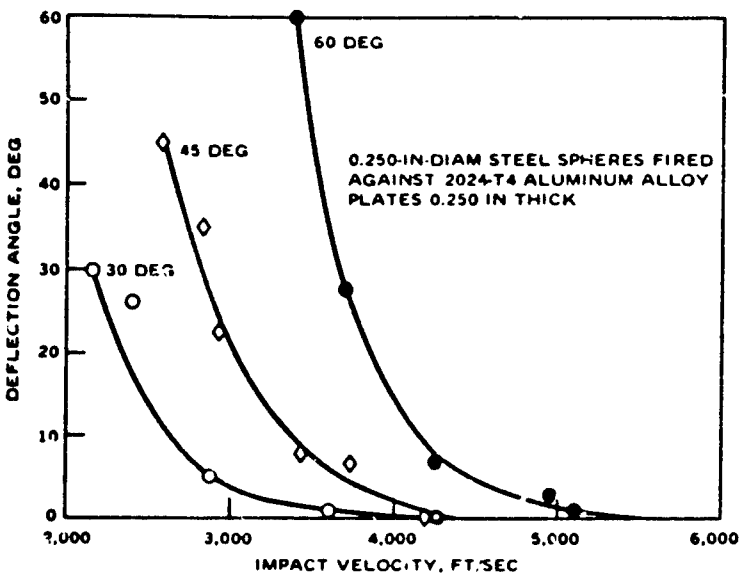

FIG. 34. Deflection Angle as a Function of Impact Velocity for the Impact of 0.250-Inch-Diameter Steel Spheres Against 0.250-Inch-Thick Aluminum Alloy Plates.

does not take into account the fact that at large obliquities the asymmetry of the contact forces changes so that deflection increases the instantaneous obliquity and the projectile ricochets off the front surface. This can be the consequence of projectile configuration. If the projectile is pointed, there is some angle of obliquity at which the projectile contacts the barrier along the side rather than at the tip. The contact configuration favors deflection more than penetration. At high obliquities it is not at all obvious that the zero stress and surface motion of the rear surface are solely responsible for the asymmetry of the contact force on the projectile. The guess about the magnitude of the deflecting force has been good enough to show the general trends in projectile deflection at moderate obliquities, but it would have to be considerably improved, and in exactly those areas where it is most weak, in order to predict the change to ricochet.

In terminal ballistics the important datum is the critical angle of ricochet, since once ricochet occurs the projectile is defeated. The angle depends on the thickness and strength of the target. The ricochet angle is significantly higher for blunt and flat-ended projectiles.

SINGLE FRAGMENT SYSTEMS

The impact of a blunt projectile against a barrier results in rapid transfer of momentum and energy to the section of the barrier immediately in contact with the projectile. Plugging perforation will cause this section to separate from the rest of the barrier at velocities above the ballistic limit. The parameters of paramount interest are the momenta and energies of the projectile and plug, but the momentum and energy transferred to the perforated barrier must be accounted for.

At velocities below the ballistic limit the conservation equations are

$$m_1 v_0 = m_1 v_1 + m_2 v_2$$

and

$$m_1 v_0^2 = m_1 v_1^2 + m_2 v_2^2 + 2E_0$$

where the velocity relations must be for *rebound*, and $E_0 \leqq (R_2 m_1 v_0^2)/2$. Above the ballistic limit the conservation equations are

$$m_1 v_0 = m_1 v_1 + m_2' v_2' + m_3 v_3$$

and

$$m_1 v_0^2 = m_1 v_1^2 + m_2' v_2'^2 + m_3 v_3^2 + 2E_1 \tag{3-36}$$

where the velocity relations are now for *perforation*, and

$$2E_0 = m_2' v_2'^2 + m_3 v_3^2 + 2E_1 \leqq \frac{R_2 m_1 v_0^2}{2} \tag{3-37}$$

where $m_2' v_2'$ are mass and velocity of the perforated barrier, and $m_3 v_3$ are mass and velocity of the plug.

It is desirable to have an explicit dependence of the projectile velocity and the plug velocity on the masses of these bodies. This can be done by a simple analytical device. The momentum $m_2' v_2'$ is treated as transformation of the impact velocity v_0

$$\overline{v}_0 = v_0 - v_0' \tag{3-38}$$

where v_0' is the velocity of m_1 equivalent to $m_2'v_2'$

so that

$$m_2'v_2' = m_1v_0'$$

Hence

$$v_0' = \frac{m_2'v_2'}{m_1}$$

Then the momentum equation

$$m_1v_0 = m_1v_1 + m_2'v_2' + m_3v_3$$

is changed to

$$m_1\bar{v}_0 = m_1v_1 + m_3v_3$$

The energy equation can be changed in an equivalent way; thus since

$$m_1\bar{v}_0^2 = m_1(v_0 - v_0')^2 = m_1(v_0^2 - 2v_0'v_0 + v_0'^2)$$

and

$$v_2' = \left(\frac{m_1}{m_2'}\right)v_0'$$

the energy equation

$$m_1v_0^2 = m_1v_1^2 + m_3v_3^2 + m_2'v_2'^2 + 2E_1$$

becomes

$$m_1\bar{v}_0^2 = m_1v_1^2 + m_3v_3^2 + m_1\left(\frac{m_1}{m_2} + 1\right)v_0'^2 - 2v_0'v_0m_1 + 2E_1$$

Designate the energy

$$m_1\left(\frac{m_1}{m_2'}+1\right)v_0'^2 - 2v_0'v_0m_1 = -2E_{BL} = -mv_{BL}^2$$

(The minus sign is required if $m_2' \geq m_1$ since $v_0 > v_0'$.) E_{BL} is a new energy variable, and the velocity v_0 is related to this variable by the equations

$$v_0' = \frac{m_2'v_0}{m_1+m_2'} \pm \frac{m_2'}{m_1+m_2'}\sqrt{v_0^2 - \left(\frac{m_1+m_2'}{m_2'}\right)v_{BL}^2} \tag{3-39a}$$

and

$$\bar{v}_0 = \left(1 - \frac{m_2}{m_1+m_2'}\right)v_0 - \frac{m_2'}{m_1+m_2'}\sqrt{v_0^2 - \left(\frac{m_1+m_2}{m_2'}\right)v_{BL}^2} \tag{3-39b}$$

The transformed equations are

$$m_1\bar{v}_0 = m_1v_1 + m_3v_3$$

and

$$m_1\bar{v}_0^2 = m_1v_1^2 + m_3v_3^2 - 2E_{BL} + 2E_i$$

The energy E_{BL} is the amount of energy that has to be subtracted from the nonkinetic energy E_1 in order to put the energy equation in the desired form. It is usually assumed that E_{BL} is constant, *but in general it is not.* The projectile never passes the plug in plugging perforations, so that the solution is

$$v_1 = R_1'\bar{v}_0 - R_2'\sqrt{\bar{v}_0^2 - \frac{2(E_1 - E_{BL})}{R_2'm_1}} \tag{3-40a}$$

$$v_3 = R_1'\bar{v}_0 + R_1'\sqrt{\bar{v}_0^2 - \frac{2(E_1 - E_{BL})}{R_2'm_1}} \tag{3-40b}$$

where

$$R_1' = \frac{m_1}{m_1 + m_3} \qquad R_2' = \frac{m_3}{m_1 + m_3} \tag{3-41}$$

The projectile and plug velocities are equal if

$$E_1 - E_{BL} = R_2' \frac{m_1 \bar{v}_0^2}{2}$$

and this is also the maximum energy dissipation compatible with momentum conservation. The barrier is usually much larger than the projectile so that

$$\frac{m_2'}{m_1 + m_2'} \to 1$$

Thus

$$\bar{v}_0 = \sqrt{v_0^2 - v_{BL}^2}$$

and the projectile and plug velocities are

$$v_1 = R_1' \sqrt{v_0^2 - v_{BL}^2} - R_2' \sqrt{(v_0^2 - v_{BL}^2) - \frac{2(E_1 - E_{BL})}{R_2' m_1}} \tag{3-42a}$$

and

$$v_3 = R_1' \sqrt{v_0^2 - v_{BL}^2} - R_2' \sqrt{(v_0^2 - v_{BL}^2) - \frac{2(E_1 - E_{BL})}{R_2' m_1}} \tag{3-42b}$$

These are equal if

$$E_1 - E_{BL} = \frac{R_2' m_1}{2} (v_0^2 - v_{BL}^2)$$

and thus

$$v_1 = v_3 = \frac{m_1}{m_1 + m_3} \sqrt{v_0^2 - v_{BL}^2} \tag{3-43}$$

This is the expression for residual projectile velocity that Recht found for plugging (Ref. 23). It applies to a large amount of firing data if empirical values of v_{BL} are used.

Examples of projectile residual velocity data are given in Fig. 35 and 36. The projectiles were spheres and cubes.

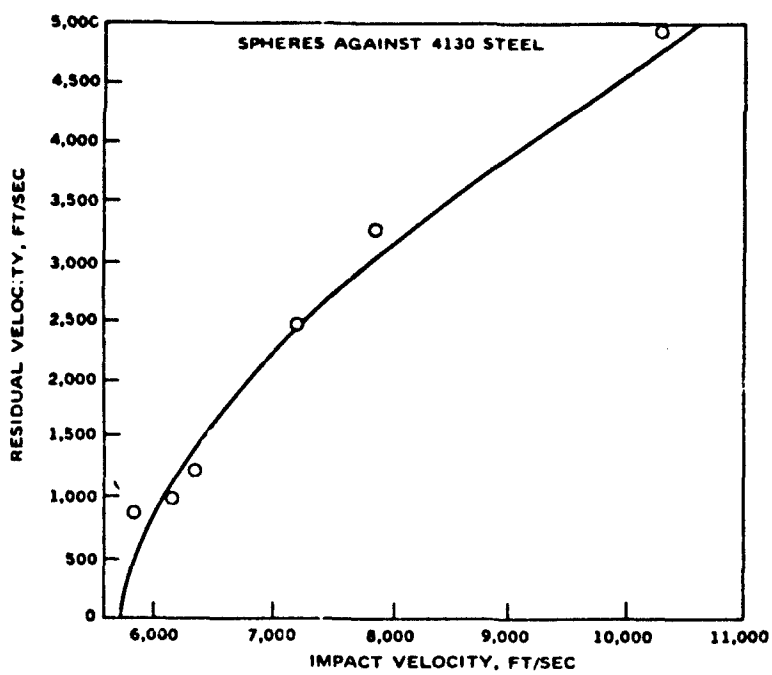

FIG. 35. Residual Velocity as a Function of Impact Velocity for 0.25-Inch-Diameter Spheres Against SAE 4130 Steel.

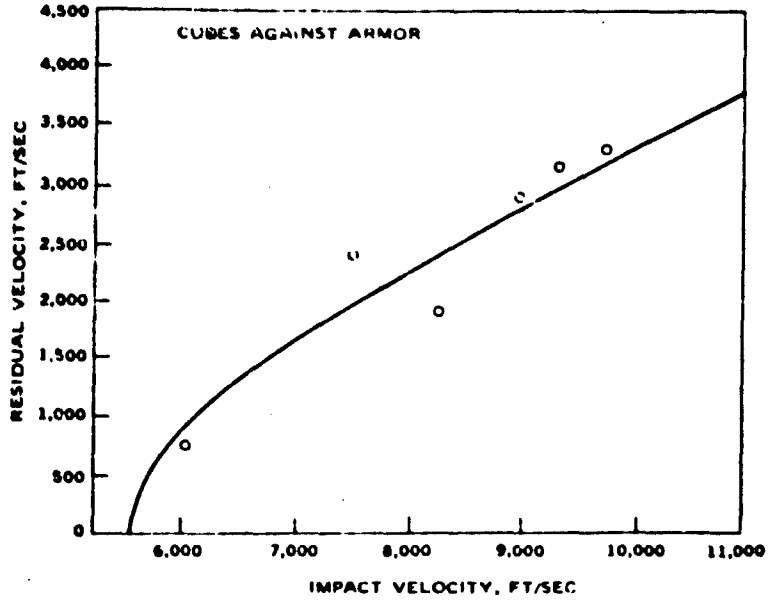

FIG. 36. Residual Velocity as a Function of Impact Velocity for 0.24-Inch Cubes Against 0.25-Inch-Thick Armor.

SUMMARY

The terminal ballistics of projectiles treats the interaction of a projectile of known shape and orientation with barriers that range from low resistance soils of large extent to highly resistant metallic armors of small thickness. It is assumed that the projectile does not deform significantly during the interaction with barriers. For the extended barriers empirical expressions can be used to relate the penetration resistance to velocity and thus account for deceleration with reasonable accuracy. The most serious problems are inhomogeneity of soils, uncertainty in the information about the composition of soils, and the intrinsic instability of most projectile shapes in soils. For finite barriers of armor the primary interest is in determining the maximum velocity of a projectile that the barrier will stop. Again, empirical expressions for penetration resistance can be used, but the mode of failure of the barrier is important in distinguishing various kinds of interaction between projectile and barrier.

PART II

WARHEAD BALLISTICS

4

The Analogy Between Warhead and Gun

The projectile has evolved from a simple moving mass set in motion by a gun to a whole family of devices that are launched from guns, propelled by rockets, or dropped from aircraft. These devices are filled with an explosive that is detonated by an impulse received from the fuzing system. The explosive and certain parts of the surrounding structure comprise the warhead. It is the function of the warhead to make the terminal contact with the target by means of high-velocity fragments and blast.

The warhead and its operation will be treated as a ballistic system analogous to a gun and projectile. The basic elements of a warhead are as follows:

1. An initiating system, which corresponds to the igniter of the gun and projectile
2. A high explosive charge, which corresponds to the propellant charge
3. A case, which corresponds to the barrel of the gun in its function of confining the charge and to the projectile in its role as the source of fragments that are propelled toward the target

The same kinds of processes are involved in warhead operations as in gun operation and the same divisions of the subject are appropriate. The explosive charge, like the propellant charge, releases energy that gives the fragments kinetic energy, and produces the pressure of the blast wave. This

is the *internal ballistic phase of warhead operation*. The system of fragments and the blast wave travel out from the warhead. The fragments lose energy and the blast wave is dissipated. This is the *exterior ballistic phase*. The system of fragments and the blast wave reach the target and interact with it, causing perforation, damage to internal components, and damage to structure. This is the *terminal ballistic phase*.

There are interesting and useful similarities between projectile ballistics and warhead ballistics which invite comparison, but there are also dramatic differences. For example, in projectile ballistics every effort is made to control the rate of energy release from the charge and to keep the pressures in the chamber and bore below the yield stresses of the barrel and projectile, but in warhead ballistics the most extreme rates of energy release from the charge and complete failure of the case are the processes that are exploited. These differences actually point out a complementary relation between projectile ballistics and warhead ballistics. Together, these two forms of ballistics represent a more comprehensive investigation of the possible forms of ballistic systems.

5

Warhead Internal Ballistics

MAIN PHENOMENA IN THE DETONATION OF A WARHEAD

As an example of a warhead consider a bomb in which there is an explosive charge with a simple metallic case. Figure 37 shows such a weapon in cross section and without the fins. The operation of the bomb from the time it strikes its target can be outlined as follows:

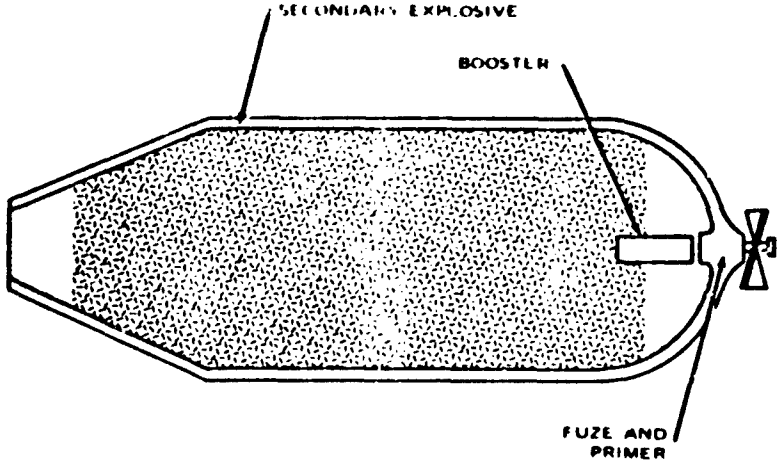

FIG. 37. General-Purpose Bomb With an Impact Fuze.

1. An initiating system (which is actuated by a fuze) delivers a shock to the main charge.
2. The shock causes the main charge to detonate, that is to say, a chemical reaction with an extremely high rate of energy release is set up and travels through the charge material.
3. The detonation propagates at a constant rate and produces constant changes of pressure, temperature, and motion of the detonation products.
4. The case is set in motion and deforms under the action of the intense internal pressure.
5. The case expands and ultimately reaches a state at which fragmentation begins.
6. The detonation products expand and for some distance continue to work on the fragments.
7. The expanding gases slow down under expansion, but these have now established a high-speed system of fragments and a shock wave in the surrounding atmosphere.

FUZE AND EXPLOSIVE TRAIN

In Fig. 37 the general-purpose bomb has an impact fuze that actuates the primer. The simple mechanical system for detonating the primer is shown in detail in Fig. 38. The sensitive explosive in the primer is the most likely part of the explosive system to be detonated prematurely, and therefore provisions are made to keep the primer isolated from the rest of the explosive in the warhead. The mechanism for isolating the primer until weapon operation is the *arming device*. In Fig. 38 this is the out-of-line mechanism, a simple mechanism that keeps the primer out of line with the striker and booster. The vanes shown in Fig. 38 are rotated during the fall of the bomb and withdraw the striker from the piece that holds the primer out of line. When the striker is completely withdrawn, it allows the primer to swing into line under spring tension. Impact then drives the pointed striker into the primer and detonates it.

The shock from the primer acts directly on a small charge called the booster charge. The booster explosive is less sensitive than the primer but more sensitive than the main charge and does not have the best properties for the functions of the main charge. The booster develops shock intensities

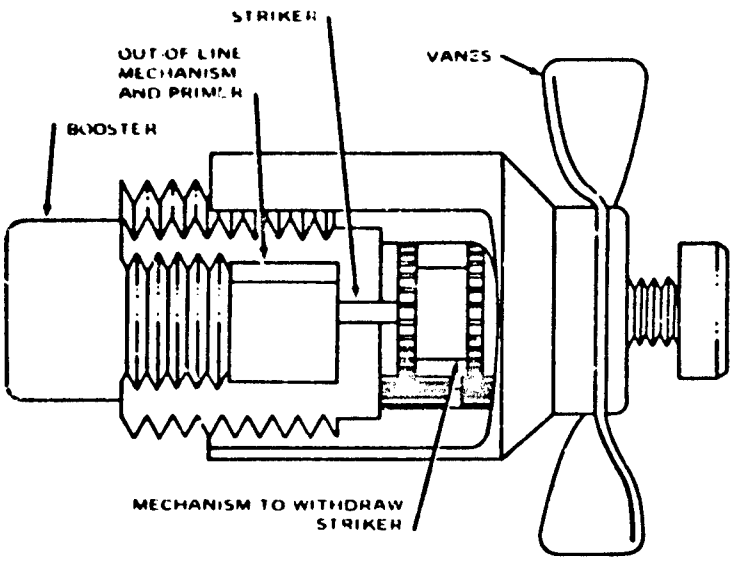

FIG. 3b. Simple Fuze Mechanism.

that are great enough to detonate the very insensitive explosive of the main charge.

DETONATION

The initiating system in a warhead differs from the ignition system in a gun in that it delivers *shock*, not heat, to the charge. The effect of the shock is to set up a detonation, which is an extremely high rate of energy release that sweeps through the charge at a rapid but *constant* rate. It will be recalled from the discussion of the internal ballistics of guns that detonation is the process that results from uncontrolled increase in the reaction rate of nitrocellulose with too high a porosity. Also the shape and size of powder grains are carefully chosen, and in some cases the surfaces are even coated with special stabilizing agents in order to control the burning rate and avoid detonation.

One of the surprising things about detonation is that while it can result from a runaway increase in reaction rate, it has stable and predictable

properties. How does this come about? Is there some reason to expect a stable limit on runaway reaction rates?

Suppose a reaction in a given material is continually increasing. For a propellant the reaction occurs by the advance of a flame front into the reactive material. Unreacted material goes into the front surface of the reaction zone, and completely reacted material comes out of the rear surface of the zone. The reaction rate determines the rate at which the zone sweeps over the material. If the reaction rate increases indefinitely, the rate of sweep increases indefinitely. When this rate of sweep reaches and surpasses the speed of sound in the material, the question of the propagation of mechanical disturbances from one point to another has a strong bearing on how the processes occur. At these speeds any mechanical effects due to the moving reaction zone cannot be communicated beyond a shock that travels just ahead of the reaction zone and at a velocity that depends on the intensity of the mechanical disturbances. In particular, increases in pressure and density due to the reaction cannot extend beyond the shock. The general properties of shocks are discussed in the Appendix.

These broad conclusions can be pictorially presented as in Fig. 39. It is assumed that the reaction zone is bounded by plane surfaces, and the drawing shows a cross section of the zone, which is moving from left to right. A plane shock wave travels in front of the reaction zone. This is the "sonic boom" for the supersonic motion of the reaction zone. *Ahead of the*

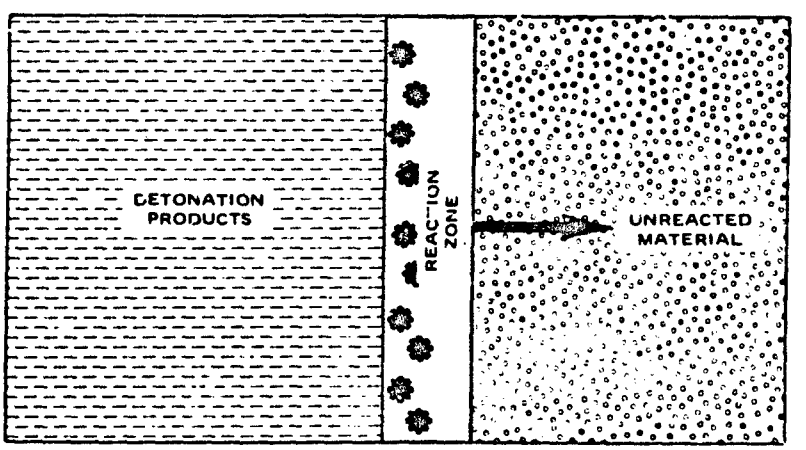

FIG 39. Plane Detonation Wave.

shock the material is undisturbed and unreacted. *At the shock* pressures and densities change abruptly because of the transmission of disturbances originating in the reaction zone. *Behind the shock and in the reaction zone* the chemical changes and release of energy take place. *Behind the reaction zone* the material is at a new pressure, density, and motion, and is composed of new chemical species the detonation products. (For further details see Ref. 1, 2, and 24.)

The notion that detonation is a shock phenomenon is verified by high-speed photography and by special instrumentation capable of measuring very rapid rises of pressure at extremely high intensity. It might be expected that the quantitative description of detonation waves could be accomplished by applying the procedures that are used in ordinary shock theory, specifically the formulation of conservation principles for a moving discontinuity. The application of shock wave theory to detonation waves leads to a theory of stable detonations that is known as the hydrodynamic theory.

Hydrodynamic Theory of Detonation

Figure 40 shows the detonation of a cylinder with cross section A and the detonation initiated at one end. The reaction zone is a disk that sweeps along the cylinder at velocity D. Conservation of mass, momentum, and energy will be applied to the flow through the reaction zone. Material flows into the front of the disk at velocity D, and detonation products flow out of the rear of the disk at velocity $D - u$, where u is the velocity given to the detonation products and is positive in the direction of the

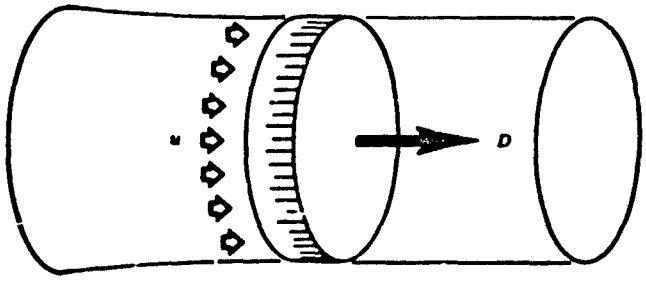

FIG. 40. Detonation of a Cylinder of Explosive.

motion of the reaction zone. Conservation of mass, momentum, or energy is satisfied if the difference between the flow of the given quantity into the zone and out of the zone is equal to the amount added within the reaction zone.

Conservation of Mass. During a unit interval of time there will flow into the reaction zone a cylinder of explosive of cross-sectional area A that has a volume

$$\tau_1 = DA$$

and the mass of the volume is

$$m_1 = \rho_1 DA$$

At the same time there will flow out of the reaction zone a cylinder of detonation products that has a volume

$$\tau_2 = (D - u)A$$

and mass

$$m_2 = \rho_2(D - u)A$$

No mass can be added within the reaction zone; hence conservation requires

$$\rho_1 DA - \rho_2(D - u)A - 0$$

or

$$\rho_1 D - \rho_2(D - u) = 0 \qquad (5\text{-}1)$$

Conservation of Momentum. The mass $\rho_1 DA$ that flowed into the reaction zone had a velocity D, and the mass $\rho_2(D - u)A$ had a velocity $(D - u)$; hence the change in momentum is

$$[\rho_2(D - u)A](D - u) - (\rho DA)D$$

The amount of momentum within the zone can be increased by the amount of force acting on the zone. The force is given by the difference in the

pressures acting over the area A:

$$p_2A - p_1A$$

thus

$$\rho_1 D_1^2 - \rho_2(D - u)^2 = p_2 - p_1 \qquad (5\text{-}2)$$

Conservation of Energy. The energy density in the material is the sum of the internal energy and the kinetic energy per unit mass

$$e = \left(E + \frac{v^2}{2}\right)$$

The flow of energy into the reaction zone is

$$A\rho_1 D\left(E_1 + \frac{D^2}{2}\right)$$

and the flow out is

$$A\rho_2(D - u)\left[E_2 + \frac{(D - u)^2}{2}\right]$$

The work done by the pressures p_1 and p_2 is Ap_1D and $Ap_2(D + u)$, which adds to the energy of the system to give

$$\rho_1 D\left(E_1 + \frac{D_2^2}{2}\right) - \rho_2(D - u)\left(E_2 + \frac{D - u^2}{2}\right) = p_2(D - u) - p_1 D$$

or this can be rearranged to give

$$E_1 + \frac{D^2}{2} + \frac{p_1}{\rho_1} = \left(E_2 + \frac{(D - u)^2}{2} + \frac{p_2}{\rho_2}\right) \qquad (5\text{-}3)$$

Detonation Velocity

The equations of conservation of mass (Eq. 5-1) and momentum (Eq.

5-2) are sufficient to determine the relationship between the shock propagation rate and the difference in pressure and specific volume across the shock.

$$D = \frac{1}{\rho_1}\sqrt{\frac{p_2 - p_1}{\frac{1}{\rho_1} - \frac{1}{\rho_2}}} \tag{5-4}$$

and also the relationship between the particle velocity u and the jump conditions (abrupt changes in pressure and density) at the shock.

Particle Velocity

The particle velocity is found to depend on the jump conditions in the form

$$u = \frac{1}{\rho_1} - \frac{1}{\rho_2}\sqrt{\frac{p_2 - p_1}{\frac{1}{\rho_1} - \frac{1}{\rho_2}}} \tag{5-5}$$

Hugoniot Relation and Hugoniot Curve

All three conservation equations can be used to determine a relationship between the difference in energy density across the shock and the jump conditions at the shock of the detonation wave. This turns out to be

$$e_2 - e_1 = \frac{(p_2 + p_1)}{2}\left(\frac{1}{\rho_1} - \frac{1}{\rho_2}\right) \tag{5-6}$$

This equation is called the Hugoniot relation for the traveling reaction zone. For a given value in the jump of the energy density and given values of p_1 and ρ_1 the Hugoniot relation defines a curve in the $p - \tau$ plane that, like the isothermal curve and adiabatic curve, defines a particular thermodynamic process. The process defined by this Hugoniot curve is thermodynamic change across the detonation wave (specifically, the change from the values p, $1/\rho_1$ in the undisturbed material to the state behind the reaction zone).

The Hugoniot curve for a detonation wave has formal similarities to the Hugoniot curve for an ordinary shock. The important differences are that it specifies the correlation of pressures and specific volume for a different material than that of the initial state so that the point p_1, $1/\rho_1$ is not on the Hugoniot curve. As for shocks, the velocity of propagation of the detonation wave is given by the slope of the line that joins the point p_1, $1/\rho_1$ and a point on the Hugoniot curve.

The major problem in determining the Hugoniot curve for a specific explosive is the calculation of e_2 and the constituents of the reaction products. The required information is an accurate equation of state of the detonation products at the pressure and density of the explosive shock and data on chemical equilibrium at the temperatures and pressures of the explosive shock.

Internal ballistic theory uses Eq. 1-12

$$p(\tau - b) = nRT$$

which is a simplified form of the van der Waals equation

$$\left(p + \frac{n^2 a}{\tau^2}\right)(\tau - nb) = nRT$$

Neither of these equations is sufficiently accurate at high pressures and densities for application to detonation theory. Other equations that have been used with varying degrees of success are the Kistiakowsky-Wilson equation,

$$p_\tau = nRT\left[1 - \frac{kT}{v}\exp\left(\frac{kT}{v}\right)\right] \qquad (5\text{-}7)$$

the Patterson equation,

$$p = nRT(1 + b\rho + 0.625b^2\rho^2 + 0.287b^3\rho^3 + 0.193b^4\rho^4) \qquad (5\text{-}8)$$

and equations like the Wilkins equation that have the form

$$p = a_1\tau + a_2\exp(-a_3\tau) + a_4\tau a_5 \qquad (5\text{-}9)$$

where a_1, a_2, a_3, a_4, and a_5 are constants that have theoretical or empirical

derivations.

The form that is universally correct or even correct for a specific material could be chosen if accurate measurements of pressure were readily available at the shock conditions. Experimental techniques are not available for doing this, so the decision must be based on attempts to get internally consistent predictions of the detonation velocity, composition of the reaction products, and available measurements of pressure and temperature.

Chapman-Jouget Hypothesis

Detonations are reproducible stable events. TNT, for example, will detonate at a velocity of about 6,700 m/sec. The exact value depends on the temperature, density, and method of preparation of the sample of explosive. If these parameters are controlled, there will be very little difference in the propagation rates for different samples or the value of the propagation rate during its travel through a given piece of explosive. The preceding applications of conservation laws to the flow associated with a propagating reaction zone do not lead to a prediction of constant propagation rate; however, these results do provide a basis for further investigation into possible causes of the constant propagation rate.

First of all, Eq. 5-1, 5-2, and 5-3 are not sufficient mathematically to establish a fixed value of D for given initial conditions. There are too many unknowns for the number of equations. In terms of physical principles this means that conservation of mass, momentum, and energy does not place enough restrictions on the flow through the traveling reaction zone to establish a unique propagation rate, and other restrictions on physical processes will have to be found. Two hypotheses were put forward by Chapman and Jouget.

Chapman assumed that the shock velocity was the minimum rate consistent with the shock conditions. The shock velocity is given by the slope of the line connecting the point 0 with a point on the Hugoniot curve. For a curve with the shape shown in Fig. 41 this hypothesis selects the point CJ, which is called the Chapman-Jouget point, as the value of the final state that determines D.

Jouget assumed that the propagation velocity would just equal the local propagation rate of finite but continuous disturbances, $D = c + u$, where c is the local sound speed. If the rate $c + u > D$, then relief processes behind the shock can catch up with it and change its rate. It can

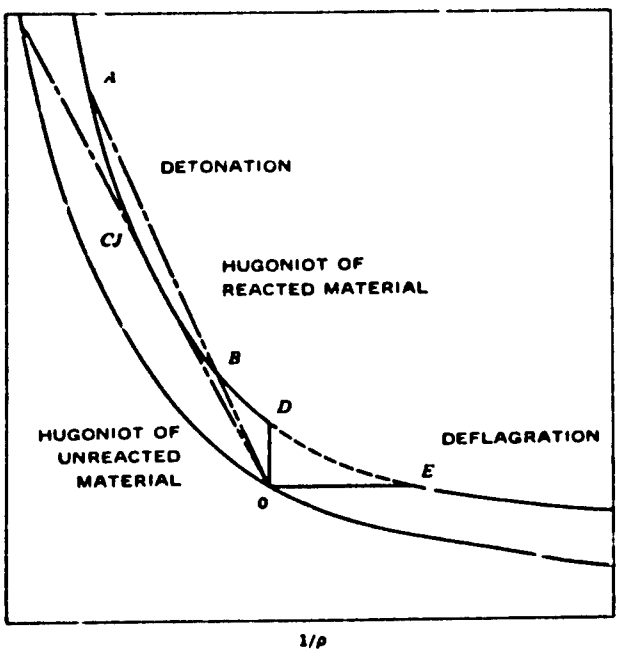

FIG. 41. Hugoniot Curves for the Unreacted and Reacted Material in a Detonation.

also be shown that the adiabat and the Hugoniot coincide at the point *CJ* so that both hypotheses are in agreement (Ref. 24). Also, points above *CJ* are states of lower entropy and therefore are thermodynamically unstable. Points below *CJ* will have propagation rates less than relief processes and are therefore mechanically unstable. The Chapman-Jouget condition is left as the only stable process.

Deflagration and Detonation

The Hugoniot curve has some properties that help to distinguish between deflagration and detonation. There is a segment *DE* that is directly above the initial state point 0 and extends to the right in which the radical of the equation for D and u is imaginary and therefore does not correspond to physically realizable situations. To the right of this segment particle velocities are in the opposite direction to the propagation of the reaction

zone, and pressures and propagation rate are low. To the left of the segment *DE* particle velocities are in the direction of propagation of the reaction zone and the pressures and propagation rate are high. Thus, the Hugoniot curve implies two distinct processes: deflagration on the right, which has all the properties that describe propellant burning, and detonation on the left.

A moving reaction zone is common to both deflagration and detonation, but the details of the events in the zone are very different. As was described in the internal ballistics of projectiles, if deflagrations are comparatively slow and the pressures are not excessively high, the reaction propagates by thermal processes, and heat is the important quantity. In detonations the chemical breakdown is started by an intense pressure in a shock. There is no time for thermal conduction in the detonation process, and the pressures are sufficiently intense to cause chemical decomposition and even ionization.

TYPES OF EXPLOSIVES

Anything that goes into an artiliery shell or a guided missile warhead has to be able to take extremely rough handling both prior to operation and during the interior and exterior ballistic phases of delivery. Explosive components must in addition respond to comparatively low-energy electrical and mechanical actuating signals. Explosive devices can meet these requirements because of the variety of materials that are available and their wide range of sensitivity to shock and heat. Explosives that are detonated most readily are called *primary explosives*. Explosives that are detonated by only the most intense shocks are called *secondary explosives, or high explosives.*

Primary Explosives

Examples of primary explosives are lead azide, lead styphnate, DDNP (diazonitrophenol), and tetracene. Mercury fulminate is another well-known primary explosive that is no longer in common use because of its poor storage properties. Lead azide has the formula $Pb(N_3)_2$. It is used either alone in detonators and primers or in combination with lead styphnate,

which serves to sensitize it to flame. Lead styphnate has the formula $(NO_2)_3C_6HO_2Pb$. DDNP has a formula

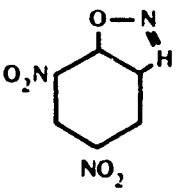

and is used in detonators. Tetracene has the formula

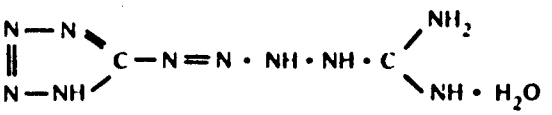

and is used with lead styphnate in primers. A summary of the properties of these explosives is given in Table 7.

TABLE 7. Properties of Some Primary Explosives.

Primary explosive	D, m/sec	Density, g/cm^3	Minimum charge (g) to detonate		
			TNT	Tetryl	PETN
Lead azide	4,500	3.8	0.25	0.10	0.02
Lead styphnate	4,900	2.6	...[a]	...[a]	0.55
DDNP	6,900	1.58	0.15	0.12	...

[a] Primary explosive will not initiate the secondary explosive.

Detonators

Devices that produce a shock in a secondary explosive that is capable of initiating a detonation are called detonators. These devices consist of a means of applying a source of electrical energy, thermal energy, or mechanical energy to sensitive explosives. The properties of the primary explosives mentioned above are further illustrated by the way these are used to initiate high explosives.

Figure 42 shows the internal structure of a commercial detonator. A bridge wire is attached between copper leads and is surrounded by lead

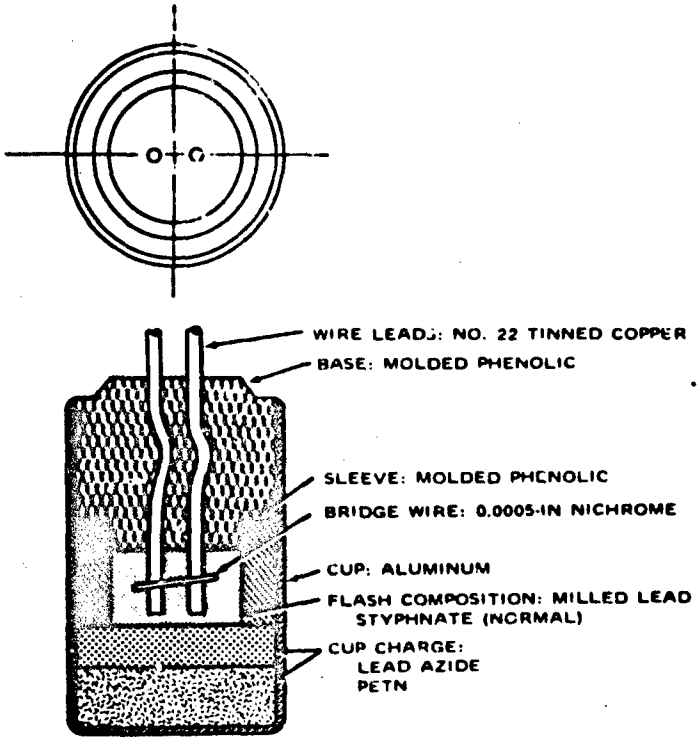

FIG. 42. Detonator With Nichrome Bridge Wire.

styphnate. The lead styphnate is particularly sensitive to friction, impact, and flame, and it reacts readily to the heat from the bridge wire. The lead styphnate is in contact with a layer of lead azide followed by PETN. Figure 43 shows a slightly different design that uses Aquadag, a commercial product with colloidal graphite in place of a bridge wire. The flash composition in this device is lead azide alone. The lead azide is in contact with PETN.

Powders used in guns are composed of a few basic ingredients: black powder, nitrocellulose, and nitroglycerin. On the other hand there is a very long list of materials that will detonate. The list can be drastically pared by the safety and storage requirements for military applications, but the

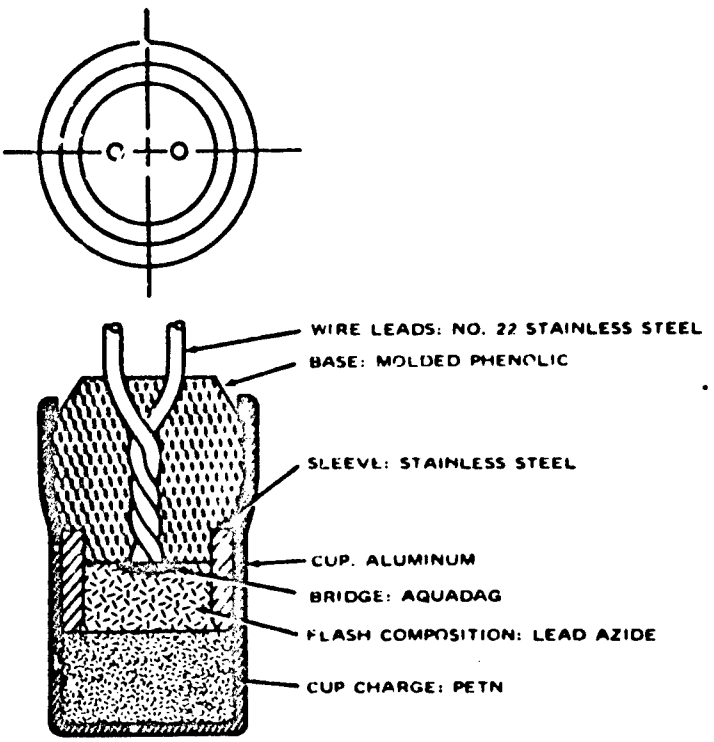

FIG. 43. Detonator With Aquadag Bridge.

number of usable explosives still exceeds the number of main propellant ingredients.

Secondary Explosives

The main constituents of military explosives are described below in just enough detail to identify the materials.

TNT (*trinitrotoluene*) is one of the least sensitive of military explosives. It has good storage characteristics and is used alone (infrequently) and in combination with other materials.

TNT

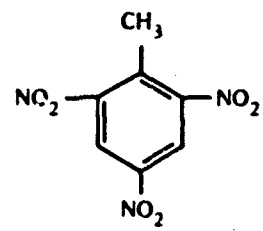

PETN (*pentaerythritol tetranitrate*) is stable chemically and thermally, but is excessively sensitive to friction and impact and is consequently used as a primary explosive but not as the main charge in a warhead.

PETN

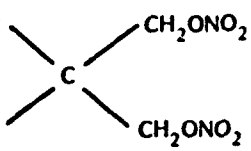

RDX (*cyclotrimethylene trinitramine*) is stable chemically and thermally and while less sensitive than PETN it is still too sensitive to be used as a warhead filling.

RDX

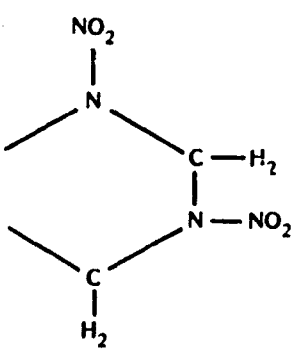

HMX (*tetramethylene tetranitramine*) is an explosive of high power and stability with somewhat the same sensitivity as RDX. It is used in combination and not alone.

HMX

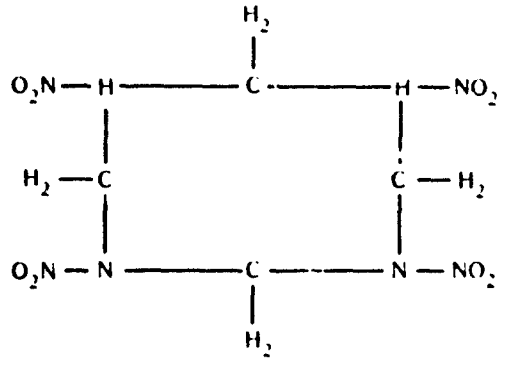

Tetryl (2:4:6 *trinitrophenylmethylnitramine*) is a moderately sensitive explosive that is usually used as a booster.

TETRYL

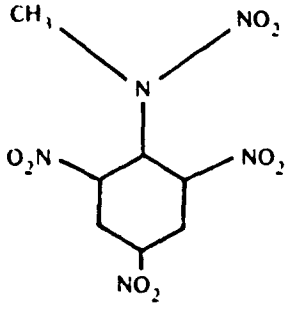

Common Explosive Mixtures

Military explosives are most often mixtures of explosives that have sensitivities and mechanical properties that are better for the given application than the pure components. For example, mixtures of TNT and PETN are called *pentolites*. Pentolites have higher detonation velocities than TNT, but also have lower sensitivities than PETN and are easier to use as a warhead case filling. Similarly, *cyclotols* are mixtures of TNT and RDX, and *octols* are mixtures of TNT and HMX. These mixtures, like the pentolites, have higher performances than TNT and better sensitivities and handling characteristics than the RDX or HMX. The cyclotol whose composition is 60% RDX and 40% TNT is known as Composition B, a very common

filling for explosive warheads. Other additives include plastic binders to give desired physical characteristics and metals like aluminum to add energy to the mixture. Table 8 lists the composition of five common aluminized explosives. An extensive list of explosives is given in Ref. 2.

TABLE 8. Aluminized Explosives.

Name	Composition			
	Ammonium nitrate, %	RDX, %	TNT, %	Aluminum, %
Minol	40	...	40	20
Torpex	...	41	41	18
Tritonal	...	...	80	20
HBX [a]	...	40	38	17
H6 [b]	...	45	30	20

[a] Desensitizer, 5%.
[b] D-2 wax 5%, CaCl 0.5%.

FRAGMENT PROJECTION BY AN IDEALIZED WARHEAD

In the analogy between guns and warheads the expanding warhead case corresponds to the expanding volume behind the projectile as it travels down the barrel. Ultimately the case breaks up and the fragments travel on as independent projectiles. This corresponds to the projectile leaving the barrel. Expansion and fragmentation of the warhead case are the next considerations in the internal ballistics of warheads.

The warheads of many weapons that are intended to inflict damage by blast and fragmentation are close to cylindrical in shape so that a cylinder is a realistic as well as a simple model of many warheads. It is also a reasonable approximation to assume that a plane wave traveling along the axis of the cylinder represents the detonation wave. The initial pressure acting on the case is the *CJ* pressure of the detonation wave. For Composition B this pressure is 2.72 kilobars, and the wave is traveling through the explosive at 7,840 m/sec. This pressure is more than 13 times the yield strength of a very tough steel (52100 steel with a yield strength of 300,000 psi) so that it is evident that yielding will occur.

The case expands as is shown in Fig. 44a. Ultimately the case ruptures or fractures, producing discrete fragments. The detonation products flow around the fragments, but the fragments are still accelerated until the

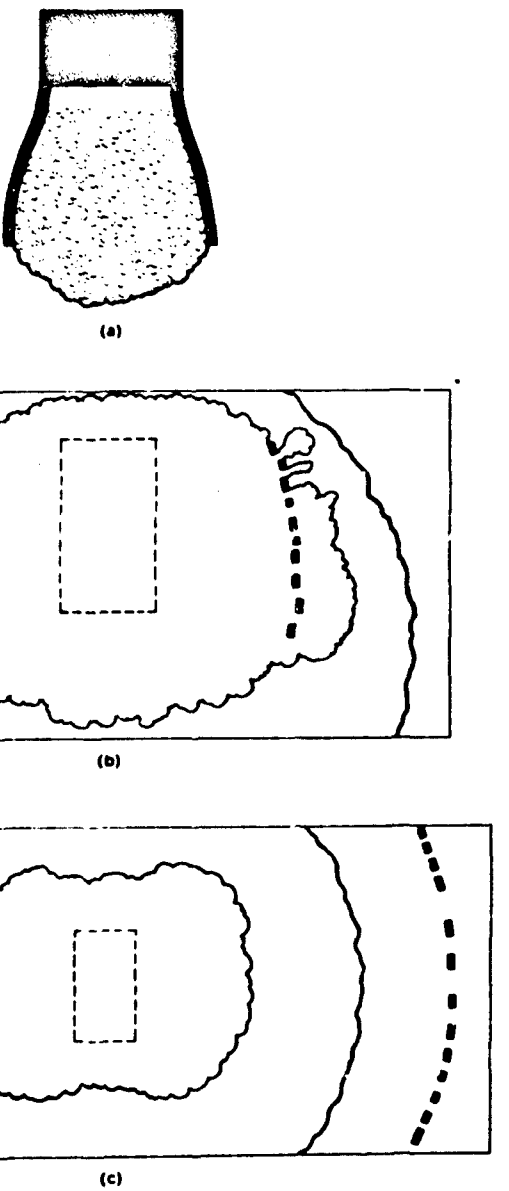

FIG. 44. Schematic Representation of the Expansion of a Warhead.

detonation products have negligible motion with respect to the fragments. While the fragments are being accelerated, the fragment system, detonation products, and blast wave (the shock from the explosive event) are qualitatively as shown in Fig. 44b. When the fragments are no longer accelerated, the internal ballistic phase is completed. (This can define the end of the internal ballistic phase, but it might be difficult to determine this time with any precision.)

After the internal ballistic phase is complete, the shock and the expanding products will have slowed down because of the attenuating effects of expansion. The fragments in general will have slowed down much less because the decelerating effect of drag forces is much less than the attenuating effects of expansion. As a result the fragments will lead both the shock and the explosive products. This is illustrated in Fig. 44c.

Figure 45 illustrates qualitatively what is happening to the detonation products during the expansion of the case. The detonation wave establishes the *CJ* pressure behind the detonation front. Lateral relief processes travel in toward the center of the cylinder at the rate c_2. Since the detonation rate D is greater than the relief wave propagation rate, the wave front is indicated by the line AB. There is also a relief wave traveling into the detonation products from the expansion of the products directly to the rear. This travels at a rate c_1 that is different from the rate c_2 because of the difference in intensity of the transmitted pressures. The arrows in the diagram indicate the relative intensity and direction of flow of the detonation products.

One of the most important kinds of information that is needed on the interior ballistics of warheads is the dependence of the velocity of the case (or case fragments) on the composition of the charge, the mass of the charge, the physical characteristics of the case, and its configuration. Fragment velocities can be estimated by an energy balance method that leads to simple formulas called the Gurney formulas (Ref. 25 and 26). These are obtained by equating the energy released by the explosive to the kinetic energy of the case and the detonation products. In the interior ballistics of guns this is equivalent to obtaining the limit velocity for a very long gun, Eq. 1-43, or setting the pressure equal to zero in Resal's equation, Eq. 1-17. The detonation products are in a cylindrical flow pattern, and the Lagrange correction k_2 must be calculated for that type of flow.

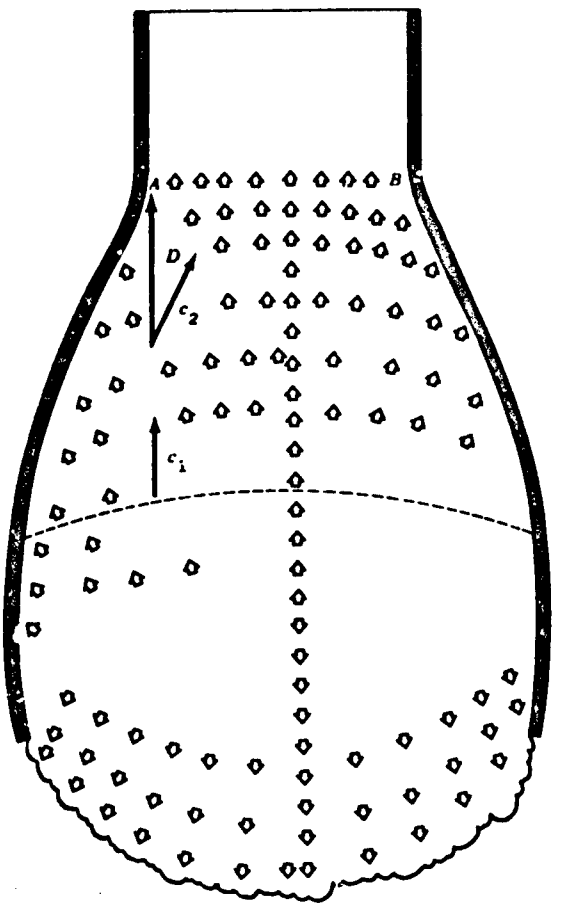

FIG. 45. Detonation Wave and Flow Velocities Within a Warhead Case.

The limit velocity of a gun is

$$v_{lim} = \sqrt{\frac{2F_c C/(\gamma - 1)}{k_2 m_1}} = \sqrt{\frac{2F_c/(\gamma - 1)}{\left(\frac{m_1}{C} + \frac{1}{3}\right)}} \qquad (5\text{-}10)$$

and the Gurney formula for the cylinder is

$$v = \sqrt{\frac{2EC}{k_2 m_c}} = \sqrt{\frac{2E}{\left(\frac{m_c}{C} + \frac{1}{2}\right)}} \tag{5-11}$$

where E is the energy released per unit mass of explosive and C is the explosive charge weight. The Lagrange correction is of course different for various configurations of a warhead. The constant $\sqrt{2E}$ is assumed to be a property of the explosive although it has been difficult to obtain agreement among measurements taken on different configurations and sizes of charges (see Ref. 26). Typical values are shown in Table 9.

TABLE 9. Gurney Constants for Various Explosives.

Explosive	Detonation rate, m/sec	Density, g/cm^3	$\sqrt{2E}$, ft/sec
TNT	6,640	1.59	7,600
RDX	8,180	1.65	9,300
HMX	9,124	1.84	10,230
PETN	8,300	1.73	9,300
Tetryl	7,850	1.62	8,200
Composition B	7,840	1.68	8,800
Octol	8,643	1.80	9,500

The Gurney constant has proved to be a useful figure of merit in the ranking of explosives according to performance in fragment projection. This suggests the use of the theory of an instantaneously burning propellant as a model for warhead case expansion. This can be done by modifying the internal ballistics of guns to account for the cylindrical expansion of the warhead. Specifically, Resal's equation and the equation of motion of the case must be modified to account for the cylindrical change of volume. It is convenient to consider the mass of the warhead case and charge in terms of weight per unit length of the cylinder, since this avoids an unnecessary explicit use of the cylinder length as a variable in the analysis.

Resal's equation with cylindrical expansion is

$$\frac{CF_c}{\gamma - 1} = \frac{pm^2}{\gamma - 1} + \frac{m_c k_2 v_c^2}{2} \tag{5-12}$$

and the equation of motion is

$$m_c \frac{dv_c}{dt} = 2\pi r p \tag{5-13}$$

In these equations m_c and C are the case and charge masses per unit length, and k_2 is a Lagrange correction. These equations have a solution

$$v_c = \sqrt{\frac{2CF_c}{m_c k_2(\gamma - 1)}} \quad \sqrt{1 - \left(\frac{r_0}{r}\right)^{2(\gamma - 1)}} \tag{5-14}$$

or in the Gurney notation

$$v_c = \sqrt{\frac{2E}{\left(\frac{m_c}{C} + \frac{1}{2}\right)}} \quad \sqrt{1 - \left(\frac{r_0}{r}\right)^{2(\gamma - 1)}} \tag{5-15}$$

Figures 46 and 47 show the velocity as a function of case expansion and the displacement of the case as a function of time for two values of γ. The literal interpretation of this model is that all the points of the case expand at the same rate. This of course is not true, since the energy release rate is known to be extremely rapid but nevertheless finite and such that the development of the release process spreads through the explosive at a finite and constant rate. A simple change of interpretation will at least qualitatively account for the finite propagation rate. This is to assume that the starting time for expansion process changes from point to point along the length of the case according to the fixed detonation rate. This implicitly assumes that the expansion at each point along the length is independent of expansion immediately adjacent to it. This is very likely approximately true.

The expansion of a cylindrical case is typical of the military application of an explosive, and this process is used as a measure of explosive performance. Current opinion is that expansion tests are the most reliable measures of explosive performance. Other tests such as the Trauzl lead block test in which the deformation of a lead block is a measure of performance, or ballistic mortar tests in which the response of a ballistic

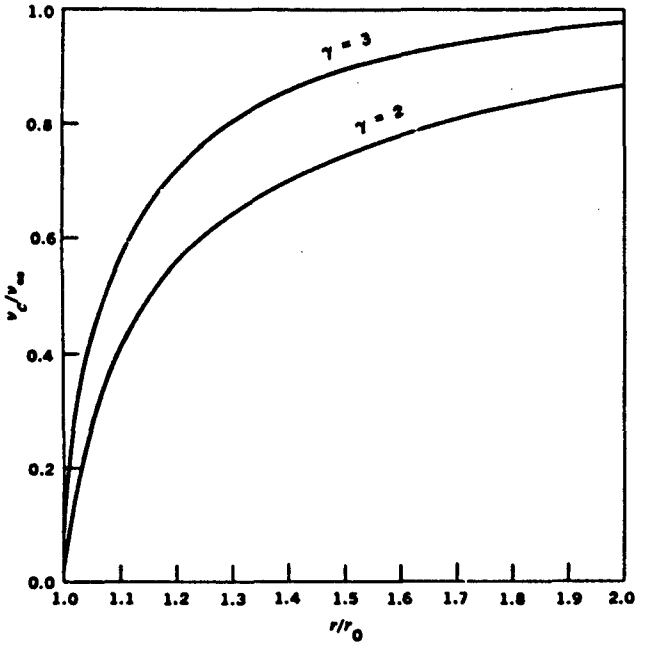

FIG. 46. Case Velocity as a Function of Case Expansion.

pendulum to standard charges of explosive is a measure of performance, do not give results that provide for consistent ranking of the explosive performance.

The cylinder expansion test consists of a standardized geometry, mode of initiation, point of observation, and mode of observation. The test geometry consists of a 1-inch-diameter, 12-inch-long explosive charge in an 0.1022-inch-thick copper tube. The charge is initiated by a plane wave lens and a 0.5-inch-thick Composition B booster. Measurements are made at a point 7 inches from the booster end. A streak camera is used to measure the case expansion, using conventional backlighting and shadowgraph techniques. Table 10 summarizes the results.

The fragment velocities from warheads can be higher than the muzzle velocities of conventional guns, as shown in Table 11.

The high pressures of detonation cause expansion of the warhead case through large plastic deformation, but eventually the plastic deformations are terminated by fractures that break the case into distinct fragments. The

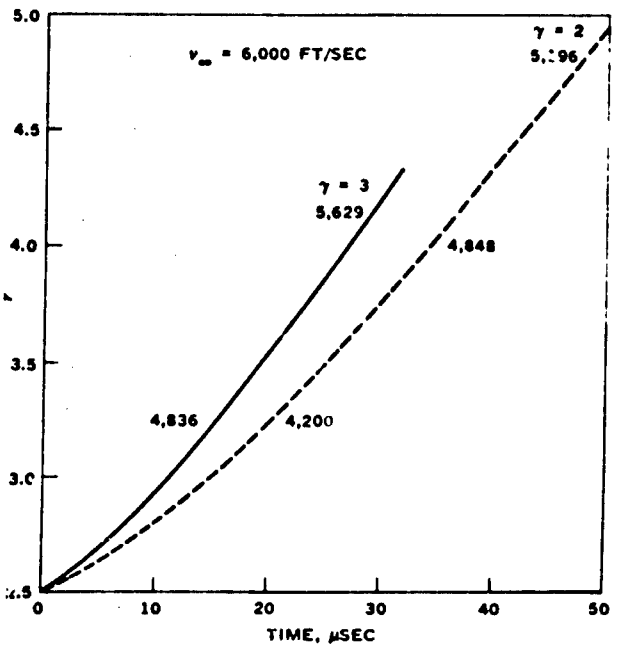

FIG. 47. Case Expansion as a Function of Time.

size and shape of the case fragments depend on the details of the fracture processes. The development of these fractures can be observed by high-speed photography and analyzed by applying static and dynamic principle-of-failure mechanics (Ref. 16).

The failure of a warhead case is complex, and it is useful to use models that simplify the description of internal ballistics. The Gurney

TABLE 10. Results of Cylinder-Expansion Tests for Various Explosives.

Explosive	Density, g/cm^3	Detonation rate, km/sec	Cylinder wall velocity, km/sec	
			$r - r_0$ = 5 mm	$r - r_0$ = 19 mm
HMX	1.891	9.11	1.65	1.86
PETN	1.765	9.16	1.56	1.79
Octol 78/22	1.821	8.48	1.54	1.77
Cyclotol 77/23	1.754	8.25	1.46	1.70
Composition B 64/36	1.717	7.99	1.39	1.63
TNT	1.630	6.94	1.18	1.40

TABLE 11. Projectile and Fragment Masses and Velocities for Various Ammunition.

Type of projectile or fragment	Velocity, ft/sec	Projectile or fragment mass
Projectiles		
.30-caliber rifle	2,800	150 grains
75-mm gun M3	2,030	14 pounds
105-mm howitzer	1,550	33 pounds
155-gun M1	2,745	100 pounds
Fragmenting warheads		
TNT-loaded, C/m = 0.05	1,700	Fragment size depends on the warhead case material[a]
TNT-loaded, C/m = 0.5	4,800	
Octol-loaded, C/m = 0.05	2,100	
Octol-loaded, C/m = 0.5	6,000	

[a] For a warhead with C/M = 0.7, firings range in size from 0 to 1,000 grains, with a majority of fragments 100 grains.

formulas for fragment velocities are equivalent to assuming a model of internal ballistics with instantaneous reaction of the explosive so that the full pressure of the detonation is developed over the entire interior of the warhead case at the start of case expansion. If this model is used for case failure, it is equivalent to using static pressure theory; the warhead case is considered to be a cylindrical tank with an internal pressure equal to the detonation pressure; the pressure exceeds the yield stress of the tank and it fails by tensile or shear fractures.

A more precise model of the internal ballistics allows for the distribution of the pressure by the detonation wave at the finite detonation velocity. The mechanics of failure in this model must allow for the rapid but finite propagation of changes in pressure through the case material by stress-wave motion, and for any mechanical properties that are affected by rapid strain rates. In the following, the theory of the failure of static pressure vessels is applied to warhead fragmentation. The conclusions are then corrected where these are at variance with the conclusions from the more precise model or with empirical observations.

One major value of the static theory is the predicting of the geometries of fractures that occur in the warhead case. The fractures are either shear or tensile forms. Shear fractures follow the trajectories of

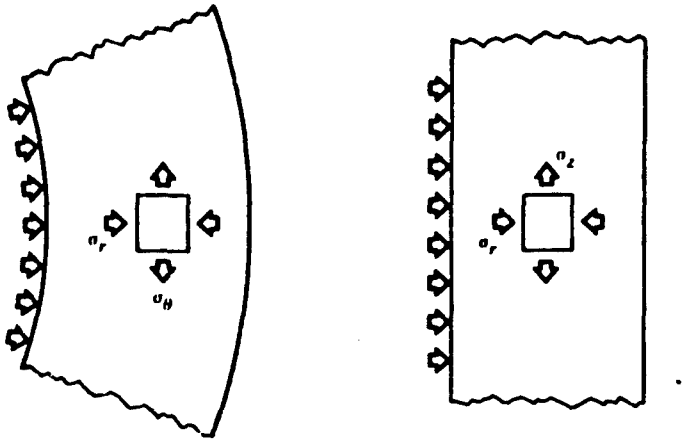

FIG. 48. Components of Stress Within the Wall of a Warhead Case.

maximum shear; tensile fractures occur on planes that are perpendicular to a principal stress. The components of stress within the wall of a warhead case are shown in Fig. 48 in cylindrical coordinates. Because of the symmetry of the load on the cylinder, these stress components σ_r, σ_θ, and σ_z are principal stresses.

Most pressure vessel theory is based on stress solutions derived by Lamé about 1832-52. The solution assumes a static load within the vessel and elastic behavior of the vessel material. These assumptions are not sufficiently realistic for a warhead to allow precise calculation of the stresses and stress distributions, but solutions based on these assumptions are qualitatively correct and have the correct geometries of the fracture systems.

The solutions are derived from an elemental force balance in terms of stress into which strains are substituted through the elastic stress-strain relations to obtain second-order differential equations. These are solved for the specific boundary conditions in the inner and outer surfaces of the internally loaded cylinder. When treated as a problem in plane strain (σ_z = 0), the solution is

$$\sigma_\theta = \frac{a^2 p_i}{b^2 - a^2}\left(1 + \frac{b^2}{r^2}\right) \tag{5-16}$$

where a and b are the inner and outer diameters of the cylinder, respectively.

$$\sigma_r = \frac{a^2 p_i}{b^2 - a^2}\left(1 - \frac{b^2}{r^2}\right) \tag{5-17}$$

$$\sigma_{\theta r} = \frac{a^2 b^2 p_i}{r^2 (b^2 - a^2)} \tag{5-18}$$

All stresses are at a maximum on the inside surface of the pressure vessel; for static loading, failure is expected to start there. This conclusion may not be valid for dynamic loading.

The orientation of the primary tensile fractures can be determined by comparing the relative stress values for the three principal stresses. In a warhead case $\sigma_z \neq 0$ due to the geometry of the distortion, and for a static pressure vessel $\sigma_z \neq 0$ as the result of the action of the pressure on the end closures. The component σ_z can be calculated for static loading by use of a force balance.

$$p_i(A)_{\text{end}} = \sigma_z(A)_{\text{cross section}}$$

so that

$$\sigma_z = \frac{p_i a^2}{(b^2 - a^2)}$$

and the values of σ_θ and σ_z on the inner and outer surfaces are

$$\sigma_\theta \Big|_{r=b} = 2\sigma_z$$

$$\sigma_\theta \Big|_{r=a} = \left(\sigma_z + \frac{p_i b^2}{a^2 + b^2}\right) > 2\sigma_z$$

Thus $\sigma_\theta > \sigma_z$, and since σ_r is compressive while σ_θ and σ_z are tensile, the component σ_θ is the greatest tensile stress component, and tensile fractures will be associated with σ_θ. Since tensile fractures will be on the plane perpendicular to the appropriate principal stress, the primary tensile

fractures will be radial. This conclusion holds for both static pressure vessels and warhead cases.

The trajectories of maximum shear are logarithmic spirals that are mutually orthogonal. A useful property of these trajectories is that they keep the same geometry in either the elastic or the fully yielded condition. The specific orientation of the primary shear fracture is determined by the fact that shear fractures will occur on planes of maximum shear stress, and thus the primary shear will be associated with $\tau_{\theta r}$, $\tau_{\theta z}$, or τ_{zr}, whichever is greatest.

When σ_θ, σ_r, and σ_z are the principal stresses, the shear stresses are

$$\sigma_{\theta r} = \frac{\sigma_\theta - \sigma_r}{2} \quad \sigma_{zr} = \frac{\sigma_z - \sigma_r}{2} \quad \sigma_{\theta z} = \frac{\sigma_\theta - \sigma_z}{2} \tag{5-19}$$

The components σ_z and σ_θ are tensile, and the component σ_r is compressive; σ_θ is greater than σ_z so that the maximum shear is $\sigma_{\theta r}$. Shear failure will occur at 45 degrees to σ_θ and σ_r. This same conclusion can also be obtained by the graphical plot of Fig. 49 (Ref. 27). This prediction of

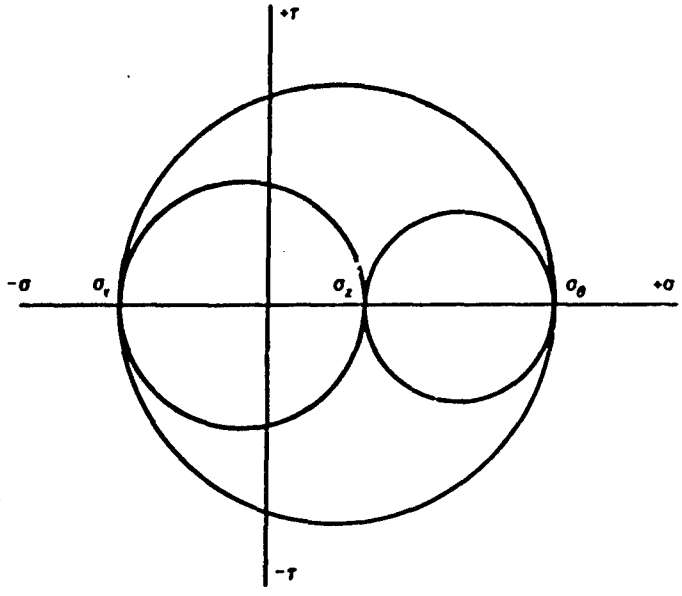

FIG. 49. Mohr's Circle Representation of Stresses.

the orientation of the primary shear fracture holds for either a static pressure vessel or the dynamic loading within a warhead.

The primary fractures of warhead fragmentation will be either tensile or shear. Criteria are needed for determining which mode of fracture will occur in a given warhead. Ductility, which is the capacity of a material to sustain plastic deformation before fracture, is found to be the material property that correlates most strongly with the primary mode of fracture. Warhead cases of very brittle materials such as high-carbon steels; or the high-strength, heat-treatable alloy steels fail by tensile fracture, and the fracture system is not conspicuously dependent on the thickness of the warhead case. Ductile materials such as the plain, low-carbon steels (i.e., SAE 1010–1020) fracture by both tensile and shear modes, and the system of fractures changes with increases of case thickness.

Ductility is a property of material that depends on its composition, internal structure, and temperature. Ductility also depends on the type of loading, in particular on two loading parameters, the strain rate, and the hydrostatic pressure. The yield strength of many materials is increased by increases in strain rate, but the capacity of the material to absorb energy by deformation is also decreased so that the material loses ductility. The loads on a warhead case are applied at extremely high rates, and therefore the materials of warhead cases might be expected to behave like brittle materials no matter how ductile they are under conventional loading. Actually, this shift toward brittleness is not evident in case fragmentation. This may be due to the fact that the effect of hydrostatic pressures on ductility opposes that of strain rate.

The properties of materials under high pressure were investigated (Ref. 26) by subjecting a rod to both a tensile force above the yield point and a hydrostatic pressure of up to 450,000 psi. Observations indicated that as the pressure increases the ductility increases, and increases in the hydrostatic pressure cause changes from tensile to shear modes of fracture—and ultimately, to no fracture at all. These results are qualitatively indicated in Fig. 50, which represents four test specimens that were subjected to increasing pressures. In the figure, the pressure applied to the specimens increases from left to right. The specimen on the extreme left was tested under ambient pressure and has failed by a tensile mode over a large zone that is surrounded by a smaller zone of failure in the shear mode. The test specimens show progressively less tensile fracture with increased hydrostatic pressure. If the pressures are sufficiently high, a sample of ductile steel can

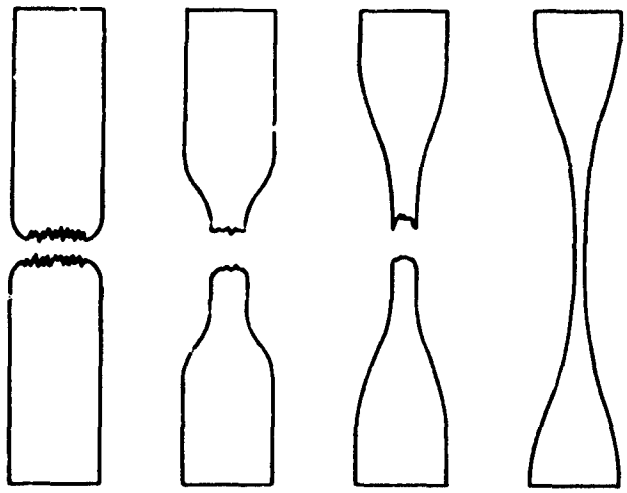

FIG. 50. Four Specimens From Tests at Different Hydrostatic Pressures.

be drawn out to a wire. This effect is not so obvious with less ductile metals. This observation is especially important since this sort of effect takes place near the inner surface of warhead cases.

At the present time there is no definitive synthesis of the strain-rate effect and the hydrostatic effect into a single measure of ductility, but experience shows that the fracture systems of warhead fragmentation can be ordered by classifying materials as "ductile" or "brittle," and, in general, materials can be so classified on the basis of quasistatic tests in a materials laboratory.

When fragmentation behavior is compared to ductility, there will be a class of brittle materials. In quasistatic tests, these materials may be very strong (have high yield strength) but go from elastic behavior to fracture with only small amounts of plastic deformation intervening. Warhead cases made of these materials fragment by tensile fractures. The fracture system is complicated, and a large number of fragments are produced. The system of fractures does not change significantly with wall thickness.

There will also be a class of ductile materials. In quasistatic tests these materials require moderate to large amounts of plastic deformation for the onset of fracture. Warhead cases of these materials are fragmented by both tensile and shear fractures. The location of the fractures and the particular

combination of tensile and shear modes of fracture in the system depend on the wall thickness so that these ductile materials exhibit a greater diversity in the forms of fragmentation than brittle materials, and warhead fragmentation has to be discussed according to case thickness. In a thin-walled case, the primary fractures are shear fractures and are initiated on the outside surface, which is contrary to the prediction of the static pressure theory. Above some thickness the fracture system includes both shear and tensile fractures, with the tensile fracture initiated on the outside surface. In very-thick-walled cases, the tensile mode will start inside the wall.

Figure 51 is a diagram of a section of a very-thick-walled case. The stress components σ_r and σ_z are indicated, and the component σ_θ is perpendicular to these components. The wall thickness is divided into radial segments A and B. For radii in segment A, the effects of σ_z and σ_r predominate to inhibit tensile fracture. Failure occurs by shear. In the region B, the effects of σ_z and σ_r are reduced so that the effect of σ_θ can be dominant, and the material fails in tension. The tensile fracture will tend to start on the inner radius of B and propagate outward.

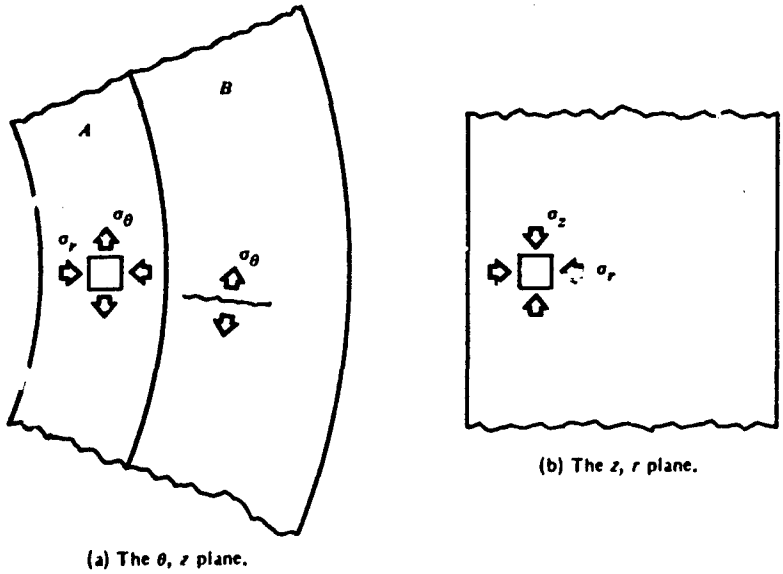

(a) The θ, z plane.

(b) The z, r plane.

FIG. 51. Cross Section of a Thick-Walled Cylindrical Case.

A thin-walled case of ductile material is capable of undergoing large deformation. and there are two phases of interest. In the first phase, the pressure of the detonation is transmitted from the inner surface outward. The stress components are those for a stress wave with stress combination well above the yield condition. The stress condition is that given in Ref. 26 and the conclusions on the increase of ductility will apply. In the second phase, the case is given significant motion, and there is a large distortion of the case along the axis of the case so that the component σ_z becomes tensile. If all the failure is by shear, the fractures start at the outside surface when the diameter is approximately 1.6 times the initial diameter. If there is a thin tensile zone near the outer surface, the tensile fractures start at the outside surface and run inward to link up with independent shear fractures.

SHAPED CHARGES

Another application of explosives as accelerators of metal is to warhead cases with specially designed cavities such that the acceleration of the metal into the cavity by a detonation wave causes a convergent flow of liner material. The resultant flow frequently forms a jet about the line or plane of symmetry of the convergent flow. For example, a symmetrically collapsing cone, shown in Fig. 52, has a convergent flow about the axis of the cone, and a jet develops along the axis. A symmetrically collapsing wedge, shown in Fig. 53, has a convergent flow about the plane that bisects the wedge angle, and a sheet-like jet develops on that plane. These are

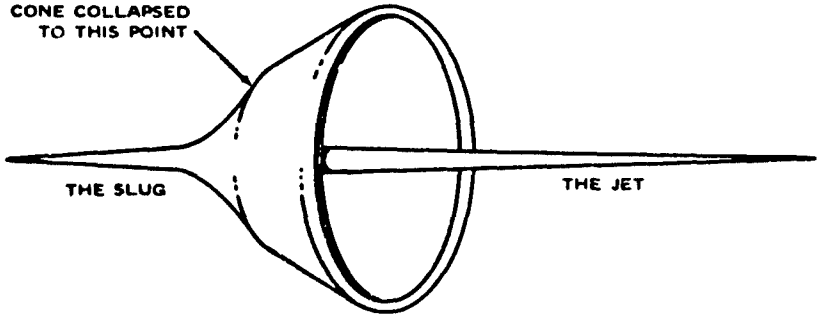

FIG. 52. Collapse of a Cone Under Explosive Loading.

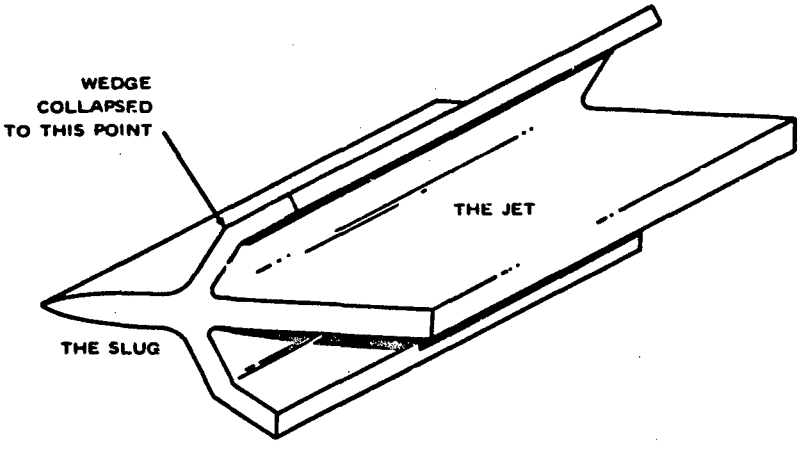

FIG. 53. Collapse of a Wedge Under Explosive Loading.

examples of what are called *conical* and *linear shaped charges*. The effect of the collapsing cavity is to concentrate the projection of case material in a single direction. With proper choice of the shape of the cavity the jets can be given high velocities and have highly desirable terminal ballistic performance.

Why does a jet form? Consider the case of wedge collapse. The collapse of a wedge cavity is a collision of two plates at an obliquity. After the collision begins, part of the plates will be mutually deformed as the result of contact, and parts will be headed toward direct contact. If these parts that are headed for direct contact are unaffected by the contact already established, then the contact develops at the intersection of the inner planes of the moving plates; however, unless the intersection is moving faster than the speed of stress waves, stress waves travel out from the intersection into the parts of the plates that are not in contact. This transmission of collision pressures must be accompanied by deformations along the free surfaces in order to maintain the stress-free boundary condition. At the very high rates of collision caused by explosive projection of the plates the pressures in the stress waves will be extreme, the response of the material of the plates will be large deformations (the material will be almost fluid in its response to the stresses), and deformations will be symmetrical about the plane of symmetry of the collapse process. This leads

to extruded material along the plane that bisects the angle between the collapsing plates.

A conical shaped charge consists of a conical metal liner surrounded by an explosive that is initiated so that the detonation wave impinges on the case and in general on the axis of the cone and from the apex to the base of the cone. Figure 54 shows a sequence of stages in the collapse of a conical shaped charge. These stages can be observed directly by high speed x-ray techniques that show what is happening to the metal parts of the warhead alone. The final results of weapon operation are a "jet" and a "slug" of metal in high-speed motion. The variables of shaped charge performance are the jet velocity and mass and the slug velocity and mass. (There is, of course an expanding gas cloud and the air shock that this generates, but for the moment these aspects are neglected.) The most obvious aspects of shaped charge design to be correlated to the performance variables are the explosive material, the mode of initiation, the liner material, liner thickness, and cone angle.

Some broad generalizations can be made on how the performance of a shaped charge, measured by its jet velocity and mass, is correlated to the shaped charge design, i.e., its explosive charge, liner material, and cone angle. The performance of a shaped charge of fixed configuration, liner material, and explosive is maximized by an initiation process that produces a detonation wave that collapses the cone symmetrically about the cone axis. In general, performance correlates next to the detonation velocity of the explosive. Explosives with detonation rates less than 5,000 m/sec are very poor, and cyclotols and octols outperform TNT. The most significant liner property is the density. The greater the density, the better the performance. Lead is an outstanding exception to this rule of thumb and is not a good liner material. Copper and steel are very efficient materials. The jet and slug masses and velocities depend conspicuously on the cone angle, which is the main configuration parameter. As cone angle increases the jet mass increases, but the jet velocity decreases. The slug mass and velocity vary in just the opposite way.

A model of the collapse process for a wedge liner has been used to explain these correlations. The model applies, at least qualitatively, to cone collapse. The essence of the explanation is an analysis of the geometry of collapse combined with an analysis of the flow of material based on incompressible fluid flow theory (Ref. 29 and 30).

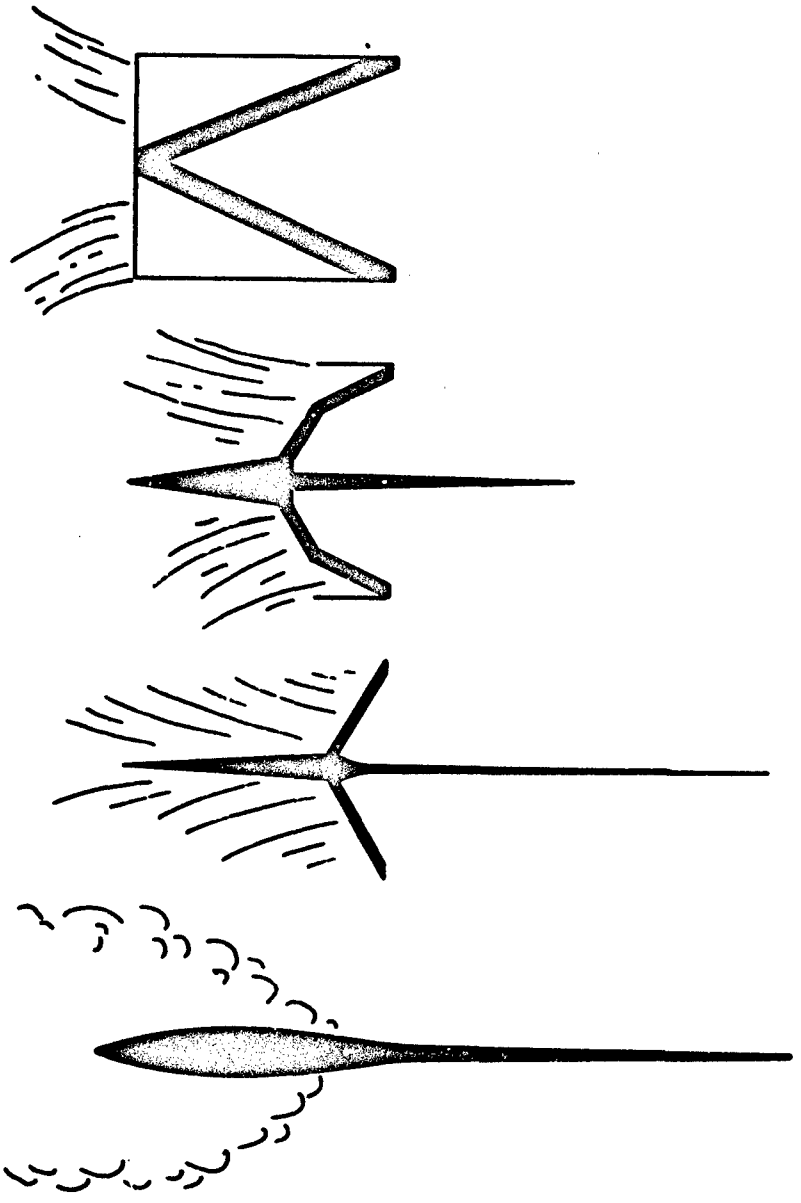

FIG. 54. Stages in the Formation of a Jet.

Figure 55 illustrates the salient features of the collapse geometry. The collapse of the wedge occurs by deformation at a hinge that moves up the wedge. The wedge changes angle from α for the undeformed state to β for the deformed state. In this process there are three velocities of particular interest, the velocity of collapse V_0, the velocity of the point in

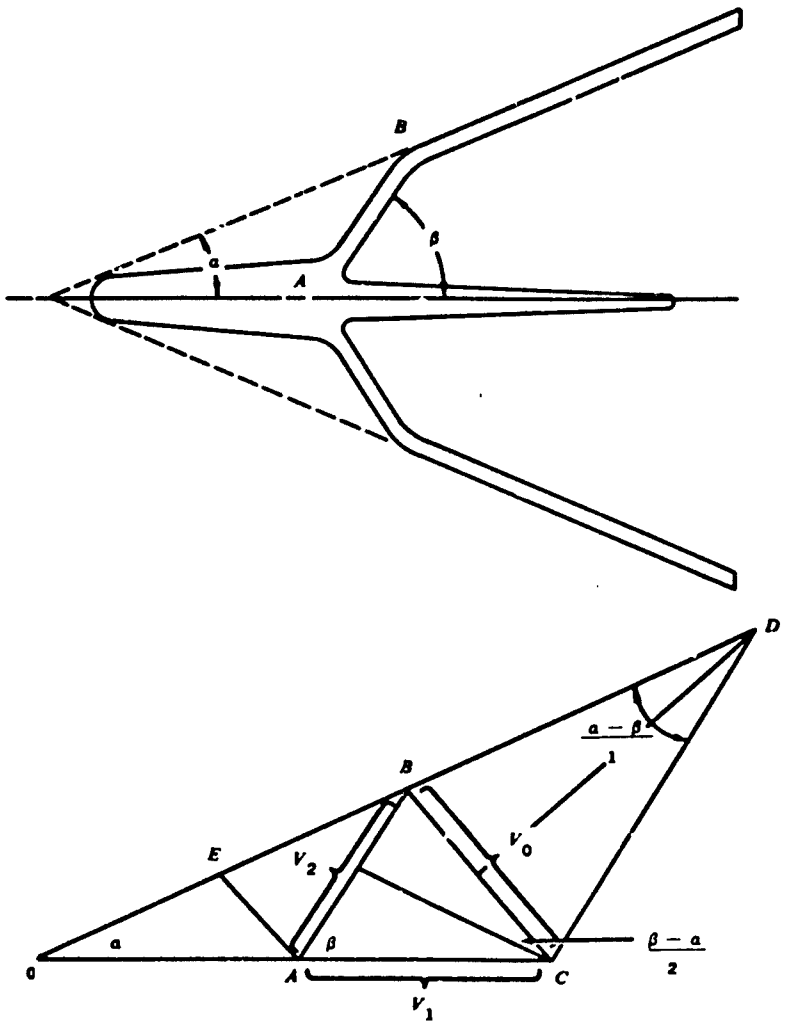

FIG. 55. Geometric Relationships of the Liner Collapse Process for a Wedge.

intersection of the collapsing walls, V_1, and the velocity of material flowing into the point of intersection, V_2. In the geometry of collapse the relationship between these velocities is given by the lines $BC \rightarrow V_0$, $AC \rightarrow V_1$, and $BA \rightarrow V_2$. The lines BD and CD are equal and the line BC bisects the angle ABD, due to the moving hinge mode of collapse. From these relationships it follows that

$$V_1 \sin \beta = V_0 \cos \frac{\beta - \alpha}{2}$$

i.

$$V_1 = V_0 \cos \left(\frac{\beta - \alpha}{2}\right) / \sin \beta$$

It can be shown that

$$V_2 = V_0 \cos \frac{\beta - \alpha}{2} \tan + V_0 \sin \frac{\beta - \alpha}{2}$$

It is assumed that the material behavior is essentially fluid-like and that Bernoulli's equation applies along streamlines. One streamline is on the inner surface of the wedge and along the jet, from which it is found that

$$V_j = V_2 + V_1$$

and another streamline is on the outer surface of the wedge and along the slug so that

$$V_s = V_2 + V_1$$

Conservation of mass in the flows requires that

$$m = m_j + m_s$$

and from Bernoulli's equation

$$m_j V_2 = m_s V_2 + m V_2 \cos$$

which give the following relations between the mass m and the masses m_j and m_s:

$$\frac{m_j}{m} = \frac{1 - \cos\beta}{2} \tag{5-20}$$

$$\frac{m_s}{m} = \frac{1 + \cos\beta}{2} \tag{5-21}$$

Formulas can also be developed to determine the collapse angle in terms of the detonation velocity and the liner angle. Experimental methods of determining this important parameter have been worked out. If α is 22 degrees, the angle α turns out to be approximately 44 degrees. The value of V_0 is 9,200 ft/sec, and the calculated value of V_j is 24,000 ft/sec.

The steady state theory outlined here has been corrected to account for nonsteady-state features and other oversimplifications.

An example of actual shaped charge designs is shown in Fig. 56. In the conical liner the jet is not uniform in velocity along its length but rather decreases back from the tip of the jet. The result is that the jet elongates as it travels and ultimately breaks into discrete elements.

Cones and wedges are the most commonly used liner shapes, but many other shapes, such as hemispherical, trumpet-shaped, and parabolic, have been tried and found to work as well or almost as well as the conical shape. Considerable experimentation has been done with the mode of initiation and with various combinations of inert and explosive materials, with the object of achieving special shapes of the detonation waves. For example, attempts have been made to cause the detonation wave to impinge on the liner at an angle closer to normal incidence. It is expected that this control of the detonation wave will result in higher collapse velocities and hence higher jet velocities. The penetration performance of shaped charges with wave shaping tends to bear out this expectation.

SUMMARY

The internal ballistics of a warhead is concerned with the conversion of chemical energy to kinetic energy through the extremely rapid process of detonation rather than the controlled release process of the combustion of a propellant. The internal forces produced by detonation exceed the strength of the toughest materials, and thus structural failure and the response of materials to stresses above yield stress have to be explicitly employed in

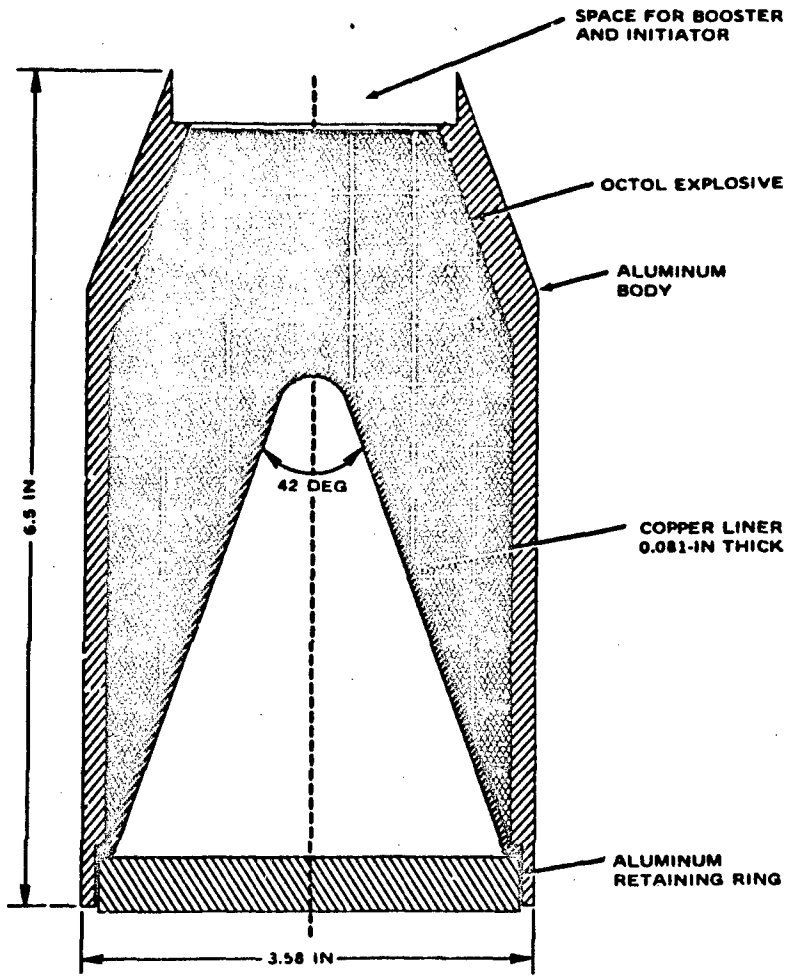

FIG. 56. Shaped-Charge Design.

warhead operation. The expansion and fragmentation of a warhead case are examples. Shaped charges are another class of devices that use the fluid-like response of materials to detonation pressures and high-speed impact to concentrate fragment acceleration in limited directions.

6

Warhead Exterior Ballistics and Blast

Exterior ballistics begins for a projectile when it leaves the barrel of the gun, the effects of muzzle blast are over, and the projectile is traveling to the target. After the muzzle blast has its last acceleration effect on the projectile, it has no further significant part in weapon operation. Exterior ballistics for warhead fragments begins when the fragments separate from the cloud of detonation products and travel from the warhead to the target. Warheads differ from guns in that the "muzzle blast" of a warhead is very large and the target is normally close to the warhead so that the pressure in the blast is not completely attenuated by expansion. The large pressure and the low attenuation combine to make blast a primary damage mechanism of a warhead. Blast refers to the shock and the flow following the shock that are caused by the expanding detonation products. Blast occurs at the same time that the fragments are flying toward the target; thus in terms of the chronological order of events, blast belongs to exterior ballistics.

The exterior ballistics of projectiles was outlined earlier. Projectile trajectories are calculated by the correction of vacuum trajectories for the effects of aerodynamic drag. The trajectories of warhead fragments are considerably shorter and therefore can be calculated by performing drag corrections of the velocities of straight line trajectories. The important differences in the calculation of drag corrections is in the inclusion of the effects of the irregularity of fragment shape, the lack of orientation stability, and the higher velocities of fragments. The inclusion of these effects is discussed next, and will be followed by a discussion of blast.

EXTERIOR BALLISTICS OF WARHEAD FRAGMENTS

Warhead fragments lose velocity along a linear trajectory according to the exponential law

$$v = v_0 \exp(-Ks) \tag{6-1}$$

where v is the instantaneous velocity, v_0 is the initial velocity, and s is the distance traveled.

The velocity decay constant K is

$$K = \frac{\rho_a A C_D}{2m} \tag{6-2}$$

where

ρ_a is the density of air
A is the cross-sectional area of the fragment
m is the mass of the fragment
C_D is the drag coefficient

Warhead fragments are often irregularly shaped and certainly not of optimum shape for minimum drag. Spheres, cubes, and cylinders may approximate the average aerodynamic performance of many fragments. Data on C_D for these shapes are given in Fig. 57.

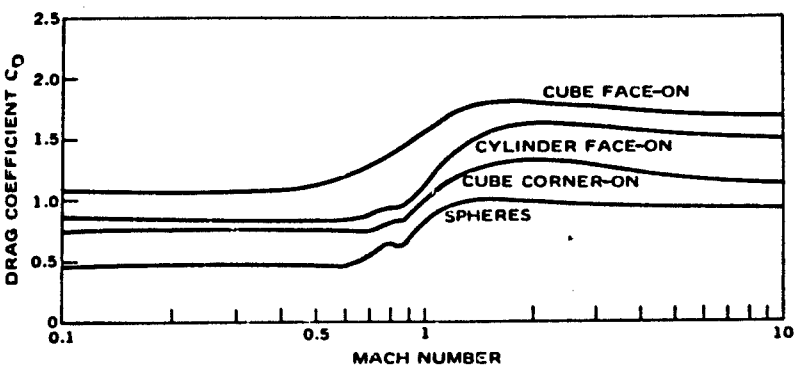

FIG. 57. Drag Coefficient as a Function of Mach Number for Cubes, Spheres, and Cylinders.

The expression for the decay factor in terms of fragment parameters can be rearranged so as to show the dependence of the decay factor on fragment density and size. Thus

$$K = \frac{\rho_a A C_D}{2\rho_f \tau_f}$$

where

ρ_f is the fragment density
τ_f is the fragment volume

and the ratio of presented area A to fragment volume τ_f for a fragment that has a single principal dimension h is proportional to $1/h$ or

$$\frac{A}{\tau_f} = \frac{k}{h}$$

and

$$K = k\frac{\rho_a C_D}{2\rho_f h} \tag{6-3}$$

where k is the shape factor. This shape factor is readily obtained from formulas for the presented area and fragment volume in terms of h. Examples are given in Table 12.

TABLE 12. Shape Factors for Fragment Shapes.

Fragment shape	k	h	$K = \frac{k}{2}\left(\frac{\rho_a C_D}{\rho_f h}\right)$
Sphere	3	radius r	$\frac{3}{2}\left(\frac{\rho_a C_D}{\rho_f r}\right)$
Cube face-on	1	side length l	$\frac{1}{2}\left(\frac{\rho_a C_D}{\rho_f l}\right)$
Cube edge-on	$\sqrt{2}$	side length l	$\frac{\sqrt{2}}{2}\left(\frac{\rho_a C_D}{\rho_f l}\right)$

The velocity as a function of distance for three steel cubes of different sizes is shown in Fig. 58. These curves are computed for constant C_D = 1.0 and for the face-on orientation Figure 59 compares the velocity as a function of distance for steel and aluminum cubes that are 0.250 inch on a side. These figures show that very small fragments will be significantly decelerated in distances that are typical of warhead operation and that lighter fragments lose more velocity than heavier fragments.

Aerodynamic heating becomes an increasingly important phenomenon

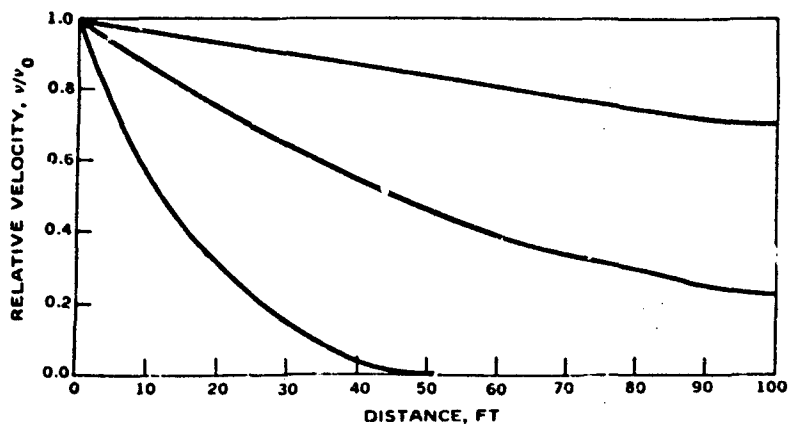

FIG. 58. Deceleration of Steel Cubes of Three Different Sizes.

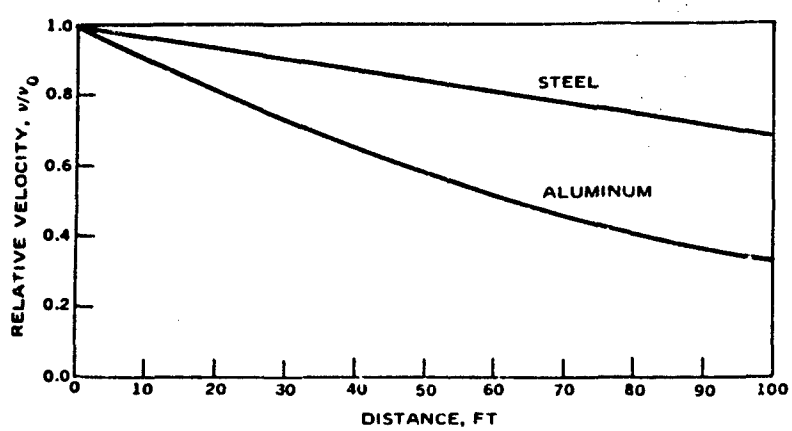

FIG. 59. Deceleration of Cubes of Steel and Aluminum.

as velocity increases. As missile speeds become supersonic, aerodynamic heating becomes a problem because of the effect on internal components, in particular the explosive in the warhead. And of course at the reentry speeds of long-range missiles aerodynamic heating is a threat to the structural integrity of the weapon. The fragments from a shaped charge weapon are in this velocity range, and the melting away of fragment surfaces is a significant effect.

Aerodynamic heating is caused in part by the compression of the air during flow around the body. The flow of air varies from point to point. In Fig. 60 the flow with respect to the body will be zero at the stagnation point and will increase downstream. The temperature in the flow will vary from point to point. At the stagnation point the temperature of the air T_0 is related to the Mach number of flow and ambient temperature T_a by the expression

$$\frac{T_0}{T_a} = 1 + 0.2M^2 \tag{6-4}$$

where M is the Mach number of the motion of the body.

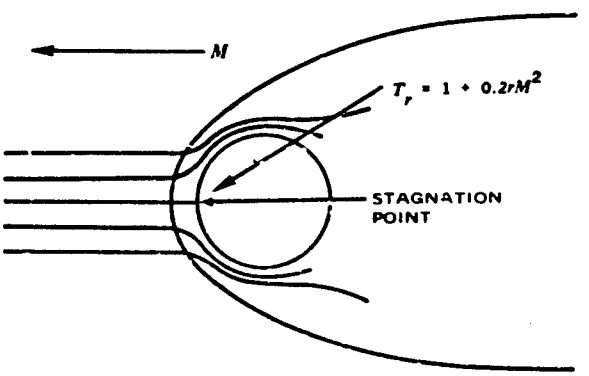

FIG. 60. Flow Around a Body

The temperature at the surface of the body is less than this value due to conduction of heat into regions of cooler air. The temperature at the surface of the body, which is called the recovery temperature, requires a correction of the above formula by a constant, r_f, called the recovery factor.

Thus the recovery temperature T_r is given by

$$\frac{T_r}{T_a} = 1 + 0.2 r_f M^2 \tag{6-5}$$

where

$$r_f = \frac{T_r - T_a}{T_0 - T_a}$$

The value of r_f is approximately 0.9 for a wide range of conditions.

Sample calculations using typical projectile, fragment, and shaped charge jet velocities show the increase in the aerodynamic heating that results from the increased velocities of warhead fragment projection. The recovery temperature for a projectile with a velocity of 2,800 ft/sec is 640°K, for a fragment with a velocity of 6,000 ft/sec the temperature is 1,840°K, and for a shaped charge fragment with velocity of 25,000 ft/sec the temperature is 26,000°K. Thus warhead fragments can be subjected to surface temperatures that are above the melting point and even above the vaporization point of the material. These high temperatures and the high-speed flow result in erosion of material from the surface of the fragment. This erosive process is called ablation.

The essential features of ablation can be described as follows: The high temperature at the surface of the body is transferred into the interior of the body by conduction, but as soon as the heated material melts it is scoured away. A detailed quantitative analysis using heat conduction and fluid dynamics would be complicated both in formulation and in execution. A simple calculation of the amount of material that is ablated can be made on the basis of energy balance between the incident energy flux and the thermal energy removed in ablated material (Ref. 31). The incident energy flux q_i is the product of the pressure and the velocity of the particle

$$q_i = \rho_g \frac{v^3}{2} \tag{6-6}$$

and the energy E_M removed from the body in the form of heat in the ablated material is

$$E_{ht} = \Delta m(C_p T + h_f)$$

where Δm is the mass ablated, h_f is the heat of fusion, and the rate of energy removal q_m is

$$q_m = \dot{m}(C_p T + h_f) \tag{6-7}$$

It is assumed that

$$q_m = C_H q_i$$

and therefore

$$\dot{m} = \frac{C_H \rho_g v^3}{2(C_p T + h_f)} \tag{6-8}$$

It is usually more meaningful to express the ablation rate in terms of the amount of mass per distance traveled. This can be obtained from the expression for $\dot{m}$ using the relation $v = ds/dt$

$$\frac{dm}{dt} = \frac{C_H \rho_g v^2}{2(C_p T + h_f)} \frac{ds}{dt} \tag{6-9}$$

The ablated mass per unit distance m' may be obtained by including the velocity decay caused by aerodynamic drag,

$$m' = \frac{\rho_g v_0^2 C_H}{2(C_p T + h_f)} \int_0^s \exp\left(\frac{-\rho_g C_D A_s}{m}\right) ds$$

The effective heating rate across the body is roughly the integrated product of the stagnation point heating rate and the cosine of the angle between the particle velocity vector and the normal to the surface. With the use of this correction the mass fraction loss from the particle will be

$$\frac{m'}{m} = \frac{C_H v_0^2 [1 - \exp(-3\rho_g C_D s/2\rho_p d)]}{3C_D(C_p T + h_f)} \tag{6-10}$$

where ρ_p is the density of the particle and d is the diameter of the particle.

Figure 61 shows this mass fraction loss for spherical aluminum particles at standard atmospheric conditions. The spheres are assumed to be initially at room temperature with a velocity of about 10,000 ft/sec.

One factor that would tend to increase the rate of ablation from the fragments would be the surface roughness of the fragments. Another is the possibility of a higher initial temperature of fragments. Similarly, factors such as rotation of the fragments and inhibition of ablation by a layer of aluminum oxide (which has a higher melting temperature than aluminum) would tend to decrease the ablation rate.

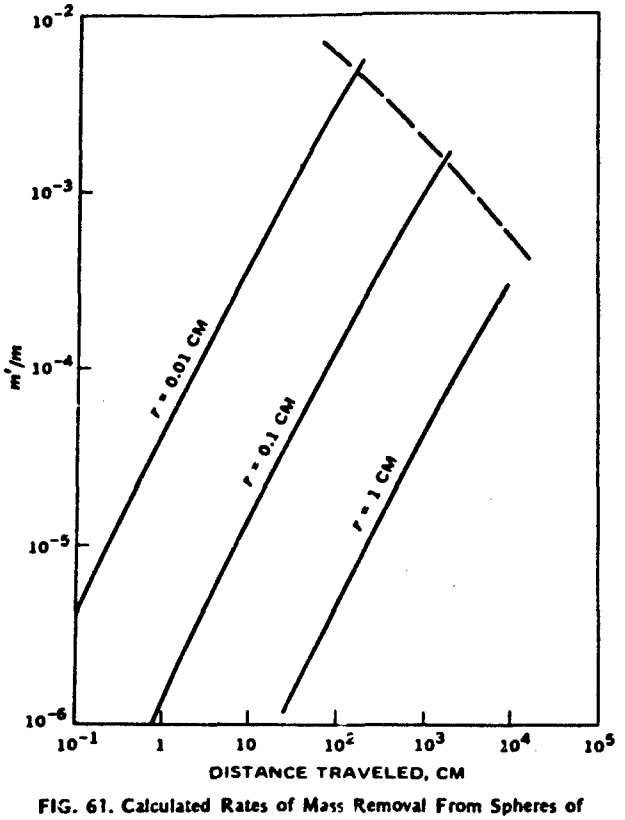

FIG. 61. Calculated Rates of Mass Removal From Spheres of Three Radii.

The ablation rates for a shaped charge particle traveling at 24,000 ft/sec would be approximately 5.8 times as great as those in Fig. 61. It is clear that it is only the very small particles that give up an appreciable percentage of their mass in the distances typical of warhead operation.

BLAST

The failure of the warhead case releases the detonation products, and rapid expansion of these products compresses the surrounding air. The pressures and velocities produced in the layer of air compressed by the product gases are sufficiently high to set up a shock that expands in a roughly spherical mode (see the Appendix). Behind the shock there are distributions of pressure and flow that transfer energy and momentum outward. This traveling shock and the flow behind it are called blast; the damage caused by these disturbances of the air is called blast damage.

In the early stages of the expansion of the shock (shock travel of 16 charge diameters or more) the expansion of the detonation products is a significant part of the dynamics of the system. After the shock has traveled beyond 16 charge diameters the products cease to expand, so that shock motion is the primary means for energy and momentum transmittal. These differences between the interaction of gases with the surrounding atmosphere in the early stages and close to the warhead, and late stages and far from the warhead are the basis for a distinction between near-zone blast and far-zone blast. In the near zone the blast can be called composite blast because both the detonation products and the shocked air are important in the transfer of mechanical effects while in the far zone only the shocked air is important in the transfer of mechanical effects (Ref. 32 and 33).

Near-Zone Processes

Calculations for a spherical charge of TNT indicate that for the near-zone phase of blast development the pressure changes are as shown in Fig. 62 and 63, with the indicated expansions of the detonation products. Figure 62a shows the structure of the disturbance in the air at a time when the initial shock has expanded to 5 charge radii, and Fig. 62b shows this structure at an expansion to 11 charge radii. The main features of the

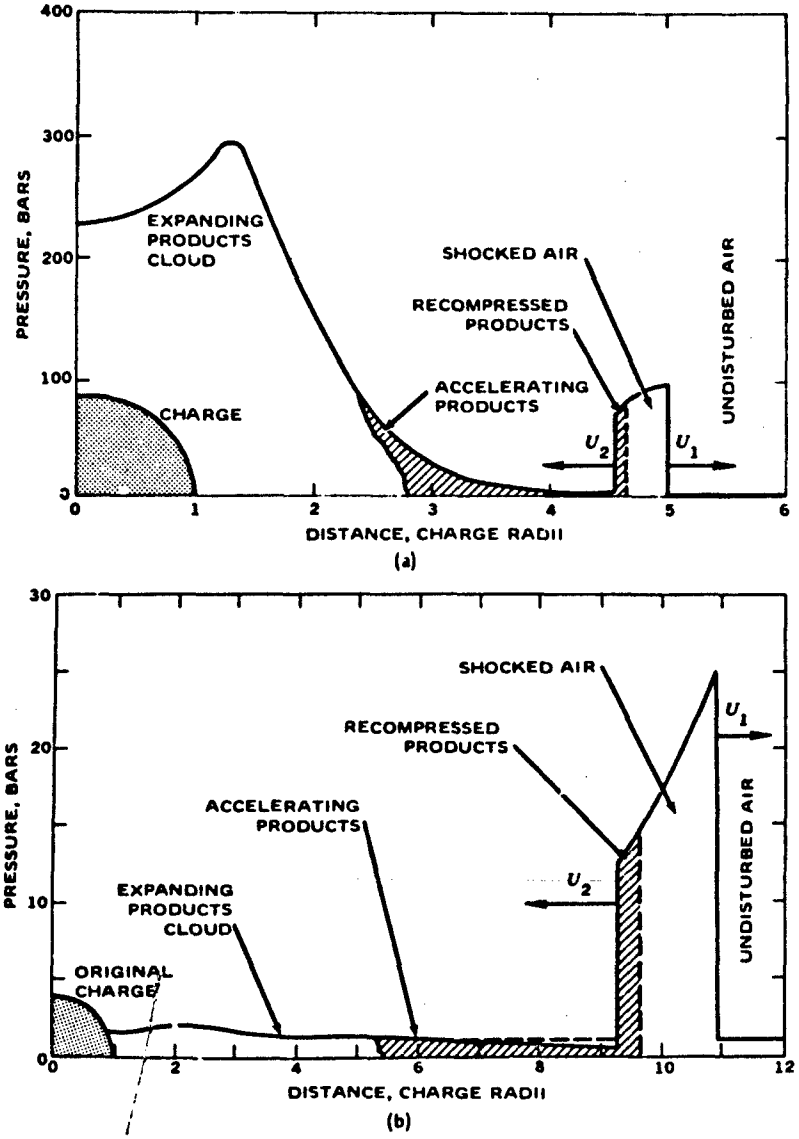

FIG. 62. Pressure Distribution in the Near Zone. (After G. F. Kinney, Ref. 33.)

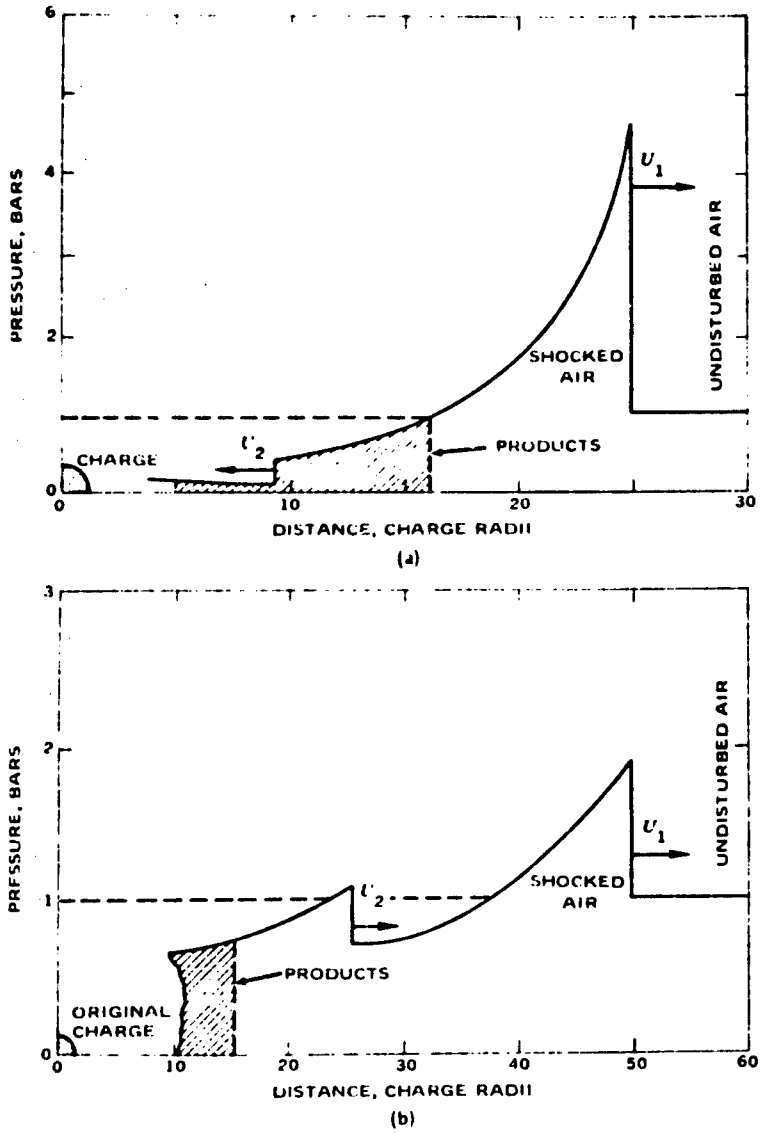

FIG. 63. Pressure Distributions in the Near and Far Zones. (After G. F. Kinney, Ref. 33.)

pressure distribution are the almost discontinuous jump in pressure at the shock, the distribution of pressure in the lamina of compressed air, and the distribution of pressure in the detonation products which includes a second shock that recompresses the detonation products that have been reduced in pressure by their expansion. The second shock initially travels inward decelerating the detonation products. It is reflected at the center and travels outward and eventually contributes to the positive impulse of the air shock.

Far-Zone Processes

Figures 63a and 63b show further expansion to 25 and 50 charge radii, respectively. The pressure distributions at these stages of the development of the disturbance are evolving into a steadily decaying shock followed by a steadily changing flow. The inertia of the detonation products causes overexpansion and the pressures drop below ambient pressures when the detonation products cease to flow outward. A region of low pressure develops well behind the shock front. An idealized configuration for the far-zone air shock is shown in Fig. 64. The main features to be accounted for are the shock strength, the pressure decay behind the shock, and the related datum, the time of the positive pulse (which is used as an index of pulse duration). It should be noted that this idealized blast wave configuration *does not apply* well to the early stages of composite blast processes in the near zone.

Shock Strength

The peak overpressure is one measure of shock strength. The Mach number of the velocity of shock expansion is an equivalent measure. The relation between the peak overpressure and Mach number is found to be

$$p^* = P - P_0 = \frac{7(M^2 - 1)}{6} P_0 \qquad (6\text{-}11)$$

where

p^* is the overpressure
P is the absolute pressure
P_0 is the ambient pressure

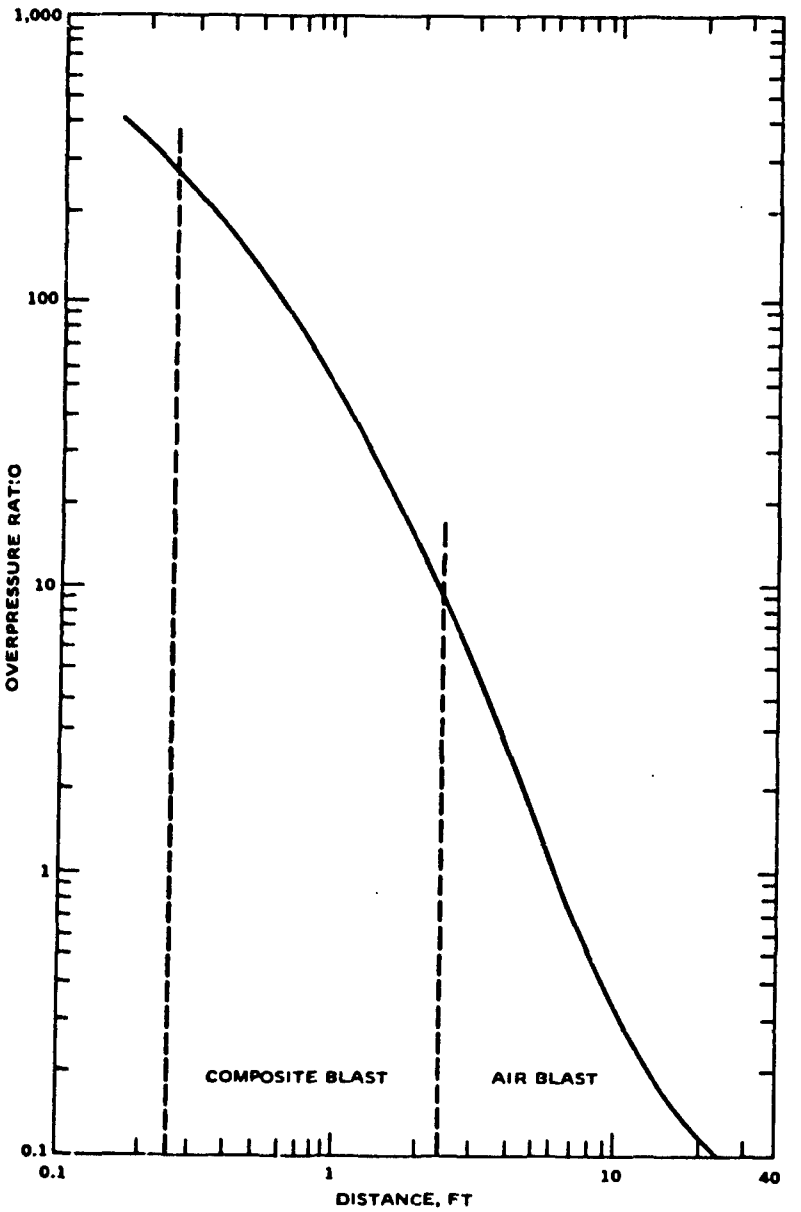

FIG. 64. Peak Pressure Versus Distance for a Reference Explosion of 1 Pound of TNT.

This formula for the peak overpressure is strictly correct for a plane shock. It applies to the shock in a roughly spherical wave since the thickness of the shock is extremely thin so that the wave is locally very close to plane.

Duration of the Positive Pulse

In the far zone the blast wave consists of the shock with its peak overpressure followed by a pressure decay to ambient pressure and below. The pressure behind the shock is found to follow the empirical relation

$$p = p^*(1 - t/t_d) \exp(-at/t_d) \tag{6-12}$$

where

- a is an empirical constant
- t is the time after passage of the shock
- t_d is the duration of the positive pulse
- p^* is the peak overpressure (or shock overpressure) for the particular distance from the explosion

This empirical expression accounts for the generally exponential shape of the decay curve but also accounts for the fact that the pressure goes to ambient pressure in a finite time t_d. The time t_d will tend to increase as the blast wave progresses because each point of the wave will travel at the rate

$$c = \sqrt{\frac{\gamma P}{\rho}}$$

so that the velocity is greatest near the shock and decays to the value

$$c_0 = \sqrt{\frac{\gamma P_0}{\rho_0}}$$

when the pressure reaches the ambient value.

The decay constant a is a separate parameter from the pulse duration and characterizes the shape of the curve as it decays to ambient pressure

within the time t_d.

The parameters p, t_d, and a vary with distance. The dependence on distance can be determined by calculations based on the basic governing equations of hydrodynamics. These require solution of hyperbolic differential equations by numerical means. The pressure distributions of Fig. 62 and 63 were obtained in this way.

Detailed Calculations for Reference Explosions

Detonation and the interaction of detonation products with the surrounding atmosphere are high-temperature, high-pressure phenomena accompanying extremely rapid energy release rates. It is extremely difficult to get reliable data on the distribution of pressure, temperature, and flow by experimental means. These phenomena are amenable to analytical treatment by the application of basic physical principles, but the resulting analytical formulations are in terms of nonlinear hyperbolic differential equations that require tedious numerical methods of solution. Solutions have been carried out for particular cases. The data of Fig. 62 and 63 are part of the output. Figure 64 shows the variation of peak overpressure as a function of distance obtained from the solutions of the fundamental equations. These particular calculations are for a one-pound spherical charge of TNT. The regions of composite blast and air blast are shown. The boundary between the two regions was chosen as 16 charge radii.

Scaling

The blast effects of a warhead depend on how mechanical effects are transmitted from warhead to target. Numerous thermodynamic and hydrodynamic details were required in order to determine the shape and scale of the curve in Fig. 64, and this shape and scale are essential for determining the transmittal of mechanical effects; however, these thermodynamic and hydrodynamic details are of no direct interest in themselves. Any scheme for avoiding the labor involved in treating these details is most useful. Scaling is one procedure by which the repetition of such calculations is avoided once a set of reference data has been developed (Ref. 34).

Scaling is an operation by which a space and time distribution of physical parameters at one charge weight is related to another space and time distribution for a second charge weight. In other words, if a distribution of physical parameters is available at one charge weight, a scaling law will provide the distribution for some different charge weight by changing the scale of distances and time in some way that depends on the charge weight.

The scaling law for explosive phenomena is based on the idea that comparable physical states should exist for comparable distributions of energy. Changes of scale that preserve energy densities are of the form

$$\frac{Z}{Z_0} = \sqrt[3]{\frac{C}{C_0}} \tag{6-13}$$

where Z is a length variable, C is explosive mass, and the subscript 0 refers to reference values, and unsubscripted symbols are actual values. The density of the atmosphere is another factor in the scaling relation and one that is very relevant to the estimation of blast effects at various altitudes. The scaling relation that holds for charge weight and atmospheric density is

$$\frac{Z}{Z_0} = \sqrt[3]{\frac{C}{C_0}}\sqrt[3]{\frac{\rho}{\rho_0}} \tag{6-14}$$

Time scales according to the relation

$$\frac{t}{t_0} = \sqrt[3]{\frac{C}{C_0}}\sqrt[3]{\frac{\rho}{\rho_0}}\left(\frac{c}{c_0}\right) \tag{6-15}$$

For explosives other than TNT an equivalent weight of TNT has to be used in scaling calculations. The equivalent weight is different for the scaling of peak pressure and impulse. Equivalent weights for common explosives are given in Table 13.

Several explosives are of special interest because of enhanced blast effects. These are all explosives to which aluminum has been added. The aluminum appears to have increased the heat of explosion, the total impulse, and the duration of the positive pulse; however, the detonation rate of the mixture has been decreased by the added aluminum. Research on aluminized explosives shows that while considerable energy can be

TABLE 13. Equivalent Weights for Free Air Effects.

Material	Peak pressure relative to TNT, %	Impulse relative to TNT, %
Composition B	110	106
Cyclotol 70/30	114	109
Minol	119	117
TNT	100	100
Torpex	124	120
Tritonal 80/20	107	111
Pentolite	117	115

contributed by the reaction of the aluminum, the reaction kinetics are very likely too slow to affect the detonation process, but rather contribute to the impulse after the detonation reactions are complete.

SUMMARY

A warhead interacts with a target not only by means of the high-velocity fragments from the warhead case, but also by the blast from the detonation of the explosive. Exterior ballistics for fragments is basically the same as for projectiles with regard to the phenomena involved but is made more complicated by the irregularities of fragment shapes and a higher velocity range. One result of the higher velocity range is the possibility of a loss of material through ablation that results from intense aerodynamic heating of fragment surfaces.

The blast from a warhead is the disturbance generated in the atmosphere by the sudden release of energy, with an attendant generation of high pressures and temperatures, in the detonation of the charge. The detonation products drive the surrounding air to produce a shock. At long distances from the warhead this shock is the principal phenomenon of blast, but close to the charge the expanding cloud of detonation products is also a potential means for interaction with the target.

7

Terminal Ballistics of Warheads

The terminal effects of a warhead on a target are caused by the blast of the warhead and the impact of its fragments. Blast and the impact of fragments are usually treated as separate and independent effects because this is expedient and reasonably accurate in many situations. These processes may interact, especially in the area close to the warhead. Contemporary analyses are beginning to treat the combined effects. In the far zone for the treatment of blast the fragments are out ahead of the air shock and the shock is attenuating severely due to spherical dispersion. Certainly here the fragments impact and inflict their damage independent of the air shock. The shock may subsequently inflict significant damage of its own, and the shock damage may be influenced by the fragment damage, but fragment impact is appropriately treated as an independent process.

IMPACT BY MATERIAL FROM THE WARHEAD CASE

The metal from a warhead case penetrates a barrier by the same processes as a projectile fired from a gun, but the warhead fragments do not have the advantages that shape, orientation, and hardness are controlled to optimize the penetration. In general the warhead fragments are moving faster than gun-fired projectiles, and shaped charges will project the metal from the warhead at many times the speed of the fastest projectile. Thus the terminal ballistics of warhead fragments may logically presume all of the

available information on blunt projectiles of moderate hardness and then be developed by considering higher and higher velocities. One of the most important differences from projectile terminal ballistics will be the fact that the impacting body will deform as it penetrates. The main interest of this chapter is the terminal ballistics of the deforming projectile.

Impact of Rods Against Plates

In impact two bodies are initially in different states of motion that bring them into contact. Each body must then deform in such a way as to achieve compatible motions. As a specific example, consider a rod moving lengthwise normal to the plane of a large plate. The two bodies must deform on contact so that there will be a consistent motion at the surface of contact and within each body (Fig. 65). At one extreme, among possible deformations, the end of the rod flattens against an unyielding plate; at the other extreme the plate indents to take the shape of an unyielding rod; and in between these extremes the rod flattens to some extent and the plate indents to some extent. Any of these deformations meet the requirement that each body has to deform to accommodate the other body. The actual deformation depends on the extent to which the bodies resist deformation. The models of material behavior and the ideas on dynamic response of materials that are discussed in the Appendix help to assign properties to the barrier and projectile that determine how each will resist deformation at a given velocity.

Elastic Behavior. Suppose a rod impacts at normal incidence against a plate over a range of impact velocities that ranges from low to moderate. The rod is assumed to be very hard compared to the plate, and at no velocity in the range does it deform other than elastically. The cylinder and plate simultaneously deform, and wave motions are induced in each. The reason for using a thick target is to eliminate consideration of its vibrations by making these vibrations have very long periods of oscillation. At low velocities both target and projectile are elastic. The deformations of the plate are cylinder-like for a small distance into the plate. Each body is stressed by its deformation; for the plate, call this stress σ_b, for the cylinder, call this stress σ_p. Both of these stresses are found from the velocities of particle motion u_b, u_p (as shown in the Appendix).

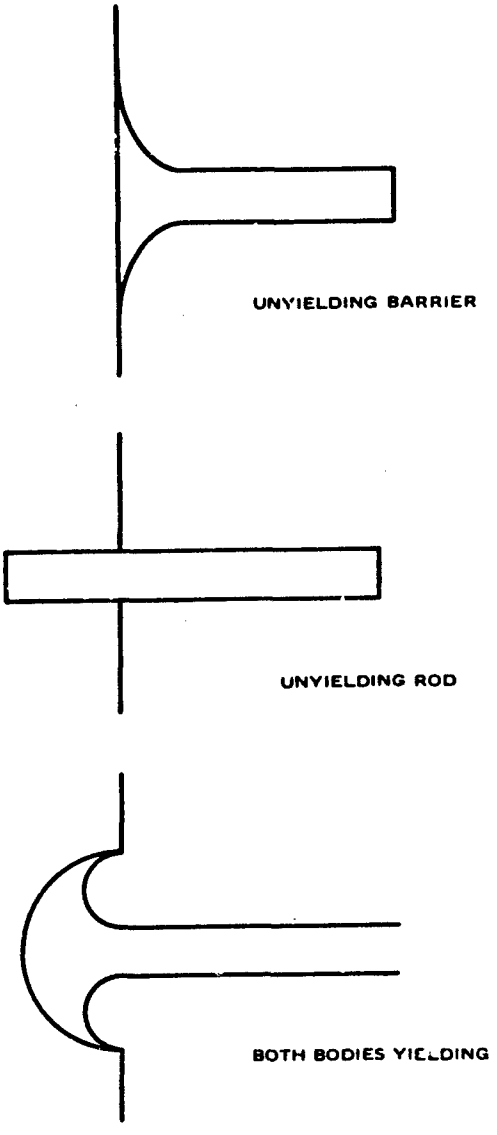

FIG. 65. Examples of Accommodations Between Barrier and Projectile Deformations.

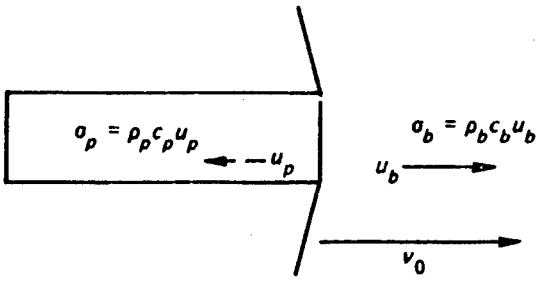

and these must be equal to the contact surface. Therefore,

$$\rho_b c_b u_b = \rho_p c_p u_p \tag{7-1}$$

The kinematics of deformation relates u_b and u_p to the impact velocity v_0 by $u_b + u_p = v_0$. From these bits of information the particle velocities u_p and u_b can be obtained from u_0 and are found to be

$$u_b = \left(\frac{\rho_p c_p}{\rho_p c_p + \rho_b c_b}\right) v_0 \tag{7-2}$$

$$u_p = \left(\frac{\rho_p c_p}{\rho_p c_p + \rho_c c_c}\right) v_0 \tag{7-3}$$

and the common stress is

$$\sigma_b = \sigma_p = \left(\frac{\rho_p c_p \rho_c}{\rho_c c_c + \rho_p c_p}\right) v_0 \tag{7-4}$$

Notice the similarity of these formulas to the formulas for the transmission of acoustic waves across a change of material. The above relation between u_p and u_0 shows that in an impact against a plate the first cycle within the cylinder changes its velocity by

$$2u_p = 2\left(\frac{\rho_b c_b}{\rho_p c_p + \rho_b c_b}\right) v_0 \tag{7-5}$$

The cylinder is now at a new velocity, v_1; then

$$v_1 = v_0 - 2u_p \tag{7-6}$$

and the process repeats. Thus the case of deceleration by contact with an elastic material is different from the constant-force case because the elastic impact stress depends on the velocity of the cylinder at the start of a cycle, and the velocity is decreased during each cycle. There is also an unrelieved force in the plate that complicates matters.

For most combinations of metals for cylinder and target, only one cycle leads to a tensile stress at the contact surface; thereupon impact ends.

These theoretical ideas have verification in the experimental studies. At lower velocities indentations are found with highly localized deformations at the edge of the surface of contact. These deformations are in fact sufficiently localized to leave unaffected most of the elastic condition over the contact surface. The indentation of the target has decelerated the project in an elastic manner but has been frozen in by the deformations at the side (Ref. 35). In other words, these side deformations have had a ratchet-like action. There is usually just one cycle before separation, and the penetration P can be computed as

$$P = \begin{pmatrix}\text{target-particle velocity}\\ \text{during the first cycle}\end{pmatrix} \begin{pmatrix}\text{duration of the}\\ \text{first cycle}\end{pmatrix} \tag{7-7}$$

This is given by the formula

$$P = \left(\frac{\rho_b c_b v_0}{\rho_p c_p + \rho_b c_b}\right)\left(\frac{2l_p}{c_p}\right) \tag{7-8}$$

Where l_p is the length of the cylinder. There is actually a constant error in this prediction due to a small elastic recovery of the side deformations, but the slope of measured penetrations P plotted against impact velocity u_0 is found to be $2[\rho_b c_b/(\rho_p c_p + \rho_b c_b)](l_p/c_p)$ for measurements on brass, aluminum alloy, iron, and mild-steel targets. In Fig. 66 the section below 500 ft/sec velocity has this slope.

Elastoplastic Barrier. At higher velocities nonelastic effects are obvious in these data. In this region the data have been found to fit a prediction based on a "perfectly plastic" model of the behavior of target material.

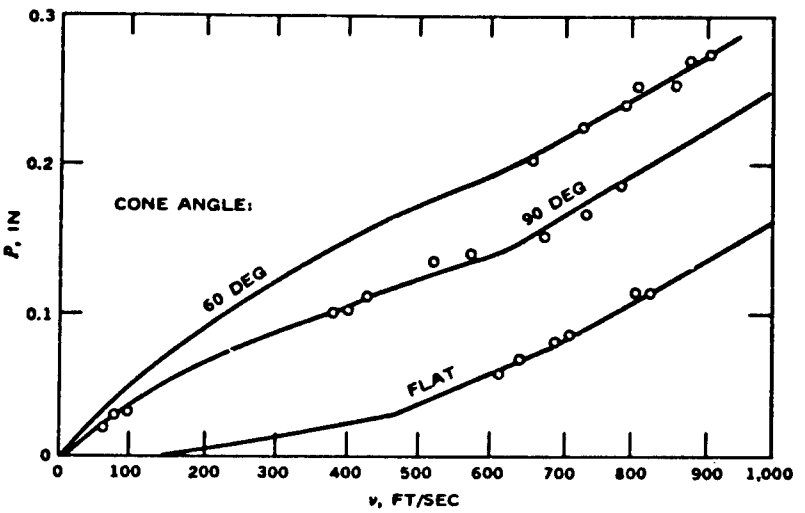

FIG. 66. Penetration of Hardened Steel Conical-Ended and Flat-Ended Projectiles Into an Aluminum Alloy.

Perfectly plastic means that the material properties are idealized by assuming there is a constant stress exerted by the material when it deforms plastically. Thus the projectile in contact with a perfectly plastic material finds a constant force of deceleration no matter what its velocity, provided it is in this perfectly plastic range of the material. In the range of velocities shown in Fig. 66 there will be one cycle under these conditions followed by another cycle under elastic conditions. The slope of this plastic section is

$$\frac{2I_p v_0}{c_p}\left(1 + \frac{\rho_b c_b}{\rho_p c_p + \rho_b c_b}\right)$$

At higher velocities there is more than one cycle in the plastic range. There is a transition section between the region of clear-cut elastic forces of deceleration and the region in which perfectly plastic conditions are achieved. This is apparently due to the work hardening of the material up to the maximum allowable amount encountered in the perfectly plastic cases.

These results are useful because of the close relation of elastic and

plastic conditions within a single collection of data. Thus the lower-velocity measurements established the decelerating stresses for elastic conditions that are then a reference point for the stresses acting during deceleration when there is plastic deformation over the contact surface. Also evident is the fact that the propagation of effects from the contact surface is a fundamental operation.

Impact by Cone-Nosed Rods

The results for cylinders show that vibration and wave motion are fundamental in penetrating processes. These projectiles, however, lack the quality of pointedness that, common experience shows, aids penetration. It is, therefore, desirable to find out how this quality affects the conclusions reached about vibration and wave propagation.

A cone has the required pointedness and is also mathematically simple. Cone-nosed projectiles have been used in tests paralleling those for cylinders. Figure 66 shows, by the circled points, indentation data obtained at impact velocities of less than 1,000 ft/sec from impacts of hardened-steel projectiles against an aluminum alloy. Included are some very low-velocity data, obtained by using a compressed-air gun, which show that the conical shape causes indentation even at very low velocities.

While the pointed projectiles penetrate more deeply than cylinders, it is interesting that in the region of deeper penetrations the slopes of the curves are parallel for the rods with 60- and 90-degree points and the cylinders of the same length. This is a surprisingly simple and direct relation that has at least a qualitative explanation.

Once the cone is fully embedded, the amount of material pushed in by an increment of penetration is the same for cone-nosed rods and for cylinders of the same diameter. This can be seen in Fig. 67. The penetration of a cone to the depth P_2 has a volume equal to that of the cone *BEC* plus the cylindrical volume *ABCD*. The penetration to the depth P_1 has the same volume as *BEC*. However, *ABCD* is just the volume displaced by a cylinder in a penetration to depth P where $P = P_2 - P_1$.

The action during the embedding of the cone involves much more complicated geometric, elastic, and plastic details. It can be approximately predicted by assuming a constant pressure of roughly the maximum value indicated in the study of cylinder indentations. The dotted sections of the penetration curves are based on this method of prediction and are seen to

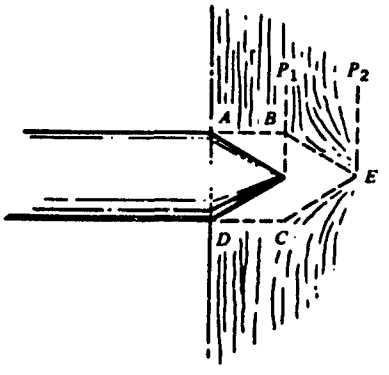

FIG. 67. Penetration of a Conical-Ended Projectile Into a Thick Target.

agree reasonably well with the measured points. The main conclusion to be drawn from this is that pointedness enhances penetrating ability primarily by providing a gradual increase of the surface over which momentum is exchanged.

The discussion thus far has emphasized that the loss of rigidity due to material failure in one of the materials reduced the magnitude of the forces of interaction between projectile and barrier. As impact velocity and deformation rates increase there is a growing inertial effect that must be taken into account. This can be done by assuming that the internal stresses within the deforming body are composed of elastic and fluid-like components so that the stress is

$$\sigma = \sigma_y + p \tag{7-9}$$

where p is a pressure. For a perfectly plastic material σ_y has a constant value, but p has a value that is determined by the boundary conditions and the instantaneous state of motion. An estimate of the value of p can be made from an analogy of plastic flow to incompressible fluid flow. Using Bernoulli's equation for the relation between the flow rate W and the pressure p along a streamline, the value of p at a stagnation point for flow around the projectile can be given by the dynamic pressure $\rho u^2/2$, and the stress is therefore

$$\sigma = \sigma_y + \frac{\rho u^2}{2} \tag{7-10}$$

The flow rate W can be estimated as $u = u_0 - u^*$ where u^* is $\sigma_y/\rho c$. The pressure elsewhere on the streamline will decrease so that the net force on the projectile will be of the Poncelet form (Eq. 3-2).

$$F = A(c_1 + c_3 v^2)$$

A graphical presentation of the relationship between stress and particle velocity can be made by plotting the above equations for each material. An example for a single material is illustrated in Fig. 68. Curves of this type for the barrier and the projectile materials determine two values of particle velocity u_b and u_p for a given stress. These values are the particle velocities in the barrier and projectile that are dynamically compatible at an impact velocity v_0

$$v_0 = u_b + u_p \tag{7-11}$$

The curve for stress as a function of the impact velocity is indicated in Fig. 68 by the dashed line. It is usually assumed that u_b is the rate of penetration and the relative values of u_b and u_p are soon such that $u_b - u_b^* = v_0$ as is assumed in the Poncelet form of the resistance force. This graphical representation of impact makes no accounting for the shape of the projectile and it assumes plane strain conditions in the elastic region and applies only to the stagnation point in the region of plastic deformation. The graphs should apply to rod impact against a very large plate or relatively blunt projectiles with large length-to-diameter ratios that are approximately plane near the stagnation point.

Elastoplastic Behavior of Projectile and Barrier. The combination of plasticity and incompressible fluid dynamics might be expected to apply to the stresses within the projectile provided that the deformations of the projectile are steady. A steady deformation is plausible for a long rod that flattens as the barrier indents. The combined flattening and indentation result in an inversion of the rod as is shown in Fig. 69, and this deformation can assume a steady state if the net effect is to form a crater of constant diameter. Experimental firings show that the craters for long rods fired at high velocities are approximately constant in diameter. The section of Fig. 68 that is above the yield point of the projectile applies to a long rod that impacts against a large plate.

The stresses that govern steady deformation of the rod should be the

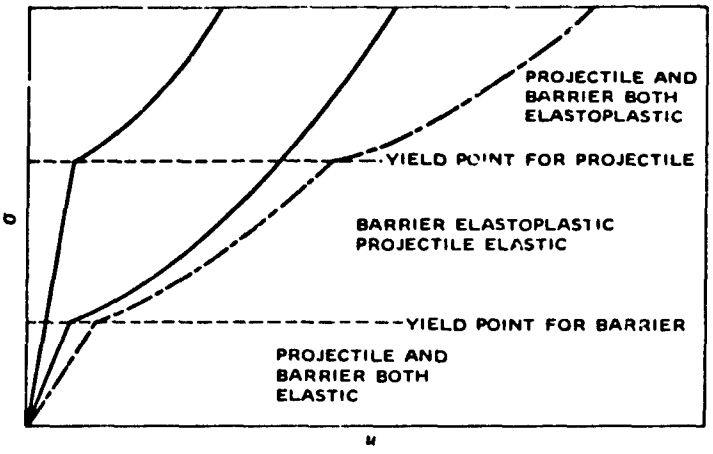

(a) Two materials with perfectly plastic behavior.

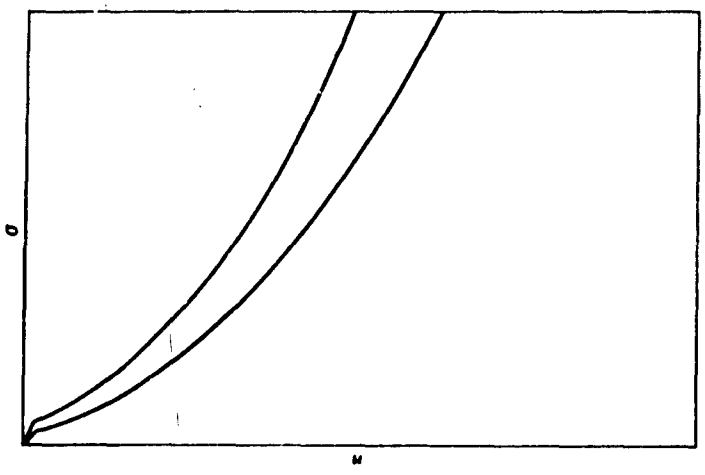

(b) Two materials with larger V scale.

FIG. 68. Stress/Velocity Curves.

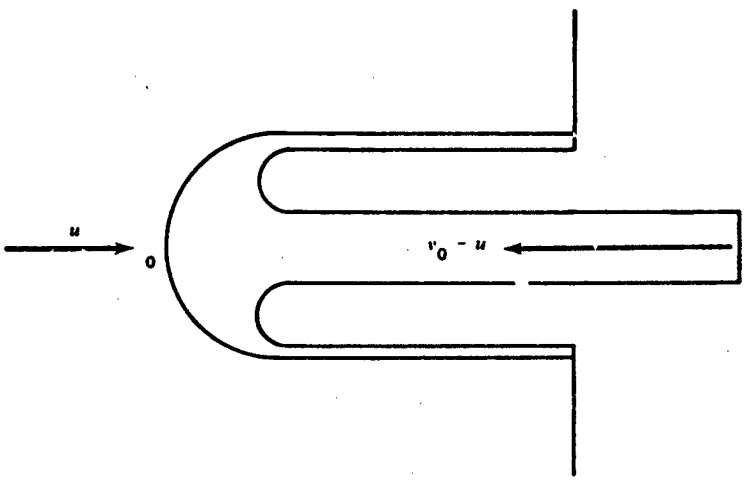

FIG. 69. Inversion of a Rod in Steady-State Penetration of a Barrier.

stress for steady penetration (Eq. 7-10).

$$\sigma^p = \sigma_y^p + \frac{\rho^p u^2}{2}$$

where u is the backward flow of the rod material.

The dynamic pressure term $\rho^p u^2/2$ increases with velocity, but σ_y does not, and eventually the σ_y term becomes insignificant compared to the dynamic pressure. This limiting condition is equivalent to treating the impact as the interaction between incompressible fluid objects. The first quantitative treatment of the penetration of shaped charge jets into thick barriers was based on this assumption. The flow of barrier and jet material is as shown in Fig. 69. This flow is assumed to be steady, so that Bernoulli's equation applies along the streamlines of the steady flow.

Let the flows be viewed from the point 0, the stagnation point, as a fixed position relative to which remote parts of the barrier flow at the rate of penetration u and remote parts of the rod flow at the rate $v_0 - u$ in the opposite direction. The flow in both bodies along the axis of symmetry comes to a complete stop at the stagnation point 0. Barrier material flows

out from the stagnation point and achieves a velocity u. Immediately next to the barrier streamline there is a rod streamline that flows out to achieve that same velocity of flow as a streamline on the outer surface of the rod. But this streamline has a constant velocity $v_0 - u$ since it is pressure-free. Hence, the equality of pressures at the point 0 requires that

$$\frac{\rho^p (v_0 - u)^2}{2} = \frac{\rho^b u^2}{2} \tag{7-12}$$

and this establishes a relation between the penetration rate and the impact velocity.

By hypothesis the deformations of the barrier and the projectile are steady so that for strict consistency the termination of penetration cannot be by loss of velocity since that would not be a steady process. An alternative that is consistent with steady state conditions is that the projectile is stopped by the complete reversal of the direction of flow relative to the stagnation point 0 through the steady deformation process. Thus, since the projectile has a steady flow rate into the base of the crater of $v_0 - u$, in a time t,

$$t = \left(\frac{l_p}{v_0 - u}\right) \tag{7-13}$$

all of a projectile of length l_p will have gone through the reversal of direction that occurs at the base of the crater. The penetration at the steady rate u will be

$$P = ut = u\left(\frac{l_p}{v_0 - u}\right) \tag{7-14}$$

but from the equation for the equality of pressures at the stagnation point

$$\frac{u}{v_0 - u} = \sqrt{\frac{\rho^p}{\rho^b}} \tag{7-15}$$

so that

$$P = l_p \sqrt{\frac{\rho^p}{\rho^b}} \tag{7-16}$$

This equation is the final conclusion of the elementary theory of jet penetration and it has enjoyed considerable success in that actual data, which are often imprecise and variable, are fit as well by this formula as by much more pretentious theories. This equation is unusual among penetration formulas in that it is *velocity independent*. This comes from the fact that the assumption that the deformation rates are steady makes the penetration and the amount of inverted rod proportional to the penetration rate and rod inversion rate, both of which are assumed to be steady. At any instant the ratio of these rates is dependent on the square root of the ratio of the densities.

The inclusion of strength into the analysis of penetration can be done by returning to Eq. 7-10,

$$\sigma = \sigma_y + \frac{\rho u^2}{2}$$

to represent the internal stress at the stagnation point for each body and thus modifying the preceding balance of pressure to give

$$\rho^b u^2 = \rho^p (v_0 - u)^2 + \sigma_y \tag{7-17}$$

in which σ_y is the combined residual elastic stress in both bodies. If this relation is used in place of the pure hydrodynamic relation, the ratio of penetration and rod inversion rates is not velocity-independent and the penetration equation is velocity-dependent

$$P = l \left(\frac{-\rho_1 v_0 + \sqrt{\rho_1^2 v_0^2 - 2(\rho_1 - \rho_2)\left[\frac{\rho_1 v_0^2}{2} - \phi\right]}}{\rho_2 v_0 - \sqrt{\rho_1^2 v_0^2 - 2(\rho_1 - \rho_2)\left[\frac{\rho_1 v_0^2}{2} - \phi\right]}} \right) \tag{7-18}$$

but approaches the equation $P = l_p \sqrt{\rho^p / \rho^b}$ as velocity increases. The velocity-dependent penetration formula and experimental data are shown in

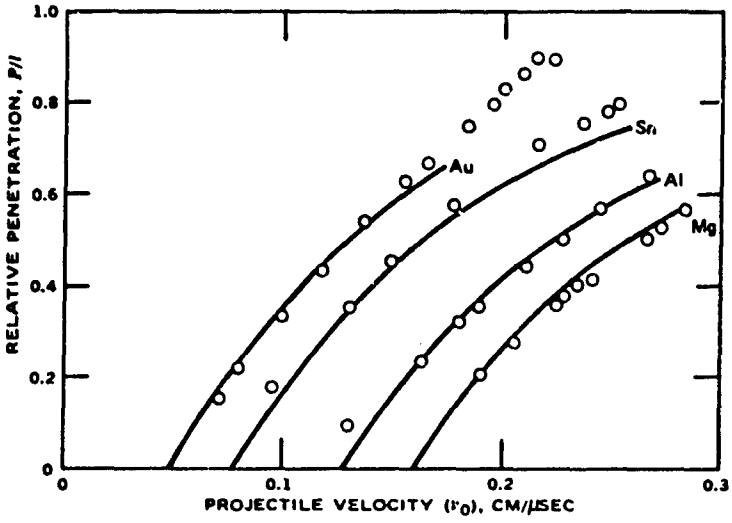

FIG. 70. Comparison of Experimental Data With Modified Hydrodynamic Theory. (From Ref. 36.)

Fig. 70. The experimental data were taken for very small scale tests using small wires for the rods (Ref. 36).

Penetration velocity predictions can be made for all three of the velocity regimes, elastic, projectile elastic, and projectile/barrier elastoplastic. There is, of course, no penetration in the elastic regime. The regime of elastoplastic behavior in the barrier alone can be represented by the formula given above. A composite plot of this type is shown in Fig. 71.

The velocity-dependent rod-penetration prediction can be corrected in another way. Since elastic effects are known to be at least a minor part of the interaction between the projectile and the barrier, there will be at least a slight deceleration due to the propagation of wave down the rod. Calculations of this kind of effect have been done using the assumption that an elastic wave of constant strength makes repeated traversals of the undeformed rod, thus changing the overall rigid body motion of the rod as the penetration proceeds. These corrections are insignificant for soft rod materials but can contribute to complete deceleration of the rod prior to complete rod inversion when the rod has appreciable strength. The shape of the penetration curves is modified as shown in Fig. 72, the penetration prediction for steel rods into steel barriers. It will be noted that the lower velocity section of the curve has roughly the Poncelet shape.

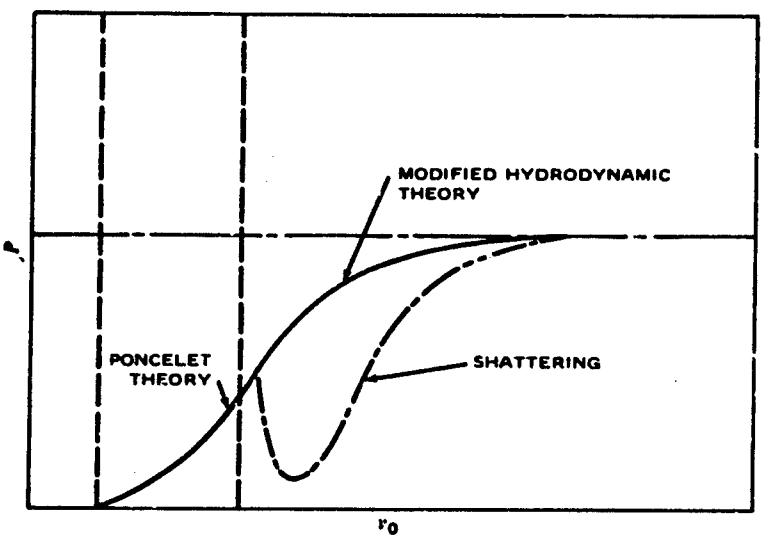

FIG. 71. Composite Penetration Curve.

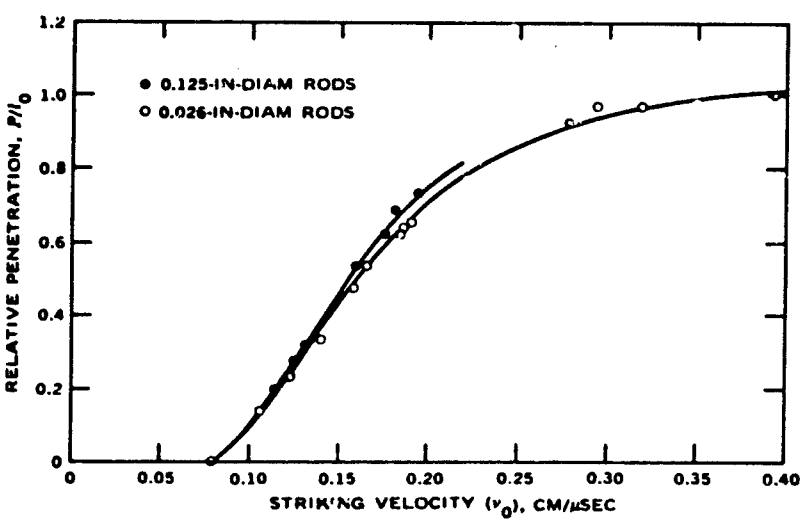

FIG. 72. Experimental Data Compared With Theory for the Penetration of Annealed SAE 4130 Steel Rods With Length-to-Diameter Ratio of 14.4 Into Annealed SAE 4130 Steel Targets.

The problem of analyzing the penetration of thick barriers by a deforming projectile can be understood in a general way for long rods that allow the projectile to deform in a nearly steady manner. The rods can also fail in a brittle mode and there is some data on this condition. Figure 73 shows the experimental data on the penetration of long hard rods into a comparatively soft barrier. The solid line is Eq. 3-9 empirically fit to the data. Penetration falls off drastically as soon as the projectile shatters. This appears to be due to complex interactions between the shattered particles along the shaft of the rod prior to the time that these contact the target. The net result is radial dispersion of fragments, and their penetration seldom has a cumulative effect. There are some indications that as the velocity increases, these interactions are not allowed sufficient time to disperse the particles so that the rod retains much of its rod shape and the

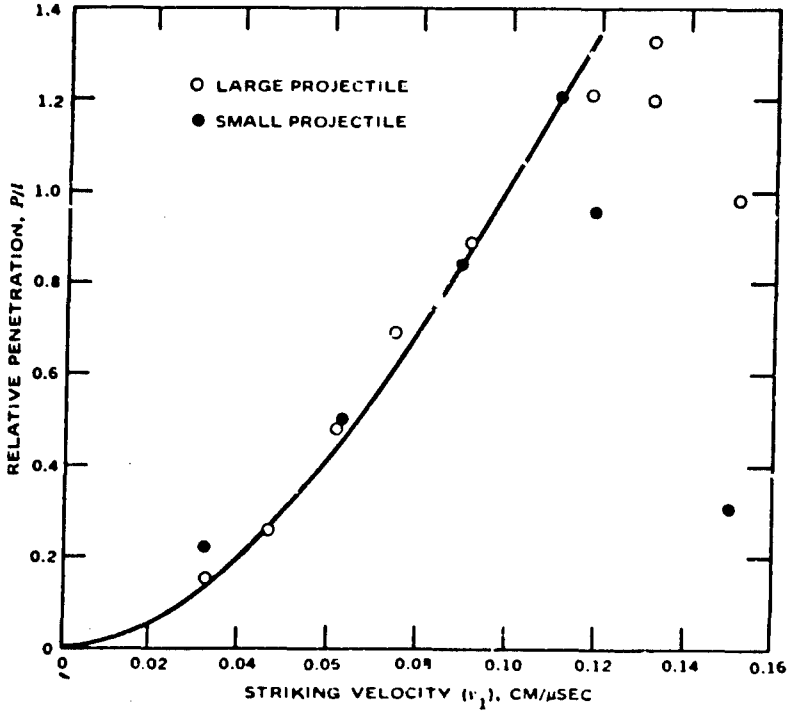

FIG. 73. Effect of Shattering on Penetration.

penetration efficiency increases and probably approaches that of the deforming rod. There is no large amount of consistent data to confirm this speculation.

Penetration Performance of Real Jets

The jet of a conical shaped charge is a long thin mass of metal that is rod shaped; therefore the theory of rod penetration should show in general what happens in jet penetration. The jet does not have a fixed length due to its velocity gradient; changing length must be included in a realistic description of jet penetration. The rod also breaks up into a number of fragments. An important practical consequence of these effects is that penetration is a function of "standoff"—the distance between the shaped charge and the barrier. The exact relationship between penetration and standoff is needed in order to design weapons for the most effective use of the conical shaped charge.

A theory of jet penetration has been worked out that utilizes three regions of standoff with distinct penetrating processes. In the first the jet is continuous but elongating; in the second the jet is continuous during part of the penetration and particulate in the rest; in the third the jet is completely particulate. Penetration relations to standoff for these three regions of standoff are discussed in summaries of work done at the Ballistic Research Laboratories (Ref. 37) and are shown in Fig. 74. For the copper

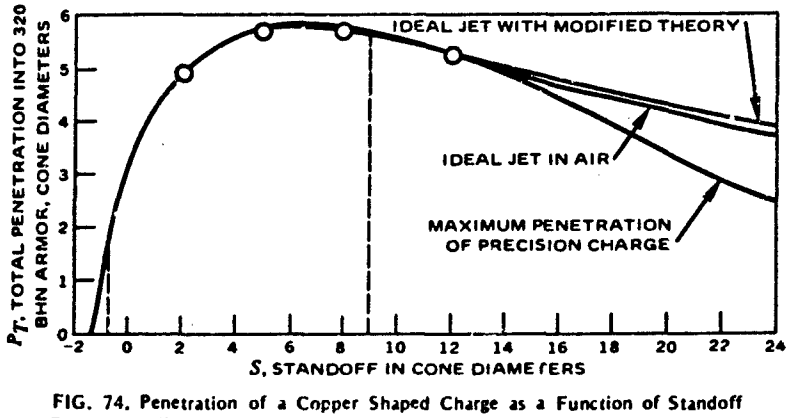

FIG. 74. Penetration of a Copper Shaped Charge as a Function of Standoff Theory and Experimental Data. (From Ref. 37.)

shaped charge of Fig. 74 the first region corresponds to negative values of the abscissa. Negative values of standoff may be interpreted as penetrations at various stages of incomplete jet formation. It is clear from the figure that for copper shaped charges this first region has no practical interest.

In the first region the continuous jet has a linear relation between penetration and standoff; in the second region there is an increase in penetration with standoff, but the breakup of the jet is responsible for reduced increases of penetration with increases of standoff; and in the third region the penetration has achieved its maximum value.

The assumptions of the theory are that the jet is initially an elongating rod that breaks up simultaneously over its entire length into segments of shorter length. The rod segments keep their orientation and lose no mass due to ablation and no velocity due to drag. The segments penetrate as individual rods of fixed length.

Actual firings of shaped charges reveal an optimum standoff distance beyond which the penetration declines markedly. The theory does not predict this decline. The preceding assumptions have been examined to determine where the theory is not realistic. Calculations of drag and ablation confirm the assumption that these are not significant factors in the loss of penetration with increased standoff. There are detectable differences due to these effects, but if ignored these differences would never have any practical consequences.

The shape of the jet is significantly influenced by comparatively small details of the design of the liner. Differences in the concentricity of the outer and inner surfaces of the liner, variations in the thickness of the liner, and malalignment of the cone axis with the axis of the explosive cavity all tend to introduce curves in the jet. Tests that compared the penetration performance of liners that are very carefully made and liners that are made to a lesser degree of precision showed that there was a significant improvement for the precision liners. This effect still does not account for the drop in penetration beyond the standoff for optimum penetration.

The assumption that appears to be most in error is that all rod segments penetrate in the classical mode. It is assumed that segments with less than some critical velocity do not penetrate, and thus there is a part of the rod length that is completely ineffective; then changes in penetration performance with standoff of the correct magnitude are predicted. The cutoff velocity can be associated with the fact that for a particulate jet the penetration crater is scalloped in contour rather than perfectly cylindrical.

At lower velocities the flow over the scalloped contour results in interference among the particles.

Penetration of Chunky Fragments

If a projectile has a length-to-diameter ratio that is close to one, it may be grossly inaccurate to assume a steady-state condition for its deformation during impact. The relation between the stresses at the contact surface and the impact velocity will be somewhere between those for an elastic projectile and those for steady-state rod penetration. The deceleration of the rod will be neither approximately rigid nor perfectly fluid but will be a combination of direct deceleration of the projectile (changes in the overall motion of the projectile) and deformation of the projectile (changes in motion due to lateral deformation and flows that reverse the direction of motion). The preceding ideas on the penetration of targets by long rods are not likely to provide a very accurate view of the penetration of a barrier by a chunky fragment.

The main features of the perforation of a barrier by a chunky fragment are qualitatively displayed by test firings with spheres, cubes, and cylinders.

It is found that projectiles that have these geometrical configurations and that have principal dimensions approximately equal to the plate thickness all perforate the plate by expulsion of a plug. This holds true for barriers of aluminum, brass, steels of several compositions and heat treatment, and titanium alloys, and thus indicates that neither the composition of the barrier material nor the shape of the projectile tends to change the mode of perforation.

At the ballistic limit the plug and the projectile are extensively deformed, but both are essentially intact (Fig. 75). When perforation occurs, the diameter of the plug is less than that of the projectile, which has flattened against the crater. The projectile has to squeeze through the hole left by the plug (Fig. 76). As velocity is increased above the ballistic limit, the plug and the projectile develop internal fractures and fragment. At the same time the region peripheral to the plug hole develops fractures, and fragments of various types are ejected from this region. The number of fragments ejected from all regions (plug, projectile, and periphery) increases with increased impact velocity.

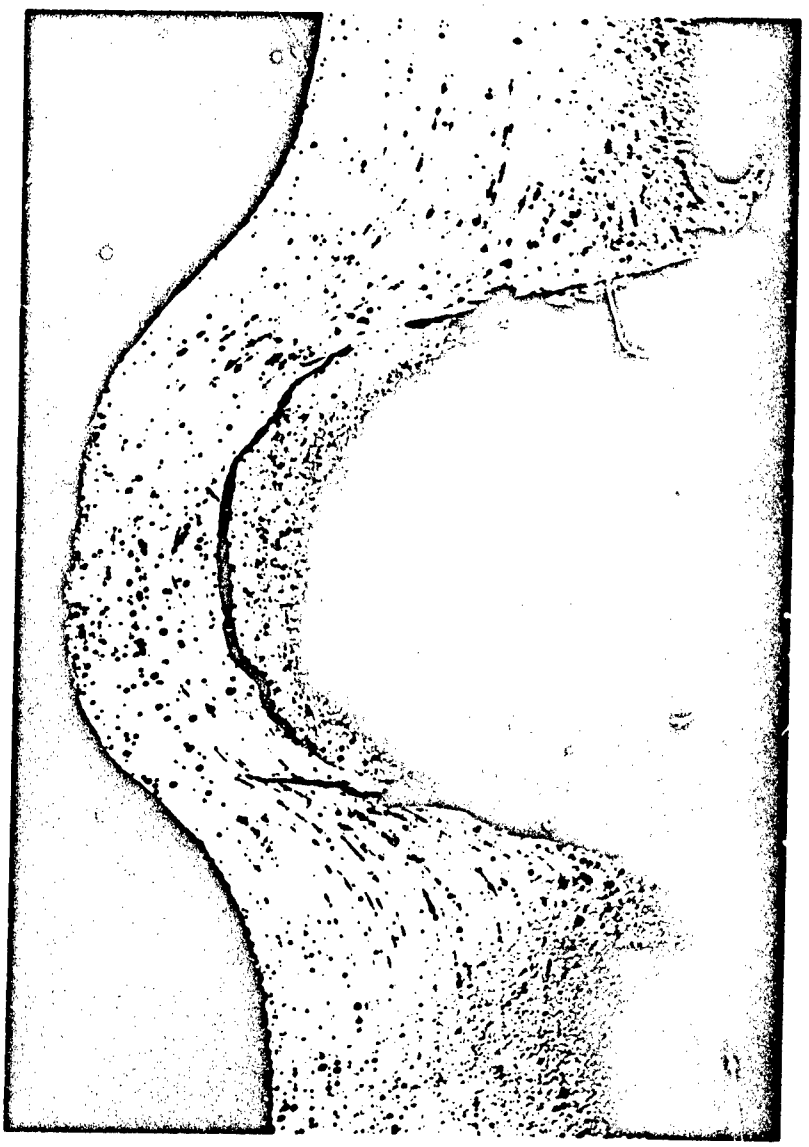

FIG. 75. Cross Section of a Plate Impacted by a Sphere Below the Ballistic Limit.

FIG. 76. Cross Section of a Plate With a Deformed Sphere Lodged in the Perforation Hole.

Since the perforation process is plugging, it is not surprising to find that the residual velocity data fit formulas of the type of Eq. 3-42a and 3-42b and in particular the special form of Eq. 3-43. Sample data are shown in Fig. 77. Note that the correlation of residual velocity to impact velocity is still good after the plug and projectile have begun to fragment. In the formula

$$v_1 = \frac{m_1}{m_1 + m_3} \sqrt{v_0^2 - v_{BL}^2}$$

the ballistic limit velocity and the ratio of fragment to plug mass are empirically determined.

Some idea of what is happening in the barrier and the projectile can be obtained by firing projectiles over a range of velocities, recovering the fragments, and sectioning the barriers and fragments. When this is done for

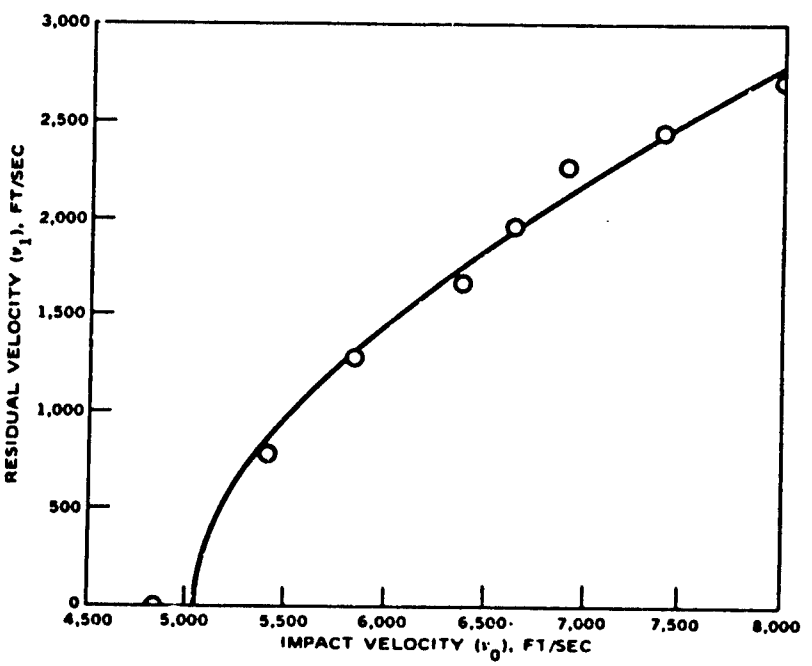

FIG. 77. Velocity Data for Plugging From Impact of 0.25-Inch Steel Balls Against 0.258-Inch Armor at 0-Degree Obliquity.

several materials, several types of fractures are found inside the fragments, and these fractures are responsible for the formation of fragments. Shear fractures dominate the fracturing of all the materials that have been examined. By shear fractures is meant complete failure of the material on surfaces that follow directions of maximum shear and that produce displacement of the material parallel to the surface of the fracture. There are many details of these fractures that separate them from the running cracks that are usually associated with the word fracture.

Consider first penetrations into very thick barriers in which the effects due to the presence of a free surface within the failure region are minimized. For a given projectile, the craters are roughly spherical in contour and increase in dimensions as the impact velocity increases. At lower velocities there are no fractures; then as velocity increases, fractures develop at the bottom of the crater. These are along directions of maximum shear, assuming that the stresses are nearly uniform compression applied normal to the surface of the crater. These fractures are like those discussed in Chapter 5. There are two directions in which the shears can go. It is most likely that the directions will be symmetrical about the axis of symmetry of the crater, and it is convenient to designate shears as *outward-directed* if they follow trajectories that travel away from the axis of symmetry and *inward-directed* if the trajectories travel toward the axis of symmetry.

The direction that the shears take depends on the macrostructure of the material. Homogeneous materials or materials that have a lamellar structure with the orientation of the structure along the axis of symmetry favor inward-directed shears. Materials that have a lamellar structure with the orientation of the structure perpendicular to the axis of symmetry (or parallel to the plane of the plate) tend to favor outward-directed shears, and the fractures frequently follow the direction of the lamellar structure. This kind of macrostructure commonly results from the use of a rolling process in the manufacture of plates. Many barrier materials may be of this type.

Plates that are of thicknesses small enough to allow perforation and to make the thickness a significant parameter are perforated by the expulsion of a plug, a mass of material that separates from the rest of the plate. This happens by a shear process, and it can easily be seen that this form of shear is inward-directed no matter how the macrostructure is oriented within the barrier. When the plug begins to break up at still higher impact

velocities, the internal fractures remain shear fractures and are inward-directed.

The peripheral fragmentation of the barrier exhibits the greatest sensitivity to the structural orientation of the material in exactly the same way as for the thick plates. Homogeneous materials and materials with structural orientation across the plate tend to form peripheral fragments along inward-directed surfaces.

The two basic modes of forming peripheral fragments are shown in Fig. 78. Materials with a rolling texture tend to form fragments by a

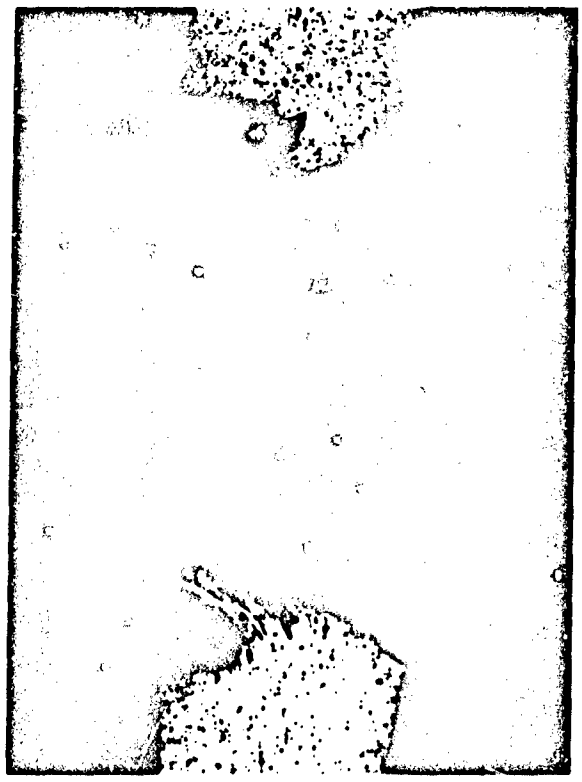

(a) Crater from a ring formed by slip surfaces affected by lamellar distributions of inhomogeneities.

FIG. 78. Two Modes of Peripheral Fragmentation.

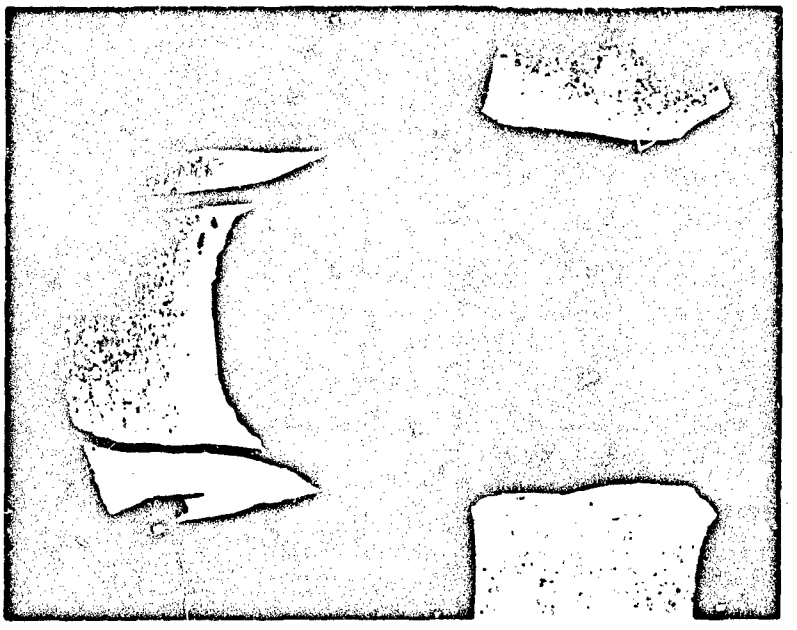

(b) Sleeves typical of homogeneous materials.

FIG. 78 (Contd.)

separation of the material along the direction of the rolling texture. Failures of this type occur along the perforation crater at impact velocities above the ballistic limit but below the velocities for peripheral fragmentation. When the velocities for the ejection of peripheral fragments are achieved, the separation of laminae is accompanied by fracture perpendicular to the laminae. Materials that are more homogeneous simply form separations along inward-directed slip lines.

The fractures that are responsible for plugging, fragmentation of the plug, and peripheral fragmentation can be examined by microscopy. Shear failures almost always are found to be preceded by highly localized plastic deformations. Bands of deformed material, and in some cases material that appears to have been structurally modified, occur along slip lines. These bands are the sites for separation of the material.

The bands of localized plastic deformation have been investigated in

order to determine the causes of their formation and the general mechanism of development. A considerable amount of evidence supports the idea that these are the result of thermoplastic instabilities that can develop under very rapid loading (Ref. 38 and 39). As the material begins to deform, it does so along a slip line since this is the direction for flow under the initial stress state. The plastic work causes heating along the slip line, and for rapid loading there is little time for the cooling effect of heat conduction. The heated material is weaker and therefore deforms more readily. The net result is that the deformation in the band along the original slip line is unstable; thus, bands of extremely intense deformation develop. For some materials these zones appear to undergo a change of phase so that the material after loading is in a different crystallographic state.

The full complexities of the analysis of barrier penetration by a deforming projectile is attacked in an approach that formulates the impact problem in terms of continuum mechanics and applies numerical methods of solution to the resultant problem. This is a highly complex analytical procedure for which the following are the major steps:

1. The formulation of a set of equations based on conservation of mass, momentum, and energy and available information on material behavior to comprise sufficient information to determine a unique solution.

2. The formulation of boundary conditions and initial conditions that specify a particular impact.

3. The conversion of the continuum mechanics equations into finite difference equations that can be solved by numerical procedures using high-speed computers. For example, continuum operations such as the differentiation of variable with respect to time and space variables are converted into ratios of finite differences.

4. The solution of the finite difference equations by numerical techniques.

The advantages of this method are the following:

1. It attacks the problem from as close to first principles as available information will allow.

2. There are a minimum of special assumptions

3. As a consequence of items 1 and 2 immediately above, all of the details of impact are revealed, not just those that are anticipated.

Some of the disadvantages are the following:

1. The extreme complexity and difficulty in the interpretation of results.

2. High cost.

3. A limitation at the present time to axisymmetric problems.

The feasibility of the solution of three-dimensional problems has been established, but it is evident that the extreme difficulty of such solutions will impose a practical limitation to two-dimensional problems and three-dimensional axisymmetric problems.

The basic outputs of this type of analysis are lengthy lists that correlate velocities, densities, and stresses to time and space variables. Fortunately these can be conveniently presented by means of automatic plotting techniques that show the spatial distribution of a given variable at some chosen sequence of times. An example is shown in Fig. 79. More detailed discussion of these techniques is given in Ref. 40 through 43.

Reference 44 presents a simplified analytical model of perforation by

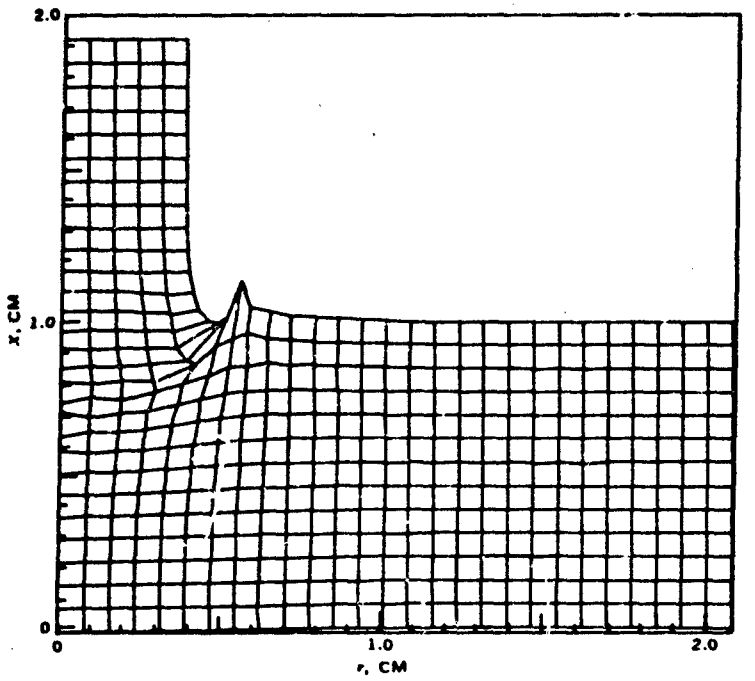

FIG. 79. Computer Solution of the Impact of a Deformable Cylinder Against a Plate. (From Ref. 43.)

a deforming projectile in which it is explicitly assumed that a pointed projectile will assume a blunt shape during penetration and finally perforate the barrier by a plugging process.

SUMMARY

The terminal ballistics of warheads treats the interaction of fragments or controlled flows of metal from a warhead with structures or vehicles. The interactions are usually similar to projectile attack of armor, except that the fragment does not have controlled orientation, its velocity range is much larger, and fragments usually deform or fracture during impact. These interaction are often more energetic than those for a non-deforming projectile but are also basically less efficient in penetration. Simple estimates of penetration for long rods can be made using fluid models of the material behavior of the projectile and barrier. The performance of shaped charge jets is approximately described by such estimates. More detailed descriptions of shaped charge performance and the performance of individual fragments at high velocity requires either combined experimental and theoretical treatment or the use of advanced computer technology and detailed descriptions of material behavior.

References

1. Fordham, S. *High Explosives and Propellants.* Oxford, Pergamon Press, 1966.

2. Departments of the Army and the Air Force. *Military Explosives.* April 1955. Washington, D.C., Government Printing Office, 14 April 1955. 358 pp. (TM 9-1910/TO 11A-1-34.)

3. Corner, J. *Theory of Internal Ballistics of Guns.* New York, John Wiley & Sons, Inc., 1950.

4. Hunt, F. R. W., ed. *Internal Ballistics.* London, His Majesty's Stationery Office, 1951.

5. Serebryakov, M. E. *Interior Ballistics.* Tr. by V. A. Nekrassoff. The Catholic University of America, 1950 (originally published in Russian in Moscow, 1949). 601 pp.

6. Binder, R. C. *Fluid Mechanics.* Englewood Cliffs, N.J., Prentice Hall, Inc., 1962.

7. Davis, L., J. W. Follin, and L. Blitzer. *Exterior Ballistics of Rockets.* New York, D. Van Nostrand Company, Inc., 1958.

8. Bonney, E. A., M. J. Zucrow, and C. W. Besserer. *Aerodynamics, Propulsion, Structures.* New York, D. Van Nostrand Company, Inc., 1956.

9. Hoerner, S. *Fluid-Dynamic Drag.* Midland Park, N.J., published by author, 1958.

10. Naval Weapons Laboratory. *A Study to Optimize the Aerodynamic Design of Naval Projectiles,* by F. G. Moore. Dahlgren, Va., NWL, September 1969. (NWL TR 2337.)

11. Headquarters, Department of the Army. *Fundamentals of Protective Design* (Non-nuclear). Washington, D.C., Government Printing Office, July 1965. (TM 5-855-1.)

12. Allen, W., E. Mayfield, and H. Morrison. "Dynamics of a Projectile Penetrating Sand," J APPL PHYS, Vol. 28, No. 3 (March 1957), pp. 370-376.

13. Allen, W., E. Mayfield, and H. Morrison. "Dynamics of a Projectile Penetrating Sand, Part II," J APPL PHYS, Vol. 28, No. 11 (November 1957), pp. 1331-35.

14. Caudle, W. N., A. Pope, R. McNeil, and B. Margason. "The Feasibility of Rapid Soil Investigations Using High-Speed, Earth-Penetrating Projectiles," in *Proceedings of International Symposium on Wave Propagation and Dynamic Properties of Earth Materials,* Albuquerque, N. Mex., Sandia Laboratory, August 1967. (SC-DC-67-1922.)

15. Young, C. W. "Low Velocity Earth Penetration Study," Wendover Operation, Albuquerque, N. Mex., Sandia Laboratory, April 1967. (SC-TM-66-2611.)

16. Rinehart, J., and J. Pearson. *Behavior of Materials Under Impulsive Loads.* New York, Dover Publications, 1965.

17. Goldsmith, W. *Impact.* London, Edward Arnold (Publishers) Ltd., 1960.

18. Massachusetts Institute of Technology, Aeroelastic and Structures Research Laboratory. *Survey of Hypervelocity Impact Information,* by W. Hermann and A. Jones. Cambridge, Mass., MIT, September 1961. (ASRL Report No. 99-1.)

19. Bethe, H. A. *Attempt of a Theory of Armor Penetration.* Philadelphia, Pa., Frankfort Arsenal, May 1941.

20. Thomsen, William T. "An Approximate Theory of Armor Penetration," J APPL PHYS, Vol. 26, No. 1 (January 1955), pp. 80-82.

21. Thompson, L. T. E., and E. B. Scott. *A Momentum Interpretation of Penetration Data.* MEM ARTILLERIE FRANC, Vol. 6 (1927), p. 1253.

22. Kraft, J. M. "Surface Friction in Ballistic Penetration," J APPL PHYS, Vol. 26, No. 10 (October 1955), pp. 1248-53.

23. Recht, R. F., and T. W. Ipson. "Ballistic Perforation Dynamics," J APPL MECH, Vol. 30 (September 1963), pp. 384-389.

24. Courant, R., and K. O. Friedrichs. *Supersonic Flow and Shock Waves.* New York, Interscience Publishers, 1948.

25. Ballistic Research Laboratories. *The Initial Velocities of Fragments From Bombs, Shells, and Grenades,* by R. W. Gurney. Aberdeen, Md., BRL, September 1943. (BRL Memo Report No. 405.)

26. Kennedy, D. R. "The Elusive $\sqrt{2}E$," presented at the 21st Annual Bomb and Warhead Section Meeting at Picatinny Arsenal, 22 April 1969.

27. Thomsen, Erich G., Charles T. Yang, and Shiro Kobayashi. *Mechanics of Plastic Deformation in Metal Processing.* New York, The Macmillan Company, 1965.

28. Bridgeman, P. W. "Fracture and Hydrostatic Pressure," in *The Fracturing of Metals.* Cleveland, Ohio, American Society for Metals, 1948. Pp. 246-61.

29. Birkhoff, G., D. P. MacDougal, E. M. Pugh, and G. I. Taylor. "Explosives With Lined Cavities," J APPL PHYS, Vol. 19, No. 6 (June 1948), p. 563.

30. Pugh, E. M., R. J. Eichelberger, and N. Rostoker. "Theory of Jet Formation by Charges With Lined Conical Cavities," J APPL PHYS, Vol. 23, No. 5 (May 1952), pp. 532-536.

31. Naval Weapons Center. *Penetration Mechanics and Post-Perforation Effects in an Aluminum-Aluminum Impact System*, by M. E. Backman and W. J. Stronge. China Lake, Calif., NWC, October 1967. (NWC TP 4414.)

32. Kinney, G. F. *Explosive Shocks in Air*. New York, The Macmillan Co., 1962.

33. Naval Weapons Center. *Engineering Elements of Explosions*, by G. F. Kinney. China Lake, Calif., NWC, November 1968. (NWC TP 4654.)

34. Cole, R. H. *Underwater Explosions*. New York, Dover Publications, 1965.

35. Backman, M. "Elastic and Plastic Behavior in the Impact of Cylinders Against Plates," J APPL PHYS, Vol. 30, No. 9 (September 1959), pp. 1397-1403.

36. Allen W. A., and J. W. Rogers. "Penetration of a Rod into a Semi-Infinite Target," J FRANKLIN INST, Vol. 272 (1961), p. 275.

37. Ballistic Research Laboratories. *Penetration of Shaped-Charge Jets into Metallic Targets*, by Robert DiPersio, Julius Simon, and Alfred B. Merendino. Aberdeen Proving Ground, Md., BRL, September 1965. (BRL R 1296.)

38. Zener, Clarence, "The Micro-Mechanism of Fracture," in *The Fracturing of Metals*. Cleveland, Ohio, American Society for Metals, 1948. Pp. 3-31.

39. Recht, R. F. "Catastrophic Thermoplastic Shear," J APPL MECH, Vol. 31, No. 2 (June 1964).

40 Sedgwick, R. T., and Mrs. D. A. Wolfgang. *CRAM: A Two-Dimensional Lagrangian Code for Elastic-Plastic Hydrodynamic Material Behavior.* King of Prussia, Pa., Space Sciences Laboratory, General Electric, February 1969. (69SD9.)

41. Wilkins, M. L. "Calculation of Elastic-Plastic Flow," in *Methods in Computational Physics*, Vol. 3, ed. by B. Adler, S. Fernbach, and M. Rotenberg. New York, Academic Press, 1964. Pp. 211-263.

42. Sedgwick, R. T. "Theoretical Terminal Ballistic Investigation and Studies of Impact at Low and Very High Velocities." Eglin AF Base, Fla., AFATL, May 1968. (AFATL-TR-68-61.)

43. Wagner, M. H. *Analytical Study of Penetration Mechanics*, by Shock Hydrodynamics Incorporated. Sherman Oaks, Calif., May 1969. (Technical Report 3030-2020FR, Naval Weapons Center Contract N00123-68-C-0838.)

44. Awerbuch, J. *A Mechanics Approach To Projectile Penetration*. ISRAEL J TECH, Vol. 8, No. 4 (1970), pp. 375-83.

Appendix

THE BEHAVIOR OF MATERIALS UNDER IMPACT AND EXPLOSIVE LOADING

The Behavior of Materials Under Impact and Explosive Loading

MECHANICAL PROPERTIES OF MATERIALS

The properties of a given material are described by the relation between the stresses and strains within the material, i.e., between the internal forces per unit area and the relative elongations or contractions and shearing of the material. The elongation of a rod in a simple testing machine is an example. The machine applies a pulling force on the rod, and allows measurement of the elongation of the rod along its axis and the amount of contraction of the rod in cross-sectional area. From these data we have the following stresses and strains

A tensile stress $\sigma_1 = F/A$
A tensile strain $\epsilon_1 = \Delta l/l$ from the extension along the axis
A compressive strain $\epsilon_2 = \Delta d/d$ from the contraction perpendicular to the axis of the rod

A test is usually carried out to the point of final failure of the rod. If the stress and strain data are plotted directly using the initial cross-sectional area A_0 in the computation of stress, and $\Delta l/l_0$ for the strain, the curve representing the data looks like the curve of Fig. 80, and is called an engineering stress/strain curve. This curve displays many of the material characteristics with reasonable accuracy and is easy to obtain. The curve is actually a plot of force on the rod and the corresponding extensions corrected by factors that remove the effect of the dimensions of the sample. It is not completely consistent with the definition of stress as force

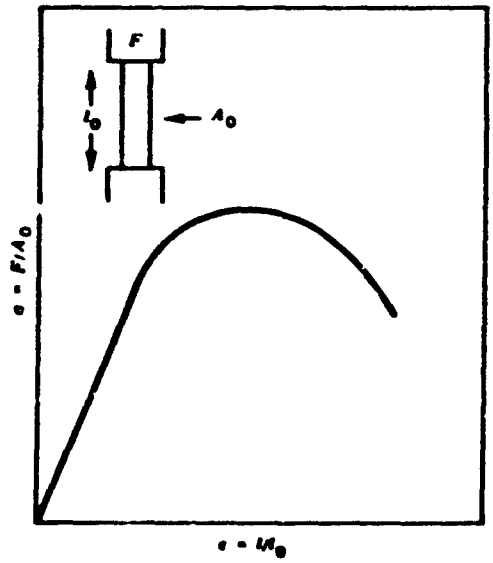

FIG. 80. Engineering Stress/Strain Data.

per unit area because the cross-sectional area changes during the test. It is not completely consistent with the definition of strain as relative elongation, since the length of the sample changes during the test.

A true-stress/true-strain curve is one computed for forces divided by the instantaneous area and for strain computed from instantaneous elongation divided by the instantaneous length. Since the instantaneous strain is $\Delta l/l$, the summation of all the instantaneous contributions is the integral of $\Delta l/l$,

$$e_1 = \int_{l_0}^{l} \frac{dl}{l} = \ln(l/l_0) \qquad \text{(A-1)}$$

The data from the testing of a rod is as shown in Fig. 81. This is a representation of the same information as Fig. 80 but this representation is more consistent in its use of the definitions of stress and strain. It is quite obvious that the two curves are vastly different in the presentation of the details above the yield point. If the curves are being used to compare materials, the engineering curve may be satisfactory, but if the use of the

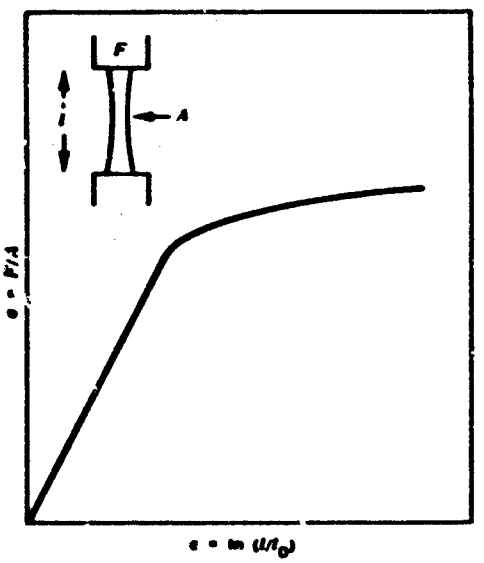

FIG. 81. True Stress/Strain Data.

curve depends on the accurate interpretation of stress and strain, the true-stress/true-strain curve would have to be used.

One of the uses of these data is the establishment of ranges of distinct material behavior. A point (σ_y, e_y), the elastic limit or yield point, separates the responses of the material into elastic and nonelastic regions. Below the elastic limit the curve is in the elastic region where the relation between stress and strain is reversible and linear (to a very high degree of accuracy), while above the yield point the curve is in the plastic region where the relation between stress and strain is irreversible and increasingly nonlinear. It is the *reversibility* of the stress/strain relation that is the defining property of the elastic region. The linearity is an advantage in analytical work and has made possible the development of a very sophisticated mathematical theory of linear elasticity, but the essential property of the elastic response is the recoverability of strains.

Figure 82 presents schematically a test of a material in which the load is repeatedly applied, removed, and then applied to a higher level. The specimen is first loaded to a stress σ_1 below the elastic limit; then the stress is removed and there is no permanent strain. The specimen is then loaded to a stress σ_2 at the elastic limit and there is still no permanent

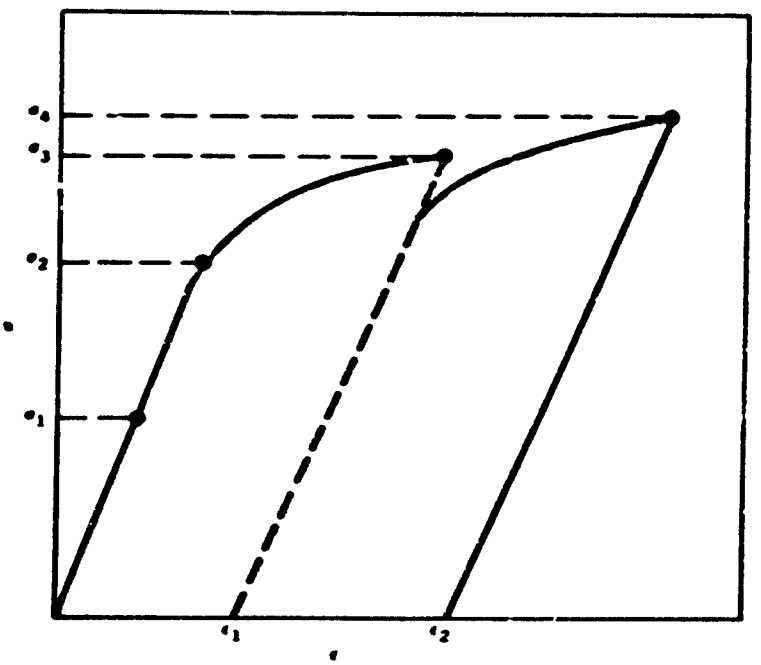

FIG. 82. True Stress/Strain Data for Cyclic Loading Above and Below the Yield Condition.

strain when the stress is removed. But when the specimen is loaded to a stress σ_3, which is above the elastic limit, and then the stress is removed, there is now a permanent strain ϵ_1. Loading to a stress σ_4 increases the permanent strain to ϵ_2. The linear paths descending from the points of maximum stress σ_2, σ_3, and σ_4 indicate the elastic nature of material response to stress relief and reloading.

The relation between stress and strain in the elastic region is linear to a high degree of accuracy. The stress is proportional to strain

$$\sigma_1 = E\epsilon_1 \tag{A-2}$$

where the constant E is Young's modulus. The axial extensions and the transverse contractions are also in a constant ratio ν

$$\frac{-\epsilon_2}{\epsilon_1} = \nu \tag{A-3}$$

that is called Poisson's ratio. These two constants determine the elastic properties of the material.

Stress/strain data are shown in Fig. 83 for a tool steel 4340 and an aluminum alloy. These are obviously very dissimilar in mechanical properties. The tool steel has a yield point that is more than three times the yield point of the aluminum alloy. The elastic moduli of the two materials also significantly differ. The aluminum alloy is widely used in aircraft construction, although it has been replaced in many modern aircraft

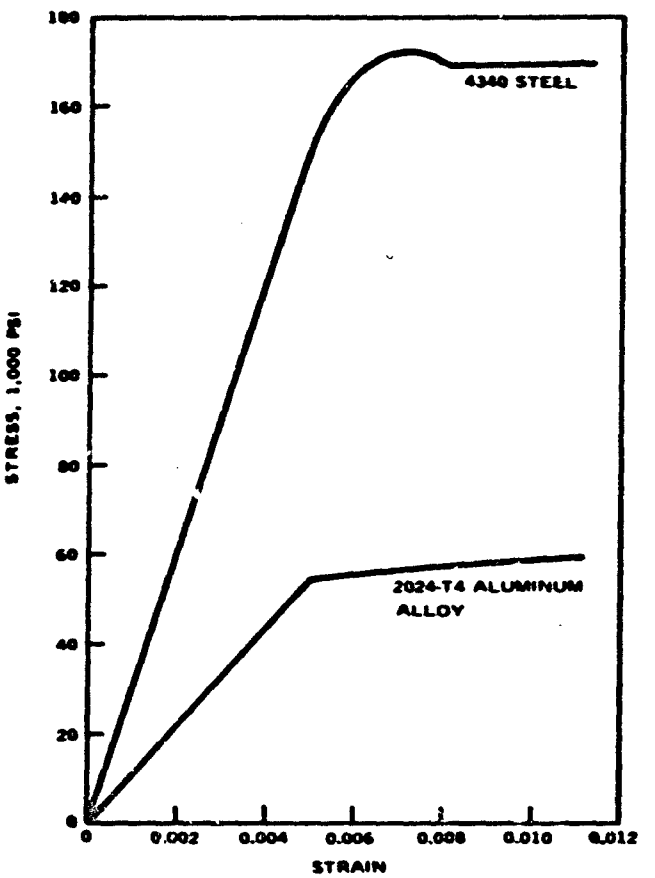

FIG. 83. Tensile Test Data for Two Materials.

by other aluminum alloys and stainless steels and titanium alloys. The steel has the general properties of the armor of armored vehicles and also the core material of projectiles.

Stress

The tensions, shearing forces, and compressions within a body can be described in a way which applies whether the body is solid, liquid, or gas. The body is imagined to be divided into many small compartments, e.g., cubes. Forces applied to the entire body result in a distribution of internal forces within the body that is described approximately by the internal forces exerted by each compartment on those compartments that are adjacent to it. The smaller the compartments are made, the finer is the description of the distribution of internal forces.

First let the compartments be cubes obtained by dividing the body by Cartesian coordinates and consider a method for listing the forces on any compartment. Number the three directions of the sides of the cubes 1, 2, and 3 and number the three different orientations of the surfaces of the cube by the direction that is normal to the surface. Now the forces can be listed in a rectangular array in which the rows correspond to the surface on which the forces act and the columns correspond to the directions of the components. An array of these forces is shown below.

Surfaces	Directions		
	1	2	3
1	F_{11}	F_{12}	F_{13}
2	F_{21}	F_{22}	F_{23}
3	F_{31}	F_{32}	F_{33}

The force components F_{11}, F_{22}, and F_{33} are normal to the surface. These are tensile forces if directed out of the cube, compressive if directed into the cube. The forces F_{12}, F_{23}, and F_{31} are parallel to the surface. These are shear forces. It can be shown that the net moment on the cube becomes zero as the cubes are made smaller and smaller, and this requires that certain of the shears must be equal

$$F_{12} = F_{21}, \quad F_{23} = F_{32}, \quad F_{31} = F_{13} \tag{A-4}$$

These internal forces depend on the surface, and in order to have a description of the internal condition that does not depend on the dimensions of the compartment, the stress is defined as the force per unit area

$$\sigma_{11} = \frac{F_{11}}{A_1}, \quad \sigma_{23} = \frac{F_{23}}{A_1} \tag{A-5}$$

for example. In the limit as the compartments become ever smaller there are six distinct components of stress at each point of the body. These are surface densities of force, which, like the mass density, are defined at each point and can be used to calculate the force on any given finite surface. The great value of the stress concept is that it makes it feasible to analyze continuous distributions of internal force.

Some simple examples of stresses may make the concept clearer. A long rod with a square cross section that is suspended on one end and has a weight W on the other will have internal forces that are directed along the rod. The array of stress components will be

$$\begin{matrix} \sigma_{11} & 0 & 0 \\ 0 & 0 & 0 \\ 0 & 0 & 0 \end{matrix} \tag{A-6}$$

The stress σ_{11} is $\sigma_{11} = W/A$ and is on the surface perpendicular to the long axis of the rod and in the direction of that axis. This is a tensile stress. There are no internal shears, and the normal forces to all other surfaces are zero.

A uniform force distribution over all very large plane surfaces will produce no shears, but there can be forces on the surfaces perpendicular to the plane surface so that the array of stress components will be

$$\begin{matrix} \sigma_{11} & 0 & 0 \\ 0 & \sigma_{22} & 0 \\ 0 & 0 & \sigma_{22} \end{matrix} \tag{A-7}$$

Hydrostatic loading produces no shears but equal stresses on all surfaces so that

$$\begin{matrix} \sigma & 0 & 0 \\ 0 & \sigma & 0 \\ 0 & 0 & \sigma \end{matrix} \tag{A-8}$$

Strain

The deformation of a body is described by considering compartments as in the definition of stress. The degree of deformation is measured by the relative elongation of a cube or the amount that the cube is sheared. Thus the elongations and contractions are

$$\epsilon_{11} = \frac{\Delta l_1}{l_1}$$

$$\epsilon_{22} = \frac{\Delta l_2}{l_2}$$

$$\epsilon_{33} = \frac{\Delta l_3}{l_3} \tag{A-9}$$

and the shears are

$$\epsilon_{12} = \frac{\Delta l_1}{l_2}$$

$$\epsilon_{23} = \frac{\Delta l_2}{l_3}$$

$$\epsilon_{13} = \frac{\Delta l_1}{l_3}$$

Deformation is expressed in an appropriate form for the continuous deformation of a body by replacing the finite quotients by derivatives. For example,

$$\frac{\Delta l_1}{l_1} \rightarrow \frac{\partial \xi_1}{\partial x_1}$$

$$\frac{\Delta l_2}{l_1} \rightarrow \frac{\partial \xi_2}{\partial x_1}$$

A shear of a 2 surface in the 1 direction has the same effect as a shear of the 1 surface in the 2 direction, and therefore it is simplest to combine these two processes so that, for example,

$$\epsilon_{12} = \frac{1}{2}\left(\frac{\partial \xi_1}{\partial x_2} + \frac{\partial \xi_2}{\partial x_1}\right) \tag{A-10}$$

An array of the strain components has the same symmetry as the stress

$$\begin{matrix} \epsilon_{11} & \epsilon_{12} & \epsilon_{13} \\ \epsilon_{12} & \epsilon_{22} & \epsilon_{23} \\ \epsilon_{13} & \epsilon_{23} & \epsilon_{33} \end{matrix} \tag{A-11}$$

The mechanical aspects of material behavior are in the relation between the components of stress and strain.

Hooke's law, which states that stress is proportional to strain, implies that each stress component is related to the strain components in a linear form. Thus for example,

$$\begin{aligned} \sigma_{11} &= C_{11}\epsilon_{11} + C_{12}\epsilon_{22} + C_{13}\epsilon_{33} + C_{14}\epsilon_{12} + C_{15}\epsilon_{13} + C_{16}\epsilon_{23} \\ \sigma_{22} &= C_{21}\epsilon_{11} + C_{22}\epsilon_{22} + C_{23}\epsilon_{33} + C_{24}\epsilon_{12} + C_{25}\epsilon_{13} + C_{26}\epsilon_{23} \end{aligned} \tag{A-12}$$

etc.

For all six stresses this would require a total of 36 elastic constants and would in general describe an anisotropic material. For an isotropic material the symmetry conditions reduce the number of constants to two, and the stress strain relations are the following:

$$\begin{aligned} \sigma_{xx} &= \lambda(\epsilon_{xx} + \epsilon_{yy} + \epsilon_{zz}) + 2\mu\epsilon_{xx} \\ \sigma_{yy} &= \lambda(\epsilon_{xx} + \epsilon_{yy} + \epsilon_{zz}) + 2\mu\epsilon_{yy} \\ \sigma_{zz} &= \lambda(\epsilon_{xx} + \epsilon_{yy} + \epsilon_{zz}) + 2\mu\epsilon_{zz} \\ \sigma_{xy} &= 2\mu\epsilon_{xy} \\ \sigma_{yz} &= 2\mu\epsilon_{yz} \\ \sigma_{zx} &= 2\mu\epsilon_{zx} \end{aligned} \tag{A-13}$$

The constants μ and λ are called the Lamé constants. The Lamé constants are related to Young's modulus and Poisson's ratio as follows:

$$2\mu = \frac{2}{1+\nu} \qquad \lambda = \frac{\nu E'}{(1+\nu)(1-2\nu)} \tag{A-14}$$

The permanent deformations of a material bring about drastic changes in the relationship between the stress and strain. These relations are described by a yield criterion that specifies the combination of stress and strain at which the changes occur from elastic to plastic behavior and determines the relation between the permanent deformations and the applied stresses.

A yield criterion is a mathematical relation between the components of stress that meet the following requirements that are based on empirical observations of the general properties of plastic deformation:

1. Permanent deformations begin when certain stress combinations exceed critical values.
2. Yielding is not influenced by hydrostatic pressure.
3. Yielding does not change the volume of the material.

Yield criteria usually use a particular resolution of the stress components into stress deviators and mean normal stress. The mean normal stress is

$$\bar{s} = \sigma_{11} + \sigma_{22} + \sigma_{33} \tag{A-15}$$

and the deviators are

$$\begin{aligned} s_{11} &= \sigma_{11} - s & s_{12} &= \sigma_{12} - s \\ s_{22} &= \sigma_{22} - s & s_{13} &= \sigma_{13} \\ s_{33} &= \sigma_{33} - s & s_{23} &= \sigma_{23} \end{aligned} \tag{A-16}$$

Examples of yield criteria are von Mises' and Tresca's criteria.

von Mises:

$$\frac{1}{2}\left(s_{11}^2 + s_{22}^2 + s_{33}^2\right) + s_{23}^2 + s_{13}^2 + s_{12}^2 = k^2 \tag{A-17}$$

Tresca:

$$\left[(s_{22} - s_{33})^2 - 4k^2\right]\left[(s_{33} - s_{11})^2 - 4k^2\right]\left[(s_{11} - s_{22})^2 - 4k^2\right] = 0 \quad \text{(A-18)}$$

The quantity s, which is like a pressure, eliminates the influence of pressure on the relationship to strain. The von Mises equation, for example, implies that s_{11}, s_{12}, etc., keep the above sum equal to k. But s may have any value.

ENERGY OF DEFORMATION

The energy of deformation can be computed from the data of the simple tension test performed on a bar of a metallic material, for example, the data of Fig. 81. The machine applies a force F corresponding to a stress $\sigma = F/A$ for the area A over which F is applied, and the bar is strained by $e = \Delta l/l$, where Δl is the increase in bar length and l is the original length of the bar.

In Fig. 82 if σ is kept less than σ_2, which is the yield point, and then reduced, the bar reverses the path and goes back to 0, but if σ goes to a point above σ_2, say to σ_3, and is then reduced, then the dashed path is followed. The work done on the bar can be measured as $\int F dl$ since dl is an increment of distance in which the force F acts. An energy density is obtained by dividing the work done by the volume of the bar, which is Al, but this is just $\int (F/A)(dl/l) = \int \sigma\, de$. (This obviously assumes uniformity in the bar.) The energy density supplied to the rod is given by the area under the stress/strain curve. Thus for cyclic loading less than σ_2 there is no area under the curve and therefore no net work done when the stress returns to zero and also, no permanent strain. But for cyclic loading that causes permanent strain e_2 the net work done is equal to the area indicated by the shading and is the energy required for the permanent strain e_2.

Other simple tests could be conducted using compression shear or torsion instead of tension. The results are essentially the same with differences in the descriptive parameters. Combinations of types of loading can also be used and are consistent with the simple tests but, of course, are much more complicated.

The perforation of a very thin plate by a pointed projectile offers one comparatively simple example of the use of a calculation of the energy of

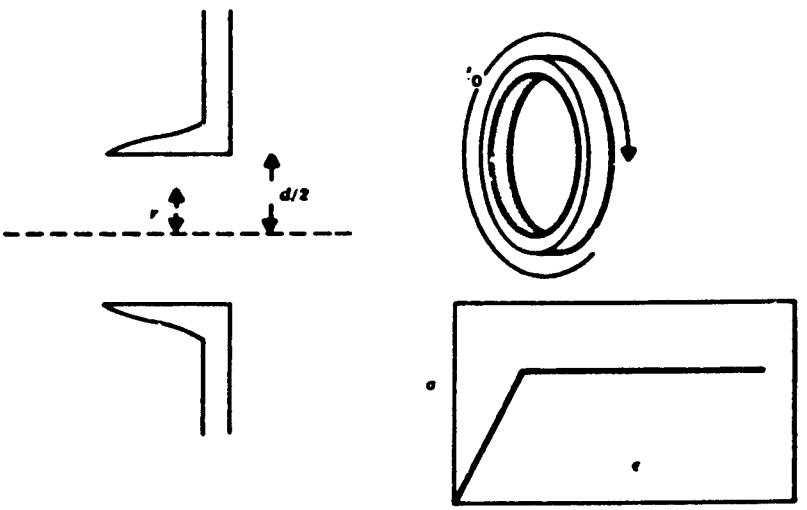

FIG. 84. Thomsen Assumptions for the Estimation of Plastic Work in Ductile Perforation Mode.

deformation in terminal ballistic theory. The starting assumptions are that the plate is thin compared to the radius of the projectile, and the relation between stress and strain is approximated by an elastic response up to a yield stress and a constant stress for all strains thereafter (Fig. 84). This kind of material behavior is called *perfectly plastic*. The perforation of the plate occurs by the piercing of the plate by the tip of the projectile followed by the deformation of the circular section of the plate of radius equal to the projectile radius $d/2$ so that this section ultimately forms a cylindrical protrusion on the exit side of the plate (see Fig. 84).

Stresses and strains are most conveniently defined for elements determined by cylindrical coordinates. The stresses are σ_r, σ_θ, σ_z, and the strains are ϵ_r, ϵ_θ, ϵ_z. It is assumed that due to the thinness of the plate and the fact that it has been pierced at the center, the stresses σ_r and σ_z are zero. The energy of deformation is estimated by calculating the work that is done in moving and deforming the circular section into the cylindrical protrusion. The stress $\sigma_\theta = \sigma_y$ because of the assumption that material behavior is perfectly plastic and the work on an element of the

circular section is

$$dW = \int_0^{\epsilon_\theta} \sigma_y d\epsilon_\theta \tag{A-19}$$

Consider an annular segment of the target that has an initial radius r and which is deformed so that it has a radius equal to the radius of the projectile; then the strain in that segment is

$$d\epsilon_\theta = \frac{\Delta l}{l}$$

where

$$l = 2\pi r$$

Hence

$$d\epsilon_\theta = \frac{dr}{r}$$

and

$$dW = \sigma_y \int_r^{d/2} \frac{dr}{r} = \sigma_y \ln\left(\frac{d}{2}r\right) \tag{A-20}$$

and the work for the entire circular section is

$$W = \int_0^{d/2} 2\pi r h_0 \sigma_y \ln\left(\frac{dr}{2}\right) dr = \frac{\pi d^2 h_0 \sigma_y}{8} \tag{A-21}$$

The energy expended in overcoming inertial forces is estimated by Thomsen through a separate calculation to give a total work

$$W = \frac{\pi h_0 d^2}{4}\left[\rho\left(\frac{v_0 d}{2l_\rho}\right)^2 + \frac{\sigma_y}{2}\right] \tag{A-22}$$

for a conical nose and

$$W = \frac{\pi h_0 d^2}{4} \left[1.86\rho \left(\frac{v_0 d}{2l_\rho} \right)^2 + \frac{\sigma_y}{2} \right] \tag{A-23}$$

for an ogival nose.

THE DYNAMICS OF DEFORMATION

The different modes of deformation, elastic, plastic, and fracture, can be demonstrated in a static testing machine. The machine exerts a force on the ends of a test specimen that is balanced by forces developed in the specimen. In dynamic loading the inertial forces within the body are balanced not by an outside agent alone but also by inertial forces. In a small region the jaws of the testing machine are replaced by material in a different state of motion.

Consider a rod with nonuniform internal motions so that the displacements of the rod, and the stresses in the rod vary from point to point. On a small segment of the rod the force applied at its upper surface is F_1; at the lower surface it is F_2.

These forces may be expressed as stresses by

$$F_1 = A\left(\sigma + \frac{d\sigma}{dx}\Delta x\right)$$

$$F_2 = A(\sigma)$$

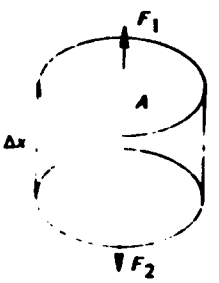

so the net force is

$$F_1 - F_2 = A\frac{d\sigma}{dx}\Delta x$$

This is balanced by the inertial force $m\dfrac{\partial^2 \xi}{\partial t^2}$ where $\dfrac{\partial^2 \xi}{\partial t^2}$ is the acceleration of the segment and

$$m\frac{\partial^2 \xi}{\partial t^2} = \rho \Delta x A \frac{\partial^2 \xi}{\partial t^2}$$

In static loading the strain is measured by the elongation per unit length. For dynamic loading the strain is the local elongation per unit length given by $\frac{\Delta\xi}{\Delta x}$. In the elastic range of behavior

$$\sigma = E\frac{\partial \xi}{\partial x} \qquad E = \text{Young's modulus}$$

Thus

$$\rho \Delta x A \ddot{\xi} = EA\Delta x \frac{\partial \xi^2}{\partial x^2}$$

or

$$\rho \ddot{\xi} = E\frac{\partial \xi^2}{\partial x^2}$$

This equation is satisfied by

$$\xi = f(x \pm ct)$$

where

$$c = \sqrt{\frac{E}{\rho}} \tag{A-24}$$

Hence it is a wave equation since it implies that disturbances travel through the body at a constant rate, c. It further implies that the dynamics of the rod can be worked out by wave propagation.

Suppose again that a force F is applied to the rod, but now in order to account for its elastic character any effects produced by F will travel at the rate $c = \sqrt{E/\rho}$. The effect of the applied force is to shorten the rod. It is therefore these deformations and accompanying internal stresses associated with this contraction that spread through the rod at the speed c. The deformation may be quantitatively measured by the contraction per unit length, for which the symbol e will be used.

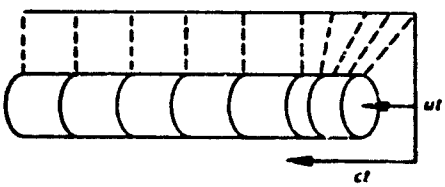

$$\epsilon = \frac{ut}{ct} = \frac{u}{c} \tag{A-25}$$

It can be seen that during a time t a total contraction u is distributed over a length ct; hence, the contraction per unit length is $\epsilon = ut/ct$. Now by Hooke's law, the force per unit area, σ, is given by $\sigma = E\epsilon$; hence, for a force F applied over a surface A, it follows that $F/A = \sigma = E\epsilon = Eu/c$, and then, since $c = \sqrt{E/\rho}$, the above becomes

$$\sigma = \rho c V \tag{A-26}$$

In this manner, the force F applied to the end of the rod produces the velocity

$$u = F/A\rho c \tag{A-27}$$

at the end of the rod. For a constant force, the velocity u is also the velocity induced at a given point as the pulse passes by. The pulse carries this velocity to the far end of the rod where it is reflected, and on its return, further increases the particle velocity by an amount u. Reflections at free surfaces will be discussed in the next section. In the present case the effect of reflection is that the pulse arrives back at the contact surface, and the rod has a velocity of $2u$. As long as the constant force F is applied, the rod will continue to vibrate in this manner, and each cycle will have the same accelerating effect.

It may turn out that u computed from $u = F/A\rho c$ is a small number compared with the initial velocity of the cylinder. In this case an individual cycle does not have much effect on the overall motion, and the rigid-body assumption is nearly as accurate and much simpler.

As an example, four computed values of particle velocity are given

below for a steel cylinder of unit area subject to the indicated forces.

Force, lb	*Velocity, ft/sec*
1	0.000488
1,000	0.488
10,000	4.88
1,000,000	48.8

This table shows that there are only small velocities associated with forces less than 1,000 pounds; however, for many applications, an analysis along the preceding lines is not the most convenient. Conversely, the table shows that large forces are generated by quite moderate particle velocities.

Stress waves in extended bodies travel at a higher rate than stress waves in rods. This is due to the differences in the relation between stress and strain that are brought about by the proximity of the lateral boundaries of the rod. It can be shown that for an extended isotropic elastic medium there are two propagation rates of elastic disturbances, one that has its particle velocity in the direction of propagation and one with particle velocity perpendicular to the direction of propagation (transverse waves). These propagation rates can be computed by Eq. A-28 and A-29. For longitudinal waves

$$c_1 = \sqrt{\frac{E(1-\nu)}{(1+\nu)(1-2)}} \tag{A-28}$$

where ν is Poisson's ratio, *i.e.*, the ratio of strain perpendicular to the direction of applied stress to the strain into the direction of applied stress.

For transverse waves

$$c_2 = \sqrt{\frac{\mu}{\rho}} \tag{A-29}$$

where μ is the torsion modulus.

Elastic stress waves in a thick barrier due to projectile impact would travel at the longitudinal propagation rate. The difference between the rod value and the extended-medium longitudinal value is as much as 15% and is therefore not insignificant. It should also be borne in mind that the rod

value is easiest to measure and therefore most likely to be given in reports on material behavior.

Stress Wave Reflection and Transmission

Free boundaries and boundaries between media that have different values of the density ρ and propagation rate c cause a change in the propagation process. Waves are reflected away from the boundaries, and these waves may be of a different type than the incident wave. Reflected and transmitted disturbances must preserve parameters. These continuity conditions determine the coefficients of reflection and transmission, which are related to material parameters, by the following:

1. The coefficient of reflection

$$u_r = u_i \frac{c_2\rho_2 - \rho_1 c_1}{c_2\rho_2 + \rho_1 c_1} \tag{A-30}$$

where ρ_1 and c_1 are for the first material and ρ_2 and c_2 are for the second material.

2. The transmission coefficient

$$u_t = u_i \frac{2c_2\rho_2}{c_2\rho_2 + c_1\rho_1} \tag{A-31}$$

It will be noted that ρc is the important parameter. This quantity ρc is directly related to the change of momentum associated with the elastic deformation of a body. An elastic body does not change momentum by the change of particle velocity at all points but by the change of particle velocity within an expanding region. This accounts for the dependence of stress on *velocity* rather than acceleration. It is the factor c that converts ρc into change of momentum by accounting for the expansion of the region.

When $\rho_2 c_2$ of the second material is small or zero, the particle velocity doubles because the incident particle velocity and the reflected particle velocity are equal. The material is also at zero stress so that the part of the material covered by both the incident and reflected wave is

moving at twice the incident particle velocity and without stress. It is consequently in local rigid body motion. Thus, reflection at a boundary produces rigid body motion. Pulses will continue to travel through the adjacent medium producing rigid body motion until the pressure inside the medium is reduced.

Wave Propagation for Materials Above the Yield Point

The stresses in a material loaded above the yield point are of the form

$$\begin{matrix} s_{11}+s & s_{12} & s_{13} \\ s_{12} & s_{22}+s & s_{23} \\ s_{13} & s_{23} & s_{33}+s \end{matrix}$$

These stresses can be resolved into an elastic stress and an imposed pressure

$$\begin{matrix} \sigma_{11}+p & \sigma_{12} & \sigma_{13} \\ \sigma_{12} & \sigma_{22}+p & \sigma_{23} \\ \sigma_{13} & \sigma_{23} & \sigma_{23}+p \end{matrix}$$

for which the elastic stress is the stress that is appropriate for the boundary conditions and the type of loading. For example, if the material is loaded on a plane surface, and the material is of great lateral extent, then the state of stress would be the elastic stress that holds for zero elastic strains in the directions normal to the direction of loading and at the yield point of the material plus a hydrostatic pressure that accounts for the remainder of the applied stress. The relations between stress and strain are then the following:

$$\begin{aligned} \sigma_{11} &= (\lambda + 2\mu)\epsilon^E_{11} + K(\epsilon^p_{11}) \\ \sigma_{22} &= \lambda\epsilon^E_{11} + K(\epsilon^p_{11}) \\ \sigma_{33} &= \lambda\epsilon^E_{11} + K(\epsilon^p_{11}) \\ \sigma_{12} &= \sigma_{13} = \sigma_{23} = 0 \end{aligned} \qquad \text{(A-32)}$$

The elastic and plastic components of these stress/strain relations represent distinct types of behavior each with a different modulus, and it has been proposed that the propagation of stresses at the yield point and stresses above the yield point simultaneously propagate at different rates. This means that the wave shape will be determined by propagation rates that are different for stress levels at the yield point and stress levels above the yield point.

If a constant load σ_1 is applied that is above the yield stress σ_y, then a wave with constant stress σ_y will travel at the elastic wave velocity and a second wave with stress σ_1 will travel at a slower rate so that the wave would have the changing wave shape illustrated in Fig. 85.

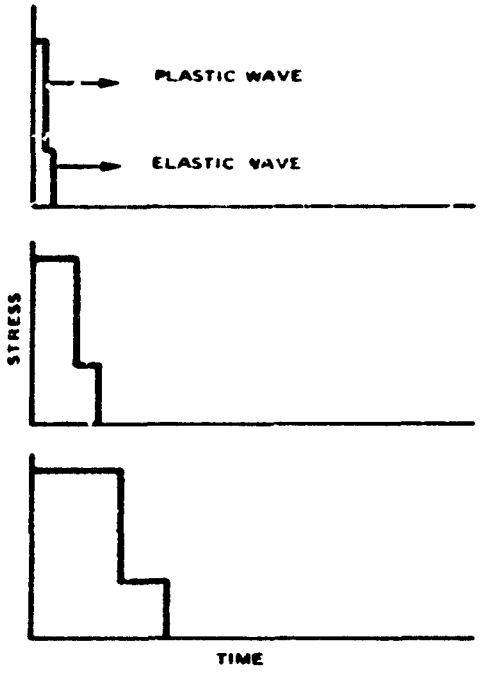

FIG. 85. The Propagation of Elastic and Plastic Waves in a Material Loaded Above the Yield Stress.

The elastic stress propagates at the rate

$$c = \sqrt{\frac{E(1-\nu)}{\rho(1+\nu)(1-2\nu)}} \tag{A-33}$$

and the plastic wave propagates at the rate

$$c = \sqrt{\frac{\left(\lambda + \frac{2\mu}{3}\right)}{\rho}} \tag{A-34}$$

The elastic wave is limited to stresses at the yield point. These stresses are very large but are still in an essentially linear region of the relation between stress and strain. The plastic wave, on the other hand, is not limited in the magnitude of its values, and at very high pressures the relation between stress and strain is nonlinear and must be described by nonlinear methods. These methods have been developed for ordinary fluids, and can be borrowed for the prediction of the fluid-like behavior of metals above the yield point.

Wave Propagation in Fluids

Changes of density and pressures are the counterparts for fluids of strains and stresses in elastic solids. The relation between the pressure and density is in general nonlinear and sometimes significantly nonlinear. For example, the adiabatic gas law

$$P = nRT\rho^{\gamma} \tag{A-35}$$

holds for many gases when changes of pressure are applied sufficiently rapidly to prevent the gas from coming to thermal equilibrium with its surroundings or within an insulated container. The simple linear methods of elastic wave propagation are not appropriate for many fluids (in particular gases) because the relation between stress and strain is nonlinear.

In order to see how the nonlinearity affects propagation, consider a plane wave propagating through a fluid that has a nonlinear relation between pressure and density. It is assumed that the propagation rate is c'. The principles of the conservation of momentum and mass can be used to

show how variations in P, ρ, and u are related to the propagation rate. This is done by examining a thin layer of the plane wave that changes location so that it moves with the wave form. Conservation of mass and momentum is computed for this layer by determining the flow of mass and momentum into and out of the layer. These flows depend on the combined effect of the motion due to the propagation of the wave form and the local motion of the material.

In Fig. 86 the wave is shown propagating to the left at a velocity c'. This means that variations in pressure, density, and velocities of the material can be described by the relations

$$u = u(x - c't) \quad \rho = \rho(x - c't) \quad p = p(x - c't) \tag{A-36}$$

where x is a coordinate in a fixed reference system. On the right boundary of the layer the density is ρ, the velocity of the material is u, and the pressure is P. On the left side of the layer the density is $\rho + \Delta\rho$, the material velocity is $u + \Delta u$, and the pressure is $p + \Delta p$. The rate at which

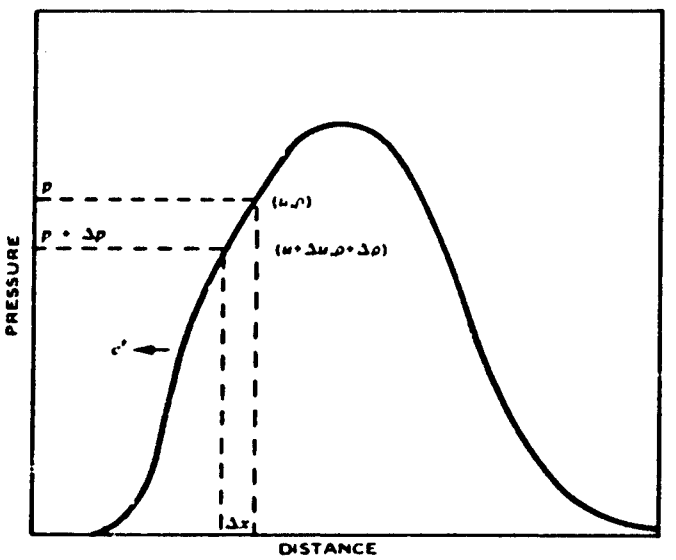

FIG. 86. Pulse Traveling Through a Fluid With Sufficient Intensity to Display Nonlinear Effects.

any parameter is carried past the boundaries of the layers are $c' - u - \Delta u$ for the right boundary and $c' - u$ for the left boundary.

Conservation of mass requires that the flow of density into the layer must be balanced by the flow out of the layer.

$$(c' - u - \Delta u)(\rho + \Delta\rho) = (c' - u)\rho$$

$$(c' - u)\Delta\rho = \rho\Delta u$$

Conservation of momentum requires that difference in the flow of the density times the material velocity must be equal to the pressure difference across the two surfaces.

$$(c' - u - \Delta u)(\rho + \Delta\rho)(u + \Delta u) - (c' - u)\rho u = \Delta p$$

The expression for the conservation of mass can be used to change the form of this equation

$$(c' - u)\rho(u + \Delta u) - (c' - u)\rho u = \Delta p$$

$$(c' - u)\rho\Delta u = \Delta p$$

The above equations for conservation of momentum and mass can be combined and solved for $c' - u$

$$(c' - u)^2 = \frac{\Delta p}{\Delta\rho} \tag{A-37}$$

$$c' - u = \frac{\partial p}{\partial \rho} \tag{A-38}$$

This quantity $(c' - u)$ is the velocity of the propagation of disturbances with respect to the material, since the velocity of the material is removed from the velocity of propagation observed with respect to fixed coordinates. Thus the velocity of propagation of disturbances with respect to the material is

$$c = (c' - u) = \sqrt{\frac{\partial p}{\partial \rho}} \tag{A-39}$$

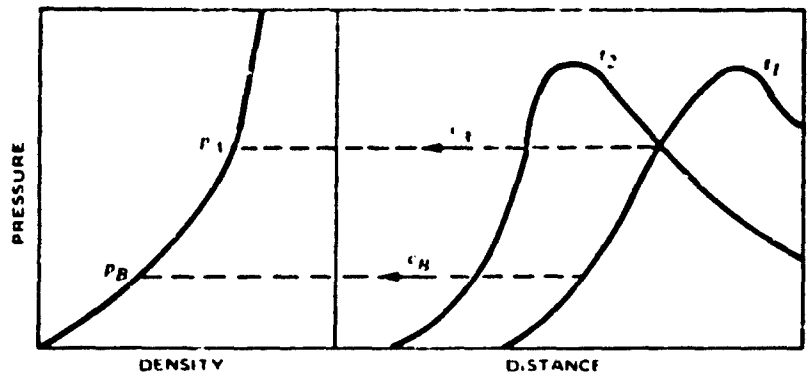

FIG. 87. Adiabatic Equation of State and Its Relation to Wave Propagation.

The dependence of the propagation rate c on the density ρ has very important consequences. Consider a fluid in which pressure and density are related as shown in Fig. 87 for an adiabatic process. Since the propagation rate c is given by $c = \sqrt{\partial p/\partial \rho}$, the pressure p_A is instantaneously propagating at c_A and pressure p_B at c_B and at some later time the point A will tend to overtake the point B and thus steepen the pulse. This process eventually tends to create a discontinuity. Thus, small disturbances preserve the shape of a pulse, but larger disturbances tend to cause steep-fronted shapes.

SHOCKS

Small-amplitude disturbances and finite disturbances during the buildup to steep leading edges, can be described by thermodynamically reversible processes because the gradients of temperature and velocity are so small that heat conduction and viscosity are not important phenomena. This is not true when the pulses take on extremely steep fronts. Thus shocks, the final result of the changes in pulse shape, are more complicated physical phenomena because dissipative processes are significant. Fortunately, the labor involved in analyzing the behavior of shocks is reduced by using the approximately discontinuous nature of the disturbances. A set of conclusions about the full-grown shock can be derived without going through the complete analysis of the more complicated processes that lead up to it.

A very abrupt change in pressure, density, and velocity is assumed to be traveling through a medium. The values of pressure, density, and velocity that are compatible with such a state are determined by applying conservation of mass and momentum to a layer that includes the abrupt changes in these quantities. The conditions are illustrated schematically in Fig. 88, which is similar to Fig. 86 for the continuous changes of pressure, density, and material velocity. The shock travels at velocity U and the fluid ahead of the shock moves at velocity u_0 and behind the shock at velocity u. The pressure and densities are p_0, ρ_0 ahead of the shock and p, ρ behind the shock. Mass and momentum flow into the shock at the velocity $U - u_0$ and out of the shock at $U - u$. Mass flow into the shock front is $\rho_0(U - u_0)$ units per second, and mass flow out is $\rho(U - u)$ units per second. To conserve mass

$$\rho_0(U - u) = \rho(U - u) \tag{A-40}$$

The flow of momentum into the shock front is $\rho_0(U - u_0)u$ units per second and the flow out is $\rho(U - u)u$. The difference in these rates of change of momentum must be equal to the pressure difference

$$\rho_0(U - u)(U - u_0) = p - p_0 \tag{A-41}$$

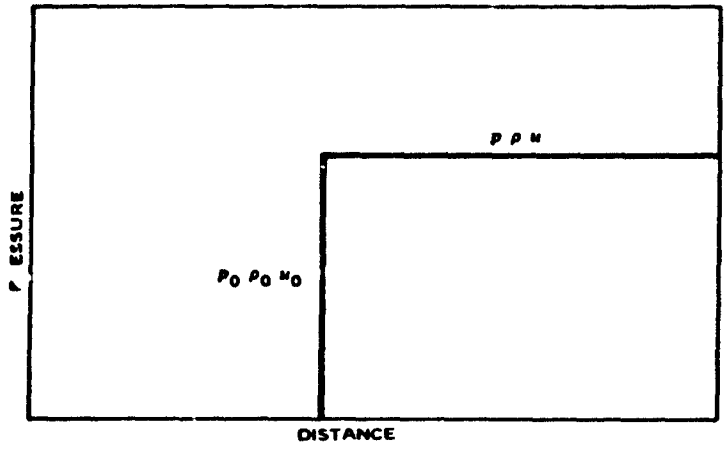

FIG. 88. Schematic Representation of "Jump" Changes of Variables at a Shock.

From these equations U and u may be calculated as

$$U = \sqrt{\left(\frac{\rho}{\rho_0}\right)\left(\frac{p - p_0}{\rho - \rho_0}\right)} \tag{A-42}$$

and

$$u = \left(\frac{p - p_0}{\rho}\right) U \tag{A-43}$$

To determine the numerical value of the shock propagation rate for a particular material we need an independent relation between the pressure and the density, such as the adiabatic gas law. The adiabatic gas law cannot be used because it is based on the assumption that there are no dissipative processes involved. An appropriate relation can be found by applying conservation of energy to the propagation of the abrupt changes in pressure, material velocity, and density.

$$pu - p_0u_0 = \rho(U - u_0)\left[E - E_0 + \frac{\left(u^2 + u_0^2\right)}{2}\right] \tag{A-44}$$

The differences in the rate of change of energy at the boundaries of the layer are equated to the rate of doing work,

$$pu - p_0u_0 + (U - u_0)\left[E - E_0 + \frac{u^2 + u_0^2}{2}\right]$$

where E and E_0 are the internal energies, usually $u_0 = 0$, and these equations can also be rearranged to have the form

$$\rho(U - u) = \rho_0 U$$

$$p - p_0 = \rho U u$$

$$E - E_0 = \frac{(p - p_0)\left(\frac{1}{\rho_0} - \frac{1}{\rho}\right)}{2} \tag{A-45}$$

The reason for rearranging the third equation is that if the equation of state is known, the internal energies can be calculated and the third equation provides pairs of pressures and densities that are compatible across a shock. This is called the Rankine-Hugoniot relation.

Shock Reflection and Transmission

The reflection of stress waves in materials with linear stress/strain relations or in fluids with very low amplitude disturbances is given by the equation

$$u_r = \left(\frac{\rho_1 c_1 - \rho_2 c_2}{\rho_1 c_1 + \rho_2 c_2}\right) u_i \tag{A-46}$$

For shocks the use of the quantities c in the above formula is usually not sufficiently accurate to describe reflection and transmission except as an approximation.

Suppose the arrival of a shock at a material boundary produces a shock in both materials. The shock in the first material is not conveniently considered as the superposition of distinct reflected and incident components, but in order to indicate the components analogous to the sum of the reflected and incident pulses the subscript $i + r$ will be used.

The shock relations in the first material are

$$\rho_i(U_i + u_i) = \rho_{i+r}(U_{i+r} + u_i) \tag{A-47}$$

$$p_{i+r} - p_i = \rho_i(U_{i+r} + u_i)(u_i - u_{i+r}) \tag{A-48}$$

and

$$E_{i+r} - E_i = \frac{(p_{i+r} + p_i)\left(\frac{1}{\rho_i} - \frac{1}{\rho_{i+r}}\right)}{2} \tag{A-49}$$

The last equation leads to the *reflection* Hugoniot

$$p_{i+r} - p_i = f(\rho_{i+r}, \rho_i) \tag{A-50}$$

Equation A-49 is similar to the impedance relationship between stress and particle velocity, but there is no simple linear relationship. By combining Eq. A-47 and A-48 the difference of particle velocities is found to be

$$u_i - u_{i+r} = (p_{i+r} - p_i)\left(\frac{1}{\rho_i} - \frac{1}{\rho_{i+r}}\right) \tag{A-51}$$

This equation and the reflection Hugoniot determine a relationship between $u_i - u_{i+r}$ and p. This and similar data for the incident shock are illustrated in Fig. 89.

In addition to the reflection curve, the curves for the direct propagation in medium I and the direct propagation in medium II are also shown. These curves are derived from the same kind of arguments as those for the shock relations for direct propagation in these media. The intersection of the direct curve for medium II and the reflection curve for medium II is the equivalent of the equality

$$\rho_1 c_1 (u_i + u_r) = \rho_2 c_2 u_t \tag{A-52}$$

From the data at this point of intersection the characteristics of the shock in both media can be obtained.

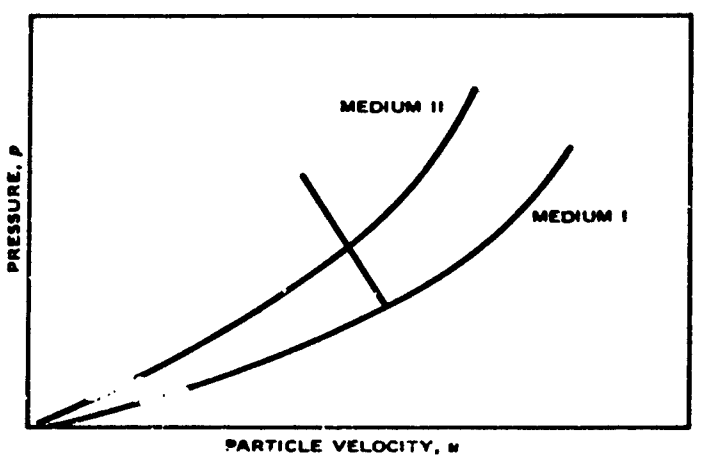

FIG. 89. Hugoniot Data for Shock Reflections.

The preceding discussion is an introduction to the basic concepts of the dynamic response of metals to impact. These concepts have been developed for the simple configurations of rods and infinitely extended bodies, since these are about the only examples in which the essential features of the dynamic responses can be illustrated in terms of elementary analytical methods. It is feasible to extend these ideas to more general configurations by the use of numerical methods in the solution of differential equations that govern conservation of mass, momentum, and energy and the description of material behavior for a continuous medium. This was discussed in the section on Warhead Terminal Ballistics.

The ideas developed thus far can be used to estimate certain stress conditions that are important in terminal ballistics and to help interpret empirical data.

MAXIMUM STRESS IN IMPACT

In the discussion of the causes of instabilities of projectiles penetrating earth media it was pointed out that the initial stresses on the projectile are high during the period of minimum flow in which the stresses are distributed through the medium. The pressure in this period was estimated by

$$p = \rho c u \tag{A-53}$$

The meaning of this formula has been demonstrated in the preceding, and methods for determining u have been developed. Strictly speaking these methods apply to a flat-ended projectile and therefore overestimate the values for common projectiles. The more pointed the projectile, the more quickly will flow relieve the stress to a value approaching

$$p = \frac{f u^2}{2} \tag{A-54}$$

where f accounts for the variation of the dynamic pressure over the surface of the projectile.

NATURAL TIME INTERVALS FOR LARGE CHANGES OF DYNAMIC STATE

The fact that stresses propagate at a constant value makes the transit time of waves through a plate and back a natural time interval for changes of dynamic state. This transit time is the minimum time interval in which a plate is identical in response to an extended medium. For impact velocities that generate stresses in the elastic region of material behavior the elastic part of the two wave systems may be important, but in general the estimate of the time interval would be based on plastic wave propagation.

THE INTERPRETATION OF DATA AND THEORIES ON RESISTING FORCE

The yield behavior of metals provides a specific phenomenological basis for the interpretation of the Poncelet form of penetration resistance forces. The velocity-independent term is naturally related to the yield strength or an empirical measurement like hardness. The velocity-dependent term is related to internal effects expressible as a dynamic pressure. Figure 90 shows data on the penetration of long projectiles into thick barriers. These data have been fitted by the solution to Poncelet's penetration equation. The correlation of experimental data to theory demonstrates the general applicability of the Poncelet form of the resisting force. This form of penetration resistance has been suggested many times. The outstanding limitation is a lack of information on the variation of the resisting forms with variation in plate thickness.

Reference 45 gives an example of the inclusion of a measure of strength in the resisting force. Assuming a resisting force of the form

$$F = aA\left(\sqrt{bH_t} + \sqrt{\rho_t u}\right)^2 \qquad \text{(A-55)}$$

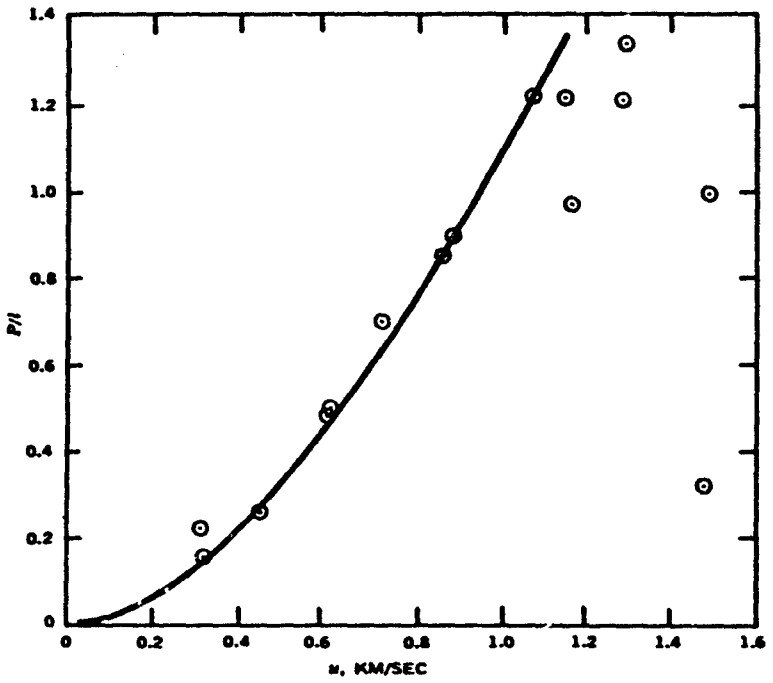

FIG. 90. Relative Penetration Plotted Against Impact Velocity.

we obtain a formula for penetration that is of the form

$$\frac{P}{l} = \frac{1}{a}\left(\frac{\rho_0}{\rho_t}\right)\left(\ln\left(1 + \sqrt{\frac{\rho_t u^2}{bH_t}}\right) - \frac{\sqrt{\frac{\rho_t u^2}{bH_t}}}{1 + \sqrt{\frac{\rho_t u^2}{bH_t}}}\right) \qquad \text{(A-56)}$$

CALCULATION OF STRESS INTENSITIES FOR SPALLING

The propagation of stress can result in the failure of the barrier ahead of the projectile as the stress waves generated by impact reflect from the free surface and interact with the latter parts of the incident wave. This is illustrated in Fig. 91, which shows different stages in the propagation and reflection of a shock from a free surface. If the incident wave has the shape shown at the top, it will reflect as a tensile wave, as is shown in the next stage, and as it combines with the incident wave it will eventually develop a net tensile stress in excess of the yield strength of the material and cause fracture.

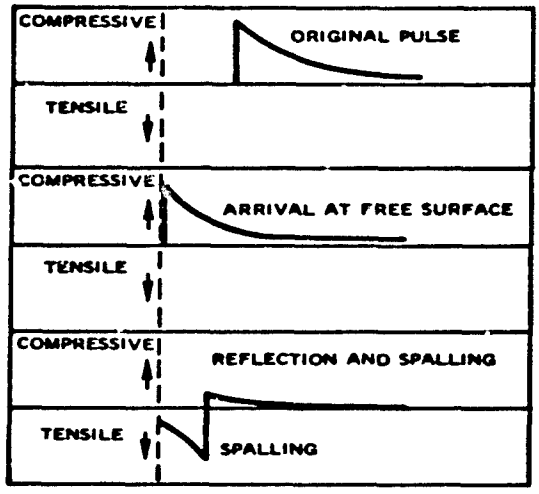

FIG. 91. Shock Reflection and Spalling.

Subject Index